AD-764 364

WIND TUNNEL DRAG AND STABILITY OF SOLID FLAT CIRCULAR, T-10, AND RING-SLOT PARACHUTE MODELS WITH CENTERLINES

H. G. Heinrich, et al

Minnesota University

Prepared for:

Air Force Flight Dynamics Laboratory

May 1973

DISTRIBUTED BY:

NTIS

National Technical Information Service
U. S. DEPARTMENT OF COMMERCE
5285 Port Royal Road, Springfield Va. 22151

AFFDL-TR-73-17

AD 764364

WIND TUNNEL DRAG AND STABILITY OF SOLID FLAT CIRCULAR, T-10, AND RINGSLOT PARACHUTE MODELS WITH CENTERLINES

H. G. HEINRICH

R. A. NOREEN

UNIVERSITY OF MINNESOTA

TECHNICAL REPORT AFFDL-TR-73-17

MAY 1973

Approved for public release; distribution unlimited.

AIR FORCE FLIGHT DYNAMICS LABORATORY
AIR FORCE SYSTEMS COMMAND
WRIGHT-PATTERSON AIR FORCE BASE, OHIO

139

NOTICES

When Government drawings, specifications, or other data are used for any purpose other than in connection with a definitely related Government procurement operation, the United States Government thereby incurs no responsibility nor any obligation whatsoever; and the fact that the Government may have formulated, furnished, or in any way supplied the said drawings, specifications, or other data, is not to be regarded by implication or otherwise as in any manner licensing the holder or any other person or corporation, or conveying any rights or permission to manufacture, use, or sell any patented invention that may in any way be related thereto.

ACCESSION for

NTIS White Section ☑

DDC Buff Section ☐

UNANNOUNCED ☐

JUSTIFICATION ....

BY ....

DISTRIBUTION/AVAILABILITY CODES

Dist.	AVAIL. and/or SPECIAL	
A		

Copies of this report should not be returned unless return is required by security considerations, contractual obligations, or notice on a specific document.

AIR FORCE/56780/25 July 1973 — 150

UNCLASSIFIED

Security Classification

DOCUMENT CONTROL DATA - R & D

(Security classification of title, body of abstract and indexing annotation must be entered when the overall report is classified)

1. ORIGINATING ACTIVITY (Corporate author)

University of Minnesota
Minneapolis, Minnesota 55455

2a. REPORT SECURITY CLASSIFICATION

UNCLASSIFIED

2b. GROUP

3. REPORT TITLE

Wind Tunnel Drag and Stability of Solid Flat Circular, T-10, and Ringslot Parachute Models With Centerlines

4. DESCRIPTIVE NOTES (Type of report and inclusive dates)

Final Report June 68 - December 72

5. AUTHOR(S) (First name, middle initial, last name)

Heinrich, H. G.
Noreen, R. A.

6. REPORT DATE

May 1973

7a. TOTAL NO. OF PAGES

~~122~~ 139

7b. NO. OF REFS

3

8a. CONTRACT OR GRANT NO. F33615-68-C-1227

b. PROJECT NO 6065

c.

d.

9a. ORIGINATOR'S REPORT NUMBER(S)

9b. OTHER REPORT NO(S) (Any other numbers that may be assigned this report)

AFFDL-TR-73-17

10. DISTRIBUTION STATEMENT

Approved for public release; distribution unlimited.

11. SUPPLEMENTARY NOTES

12. SPONSORING MILITARY ACTIVITY

AFFDL/FER
WPAFB, OH 45433

13. ABSTRACT

Wind tunnel measurements of the aerodynamic force coefficients of solid flat circular, T-10, and ringslot parachute models with and without centerlines were made. Test conditions were M = 0.1 and Re/ft = 6.7 x 10^5 on models with a nominal diameter of approximately 16 in. The results showed general similarities in the effects of various centerline lengths on the different models. With centerline lengths about equal to the suspension line length, tangent force increases from 20% to 26% were obtained. At these configurations the force in the centerline is about one-half the total tangent force. The model trim angle and slope of the moment curve at that point were determined. These show the solid flat circular and T-10 models to be less stable, while the ringslot parameters were nearly unchanged.

Details of illustrations in this document may be better studied on microfiche.

DD FORM 1 NOV 65 1473

UNCLASSIFIED

Security Classification

UNCLASIFIED
Security Classification

14 KEY WORDS	LINK A		LINK B		LINK C	
	ROLE	WT	ROLE	WT	ROLE	WT
Parachutes						
Centerlines						
Tangent Force						
Moment Coefficient						
Stability						
Drag						

☆U.S.Government Printing Office: 1973 — 759-495/637

UNCLASSIFIED
Security Classification

WIND TUNNEL DRAG AND STABILITY OF SOLID FLAT CIRCULAR, T-10, AND RINGSLOT PARACHUTE MODELS WITH CENTERLINES

H. G. HEINRICH
R. A. NOREEN

UNIVERSITY OF MINNESOTA

ic

FOREWORD

This report was prepared in the Department of Aerospace Engineering and Mechanics of the University of Minnesota in compliance with U. S. Air Force Contract No. F33615-68-C-1227, "Theoretical Deployable Aerodynamic Decelerator Investigations," Task 606503, "Parachute Aerodynamics and Structures," Project 6065, "Performance and Design of Deployable Aerodynamic Decelerators." The analysis presented in this report was performed between June 1968 and December 1972.

The study was sponsored jointly by the U. S. Army Natick Laboratories, Department of the Army, and Air Force Systems Command, Department of the Air Force, and administered under the direction of the Recovery and Crew Station Branch, Air Force Flight Dynamics Laboratory, Wright-Patterson Air Force Base, Ohio, with Mr. James H. DeWeese, AFFDL/FER, as Project Engineer.

The study was accomplished in cooperation with Mr. T. R. Hektner and several students of Aerospace Engineering at the University of Minnesota. Mr. Edward J. Giebutowski, U. S. Army Natick Laboratories, participated in this study by providing valuable guidance and identification of the principal requirements.

This report was submitted by the authors in December 1972.

This technical report has been reviewed and is approved.

Rudi J. Berndt

RUDI J. BERNDT
Acting Chief, Recovery & Crew Station Branch
Air Force Flight Dynamics Laboratory

ABSTRACT

Wind tunnel measurements of the aerodynamic force coefficients of solid flat circular, T-10, and ringslot parachute models with and without centerlines were made. Test conditions were $M \approx 0.1$ and $Re/ft = 6.7 \times 10^5$ on models with a nominal diameter of approximately 16 in. The results showed general similarities in the effects of various centerline lengths on the different models. With centerline lengths about equal to the suspension line length, tangent force increases from 20% to 26% were obtained. At these configurations the force in the centerline is about one-half the total tangent force. The model trim angle and slope of the moment curve at that point were determined. These show the solid flat circular and T-10 models to be less stable, while the ringslot parameters were nearly unchanged.

TABLE OF CONTENTS

Preceding page blank

FIGURES

FIGURES (CONT.)

Appendix Figures

FIGURES (CONT.)

Appendix Figures (Cont.)

FIGURES (CONT.)

Appendix Figures (Cont.)

FIGURES (CONT.)

Appendix Figures (Cont.)

FIGURES (CONT.)

Appendix Figures (Cont.)

TABLES

TABLES (CONT.)

SYMBOLS **

C_m	moment coefficient
C_m'	moment coefficient of standard, no centerline configuration
C_{m_α}	$dC_m/d\alpha$, generally at α_T
$C_{m'_\alpha}$	$dC_m/d\alpha$ of standard, no centerline configuration
$C_{m^*_\alpha}$	ratio of C_{m_α} at α_T for a centerline configuration to C_{m_α} at α_T of the standard configuration
C_N	normal force coefficient
C_T	total tangent force coefficient
C_T'	tangent force coefficient of standard, no centerline configuration
C_{T_C}	centerline force coefficient
$C_{T^*_C}$	ratio of C_{T_C} for a centerline configuration to C_T' of standard configuration at a defined angle of attack
$C_{T^*_T}$	ratio of C_T for a centerline configuration to C_T' of standard configuration at a defined angle of attack
D_o	nominal diameter
h	distance from vent to skirt, Fig 1
L_C	centerline length
L_S	suspension line length
ℓ_1	distance from confluence point to moment center, Fig 1
ℓ_2	distance from vent to moment center, h + D_o, Fig 1
M	aerodynamic moment

** All coefficients are based on nominal areas and diameters.

N_1 confluence point normal force

N_2 vent normal force

q dynamic pressure

S_o nominal area

T total tangent force, $T_C + T_S$

T_C centerline force

T_S suspension line component of tangent force at confluence point

α parachute angle of attack

α_T parachute trim angle of attack, $C_m = 0$, $C_{m_\alpha} < 0$

Subscripts

o nominal

Superscripts

indicates characteristics of the standard, no centerline, configuration

I. INTRODUCTION

For some time it has been known that adding a centerline to a parachute configuration, which pulls the vent down closer to the suspension line confluence point by relatively small amounts, increases the drag of a parachute within certain limits. Even though centerlines have been used or investigated frequently, there is no compilation of data on the effects of the centerline on the aerodynamic characteristics of the parachute and on the forces in the centerline. This report presents the results of wind tunnel measurements of the aerodynamic coefficients and centerline forces on model solid flat circular, T-10, and ringslot parachutes with various centerline lengths.

II. COORDINATE SYSTEM AND COEFFICIENTS

Figure 1 shows the coordinate system used and the forces measured in this study. It differs from the one in Ref 1 in view of the normal forces which now are resolved in one component N_1 acting at the confluence point and in another component N_2 at the junction of the center vent and the centerline. Both components can of course be combined to a single normal force N. Also one notices that tangent force components T_C and T_S were measured. T_C is the center-line force, while T_S is the tangent force component transmitted through the suspension lines. Both tangent forces and their coefficients can also be combined to a single term. The moment amounts to

$$M = N_1 l_1 + N_2 l_2$$

with the moment center D_o below the skirt of the parachute canopy. The respective coefficients are defined as follows:

$$C_{T_o} = \frac{T_S + T_C}{qS_o} \qquad C_{M_o} = \frac{M}{qS_oD_o}$$

$$C_{N_o} = \frac{N_1 + N_2}{qS_o} \qquad C_{T_{C_o}} = \frac{T_C}{qS_o}$$

Since all of the coefficients are based on nominal area and diameter, the subscript "o" is omitted in the remainder of this report.

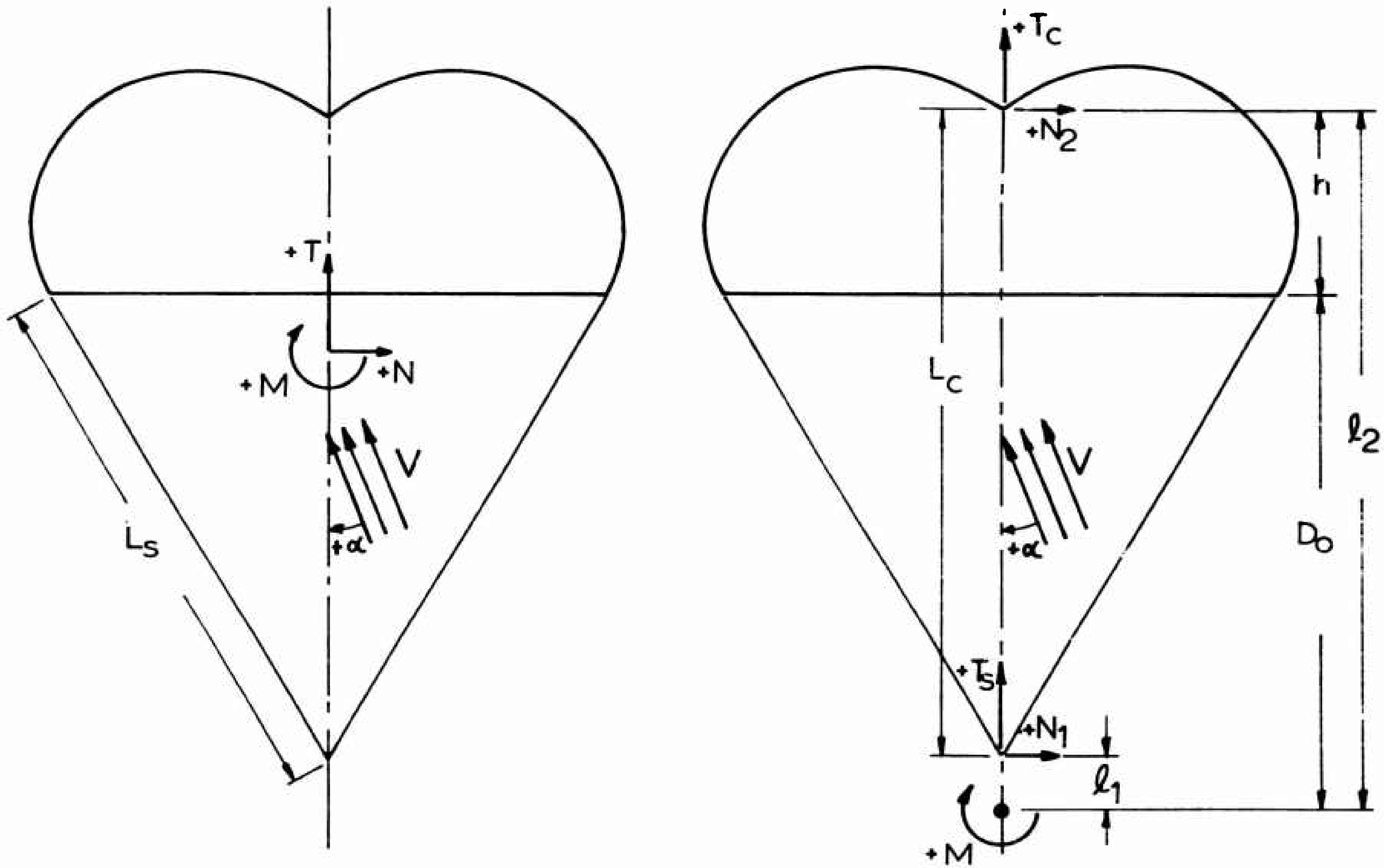

a) GENERAL SYSTEM b) WIND TUNNEL SYSTEM

Fig 1 Parachute Coordinate System and Forces

III. MODELS

Table 1 summarizes the pertinent parameters of the solid flat circular, T-10, and ringslot parachute models. Figure 2 shows the gore pattern of the ringslot model. The solid flat circular and the T-10 models were built to be as flexible as possible in accordance with Ref 2; namely, they were made from a single piece of cloth with gores simulated by running the suspension lines over the canopy and fastening them with a zig-zag stitch. Each ring of the ringslot was made from a single piece of ribbon seamed together at the ends and then darted to form the 28 gores. The seven separate rings were then connected by sewing the suspension lines from vent to skirt at the "gore" edges; there were no other radial lines or tapes.

TABLE I
MODEL PARACHUTE CHARACTERISTICS

PARACHUTE MODEL	D_o (in)	S_o (in)	L_S (in)	NUMBER OF GORES	CANOPY MATERIAL	CLOTH NOMINAL POROSITY	GEOMETRIC POROSITY	STIFFNESS INDEX,
Solid Flat Circular	15.5	188.69	15.5	28	Mil-C-7020D Type I (1.1 oz/yd^2)	100 $\pm$ 20	- - -	1.18
T-10	15.7	193.59	12.78	30	Mil-C-7020D Type I (1.1 oz/yd^2)	100 $\pm$ 20	- - -	
Ringslot $\lambda_T = 9.8\%$	14.56	166.50	16.5	28	Mil-T-5608E Class A Tape	150 $\pm$ 30	4.6%	1.58

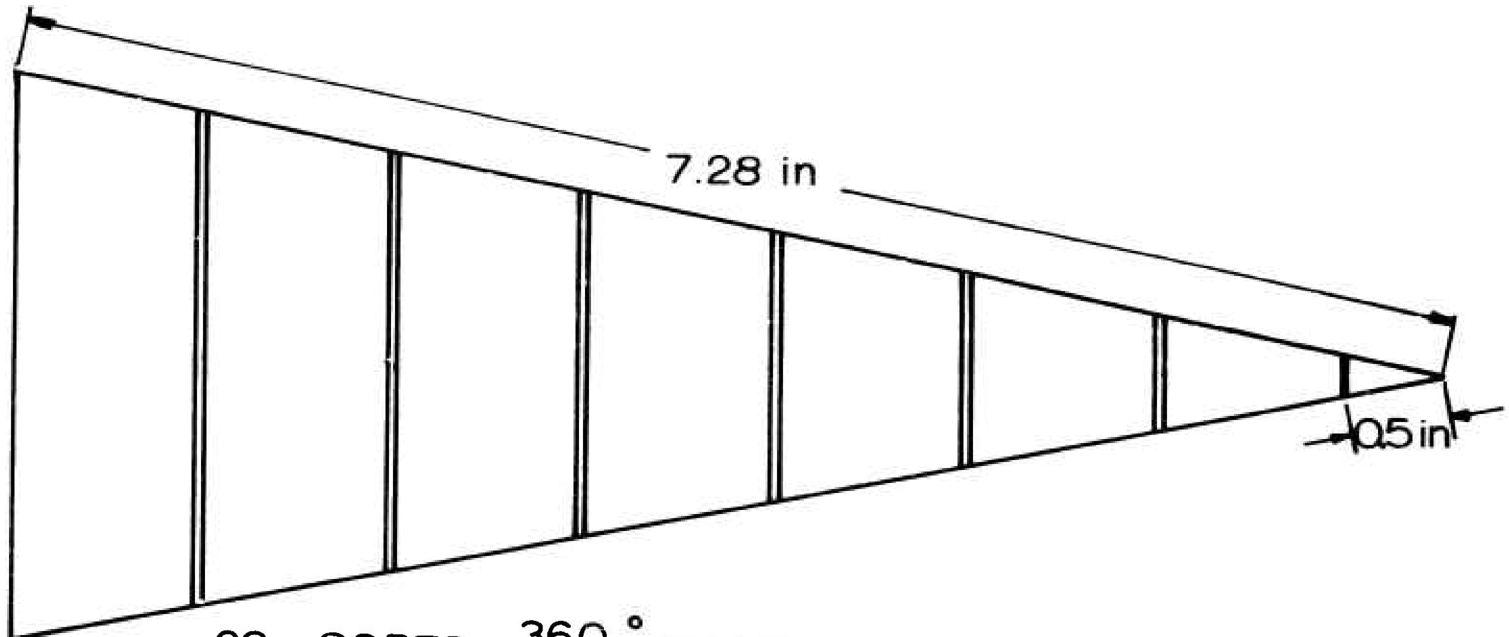

28 GORES, $\frac{360}{28}^{\circ}$ EACH

6 SLOTS, 0.05 in EACH

7 RINGS, 0.93 in EACH

Fig 2 Gore Pattern for Ringslot Parachute Model

IV. WIND TUNNEL APPARATUS AND TEST PROCEDURE

A. Apparatus

A major part of this effort was designing and building a model support system that could accurately measure the aerodynamic forces while maintaining a model geometry which would closely approximate a full scale parachute with a centerline. In full scale parachutes a centerline is an actual line, and as such pulls the vent down into a conical shape, nearly pointed at the centerline. For a correct model simulation, this means that the vent area of the model cannot be forced flat over any significant percentage of the model diameter, and thus if an axial sting is used, it must be quite small. This constraint on vent geometry and the fact that at the confluence point the normal forces are at least an order of magnitude lower than the tangent forces, combine to give a very difficult wind tunnel force measurement problem. Many different support systems were considered and several tried before one was finally found to be acceptable. It would be too tedious to describe all, but it should be noted that the system used was selected after a very thorough investigation. Also, photographic shape studies were made on the effects of various sting diameters, including a wire, and the effects of terminating the suspension lines in a manner other than a perfect confluence point. Force measurements were made with several other installations but none gave a separation of the various forces as satisfactory as in the system selected.

The sting mount system used for the force measurements derives from the one described in Ref 1 and is shown in Fig 3. The downstream end of the axial sting was supported by a ball bushing in a vertical strut. The upstream end of

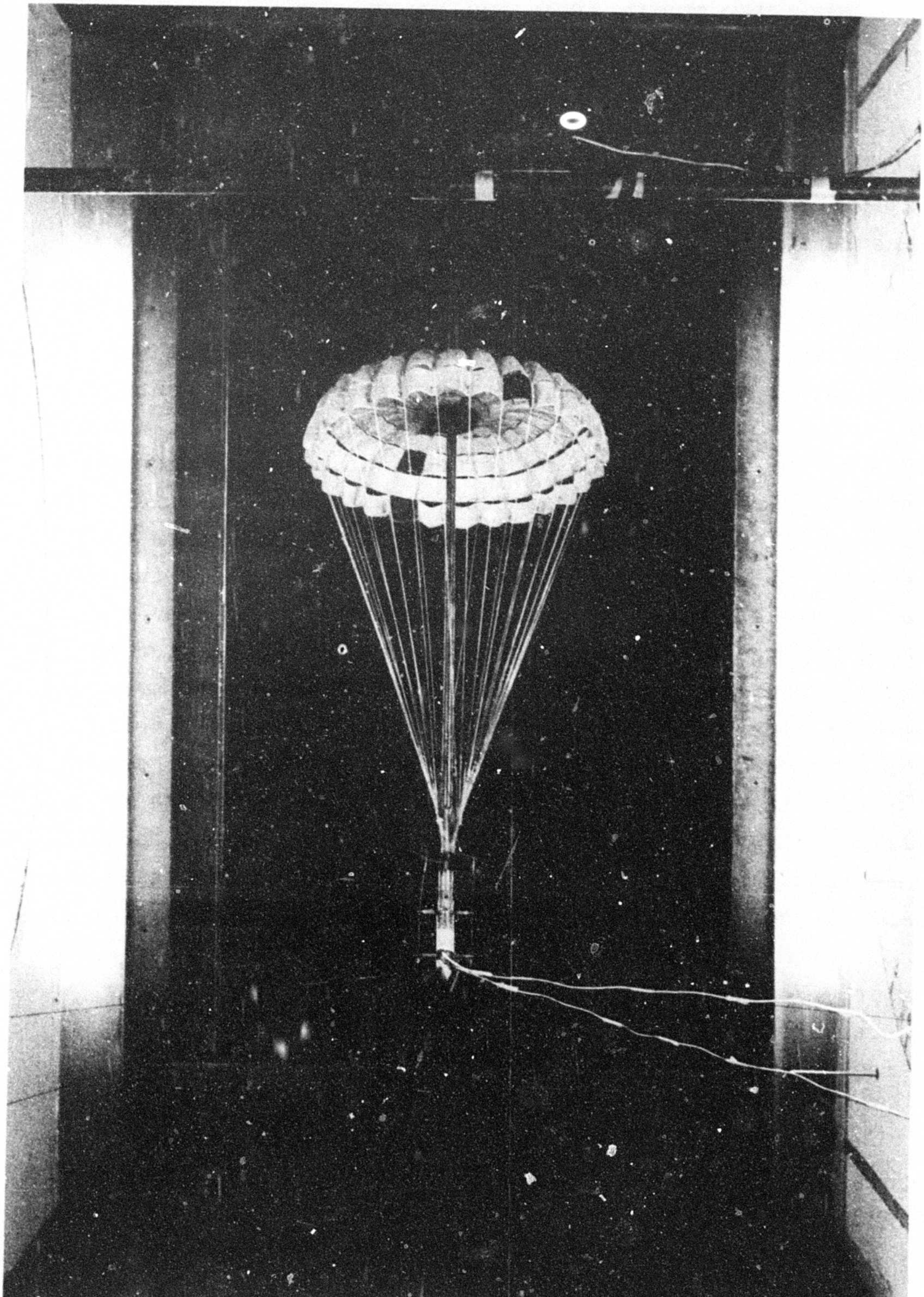

Fig. 3 PARACHUTE MODEL IN WIND TUNNEL

the sting was supported by a ball bushing in a small forebody which was held in place with 0.024-in wires. This entire system was mounted on a turntable which enabled changing the parachute angle of attack.

Figure 4 illustrates the functioning of the force sensors. The model suspension lines were brought to a single confluence point in order to preserve the canopy shape. From the confluence point the forces in the suspension lines were transferred to the upper and lower halves of the strain-gaged cantilever beams of the front force sensor. Figure 5 shows more details of this sensor. Any normal force at the parachute confluence point causes a small deflection of the confluence point. and thus a deflection of the normal force cantilever beam. The friction between the fine cables and the hole edges at the top of the normal force sensors was low enough so that its effect could be neglected, and tangent force measured on the upstream cantilever beams.

Figure 6 shows the vent normal force sensor and the method for transmitting the "centerline" force to the axial sting. As Fig 6 shows, there was no actual centerline, rather the parachute vent was restrained to a known position on the axial sting. The parachute models had thin discs attached to the inside of the canopy at the vent. The vent normal force was transmitted from the canopy to the inner ring of the disc, then from the inner ring to the disc outer ring. The disc outer ring was fastened to the outer ring of the vent normal force sensor. Two thin strain-gaged beams connect the sensor outer ring to the sensor inner ring which fits over the axial sting. These two beams then provide a measurable deflection when any vent normal force is restrained by the axial sting. The inner ring of the disc sewn in the parachute vent was such that it did not touch the axial sting, and the inner ring of the normal force

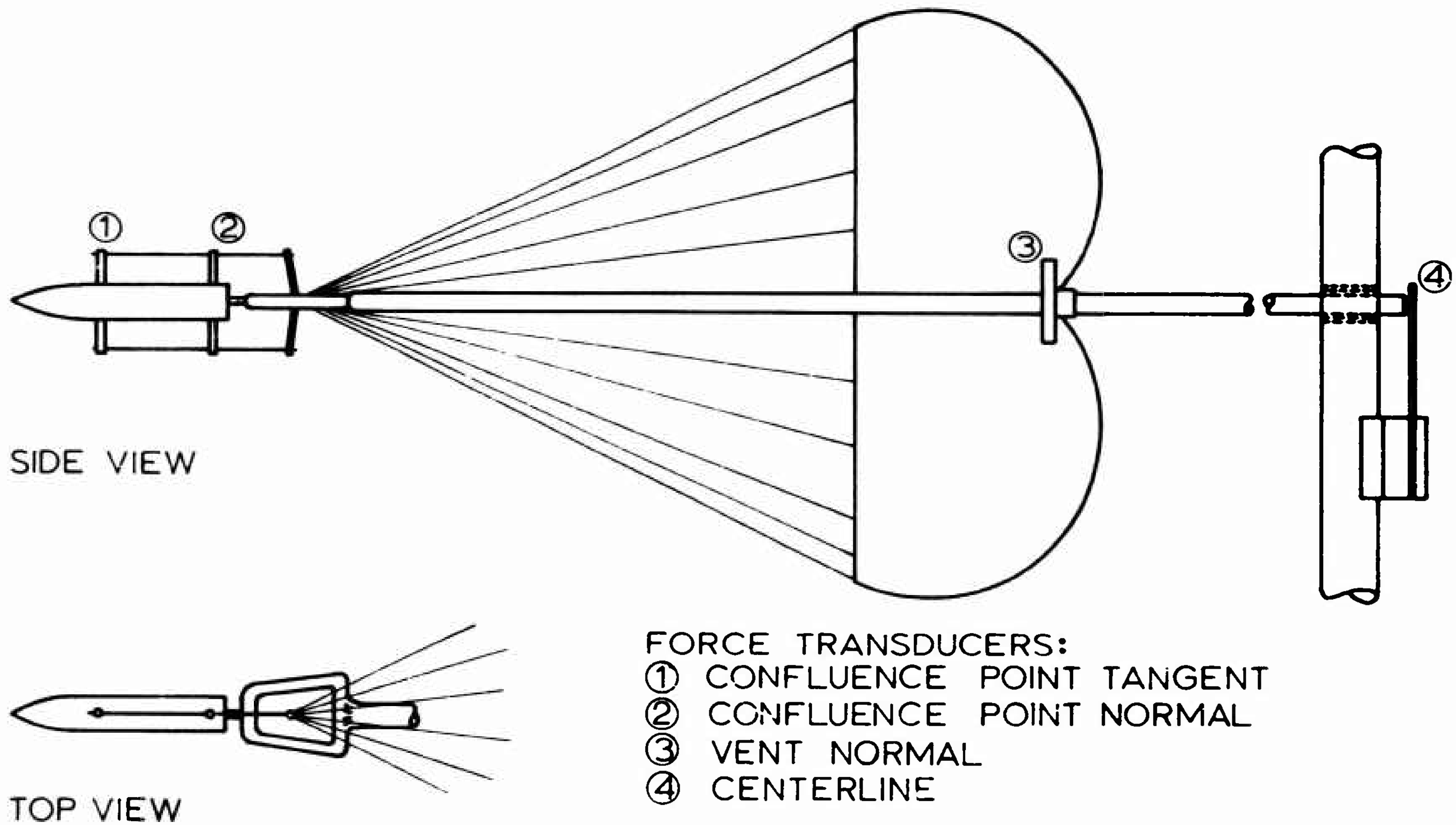

Fig 4 Wind Tunnel Apparatus

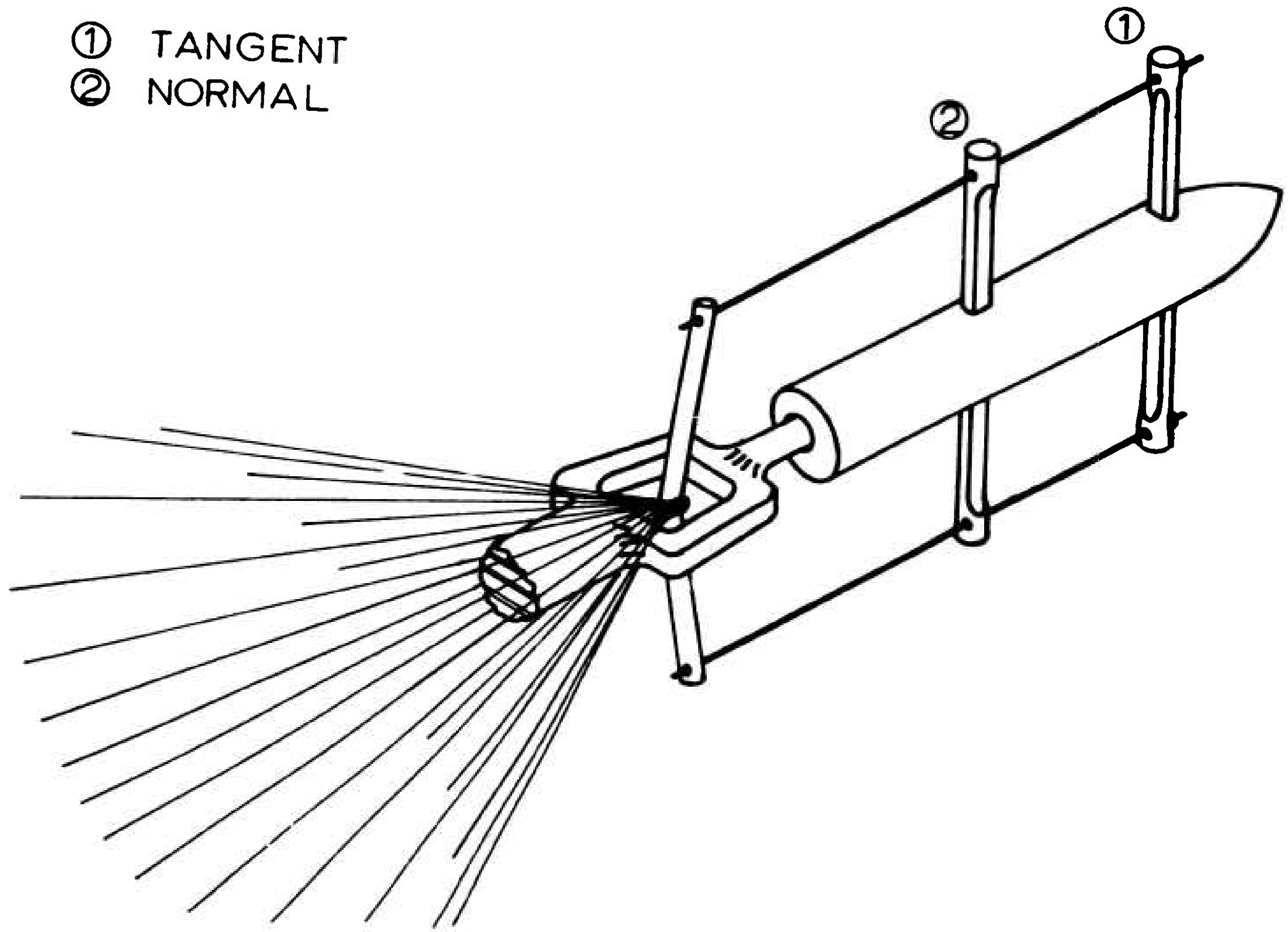

Fig 5 Confluence Point Force Sensors

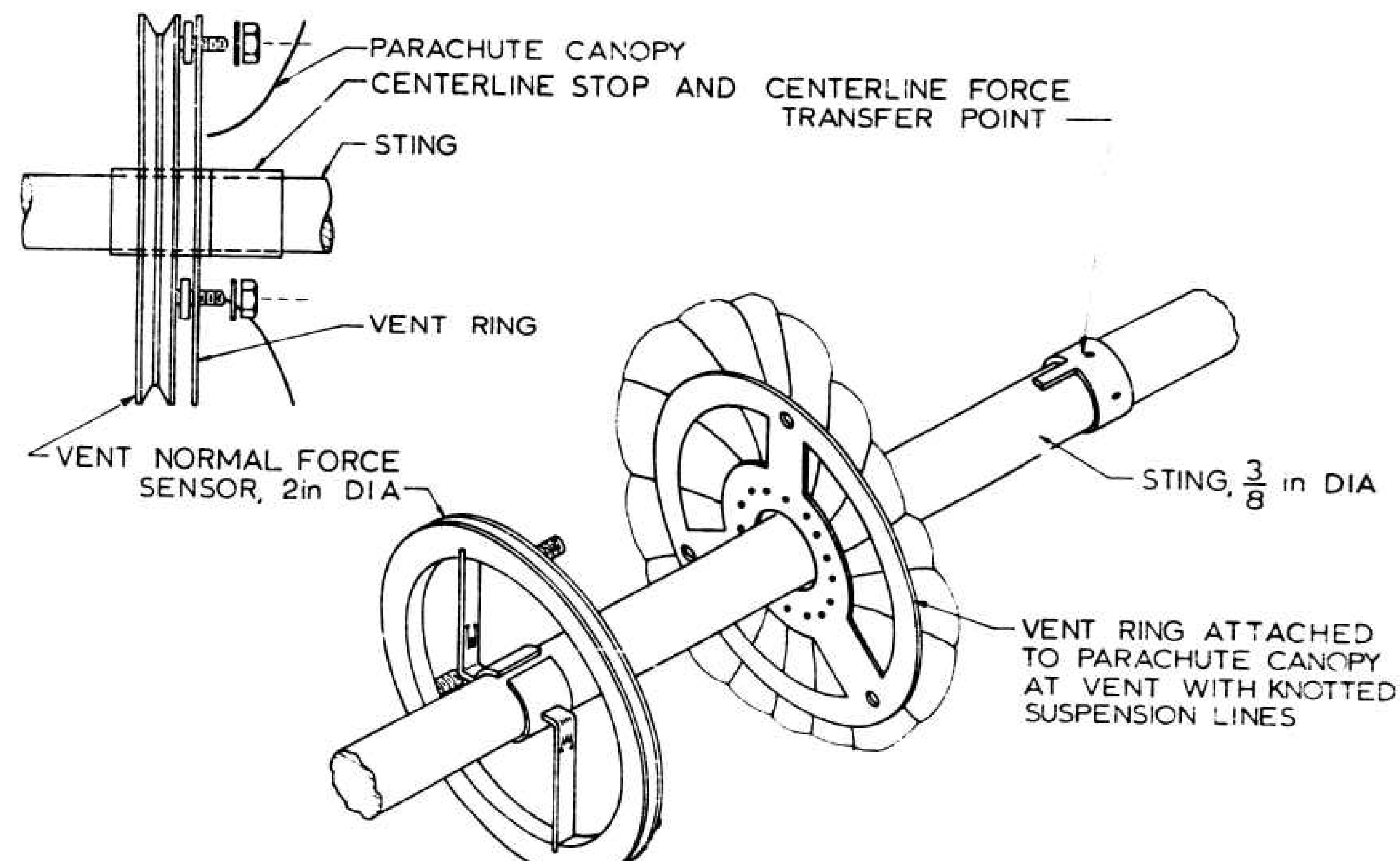

Fig 6 Vent Normal Force Sensor

sensor fit snugly on the sting. The centerline force in the axial sting was sensed by a simple cantilever beam mounted on the downstream vertical strut. Thus, with this system the geometry of a parachute with a centerline is accurately preserved, and the aerodynamic forces are separated for reliable measurement.

All of the deflecting beams on the force sensors were instrumented with strain gages which were wired into four active gage Wheatstone bridges. For the sensors which used two beams, the bridges were wired so that the deflection from each beam would be added algebraically. The output from these bridges was amplified and recorded on an oscillographic recorder.

All force sensors were calibrated before and after each wind tunnel run. The only interaction that was at all significant was the confluence point tangent force upon confluence point normal force. This interaction could cause a calibration deviation of at most 5%, and this was calibrated out.

B. Test Procedure

1. Determination of Centerline Lengths.

The first tests conducted were measurements of total tangent force over the range of centerline lengths which would be effective in increasing the parachute tangent force. As the centerline is shortened there is an increase in tangent force to a maximum, then further shortening decreases the tangent force. Measurements were made to determine the tangent force with no centerline, then to determine the particular centerline length where the models began to collapse. The difference in length between this value and that for a centerline which would give no vent pull down was divided into four

equal increments to give five different centerline lengths plus no centerline as test configurations. These preliminary tests were conducted at the approximate α_T of the particular model parachute, and all centerline lengths are associated with the inflated parachute.

2. Test Performance and Conditions.

After selecting the centerline lengths to be tested, the model was installed in the wind tunnel and its angle of attack increased until gore bulges near the skirt began to collapse. This angle was considered as the maximum angle of attack for testing this particular parachute configuration. In some cases the maximum angle up to which the measurements were made was slightly less than this angle. The parachutes were then measured at angles of attack varying in increments of 2.5^o between plus and minus values of the maximum angle. The forces were measured at each angle of attack at least four times by sweeping the parachute models back and forth over the angle range.

The wind tunnel conditions for most of the data points were $M = 0.1$ and $Re/ft = 6.7 \times 10^5$. For some data points near 0^o on the solid flat circular and T-10 models the velocity had to be reduced to $M = 0.07$, $Re/ft = 5 \times 10^5$ because of the violent model vibrations.

V. RESULTS

A. Data Reduction

After the measurements, the data from individual tests were reduced to forces and moments and these were averaged for their respective angles of attack. These averages were then plotted and symmetrized to correct for a flow angularity in the wind tunnel of approximately 2°. The symmetrized data points were plotted against the magnitude of the angle of attack so that points from positive and negative angles fell in the same quadrant of the graph. Smooth curves were then drawn through these symmetrized data points. This process averages out minor test inaccuracies and model irregularities, but the averaged data points presented generally do not deviate from individual measurements by more than 5%. Force and moment values were then read from the smoothed curves, and the related coefficient was calculated.

The complete results of this effort are presented in graphs and tables in the Appendix; the remainder of this section presents the results of the configurations without a centerline and the comparative effects of centerlines of various lengths.

B. The Standard Configurations

The aerodynamic force and moment coefficients for the "standard configurations," those without effective centerlines, are shown in Table II and Figs 7, 8, and 9. These coefficients are designated as C_T', C_N', C_M', etc. The vents of these configurations were restrained at a position determined in the preliminary tests just beyond the point where a centerline would have any effect. The value of this "ineffective" centerline length is shown in Table II, and

TABLE II
AERODYNAMIC CHARACTERISTICS OF THE STANDARD CONFIGURATIONS

MODEL	C_T' $\alpha=0$	α_T	C_T' $\alpha=\alpha_T$	$C_{D_{eff}}'$	C_M' (per deg)	L_C/L_S
SOLID FLAT	0.65	20.8°	0.645	0.727	-0.0029	1.26
T-10	0.57	20.4°	0.595	0.677	-0.0056	1.30
RINGSLOT	0.535	5.6°	0.545	0.550	-0.0045	1.22

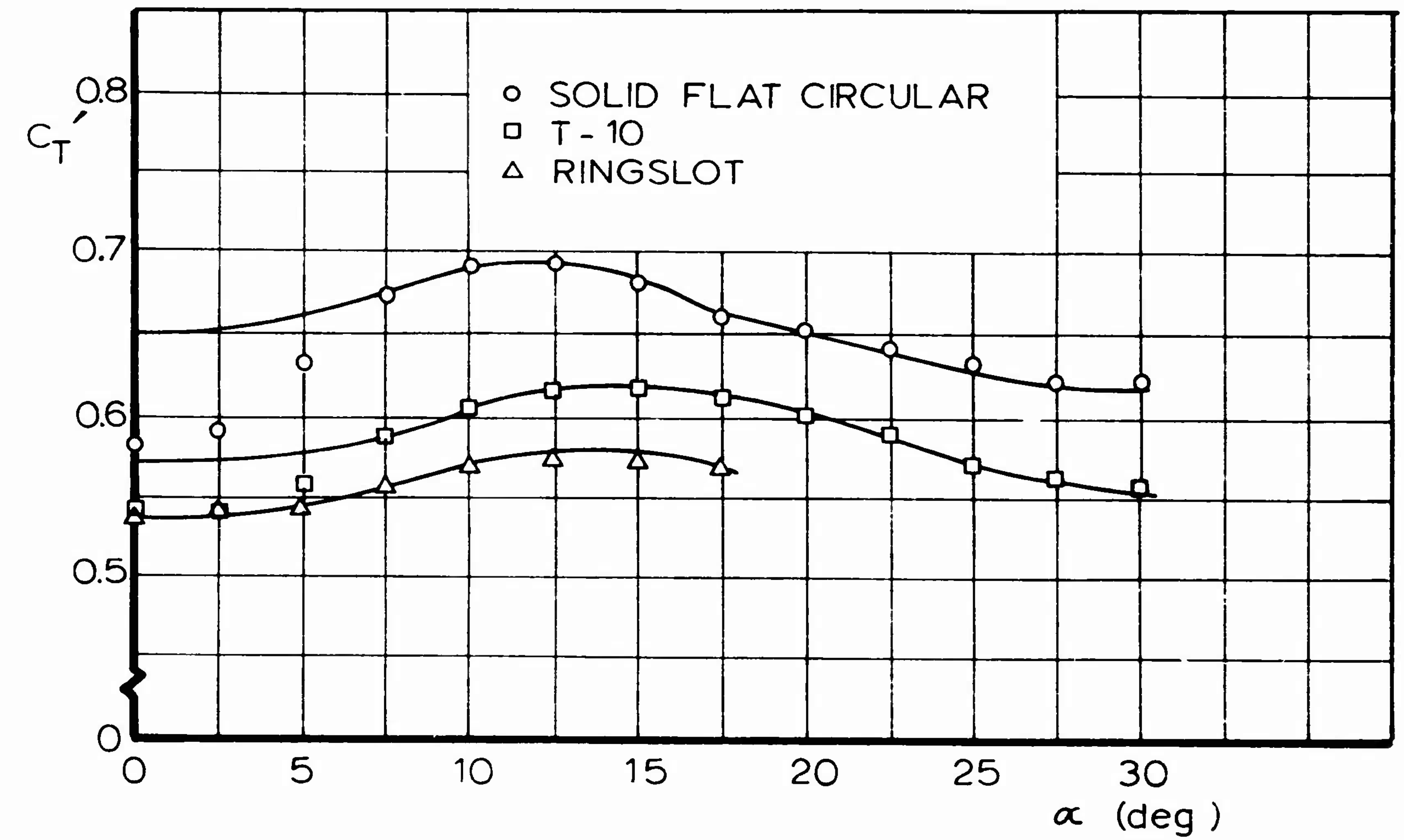

Fig 7 Tangent Force Coefficients for the Standard Configuration

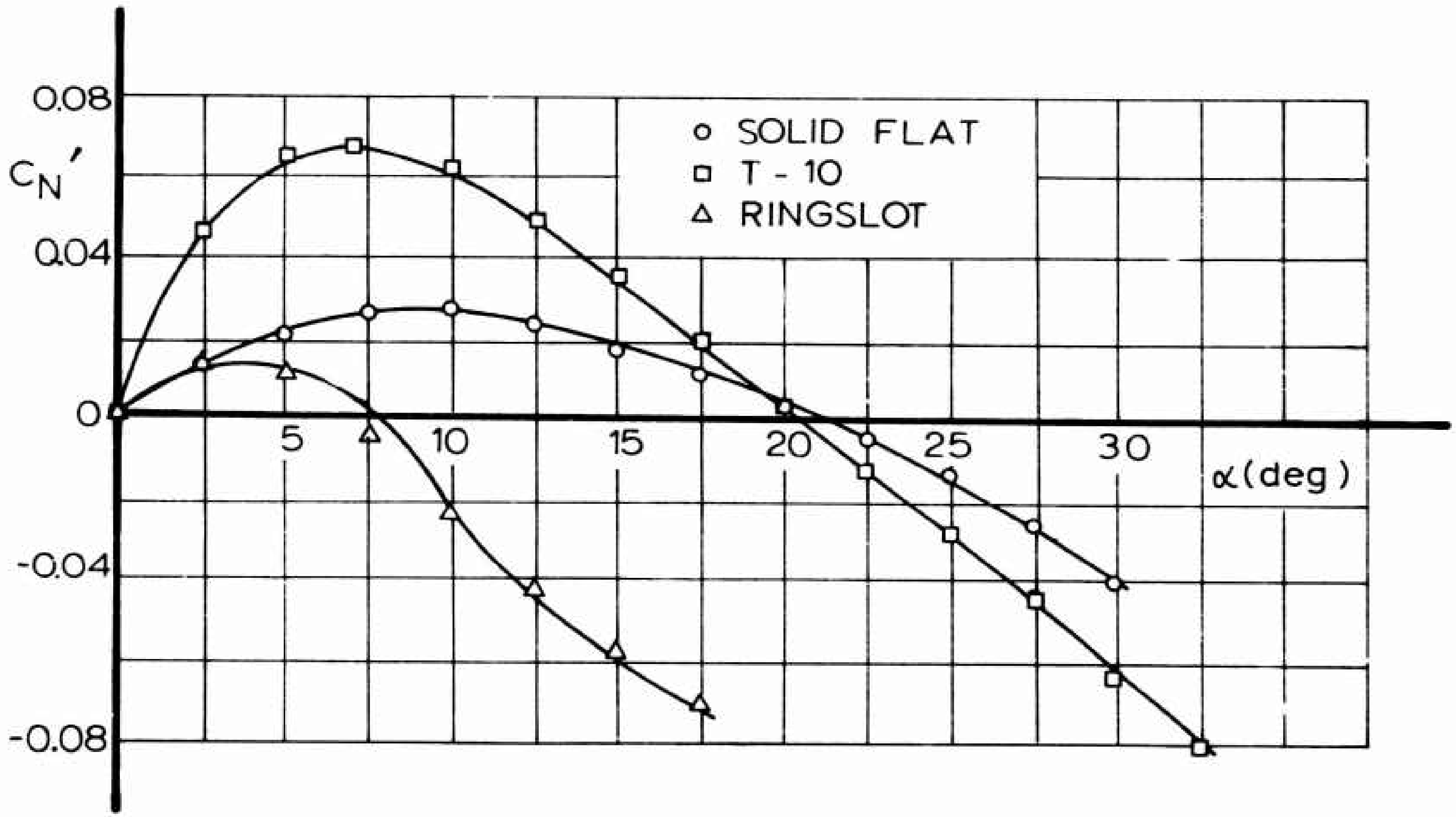

Fig 8 Normal Force Coefficients for the Standard Configurations

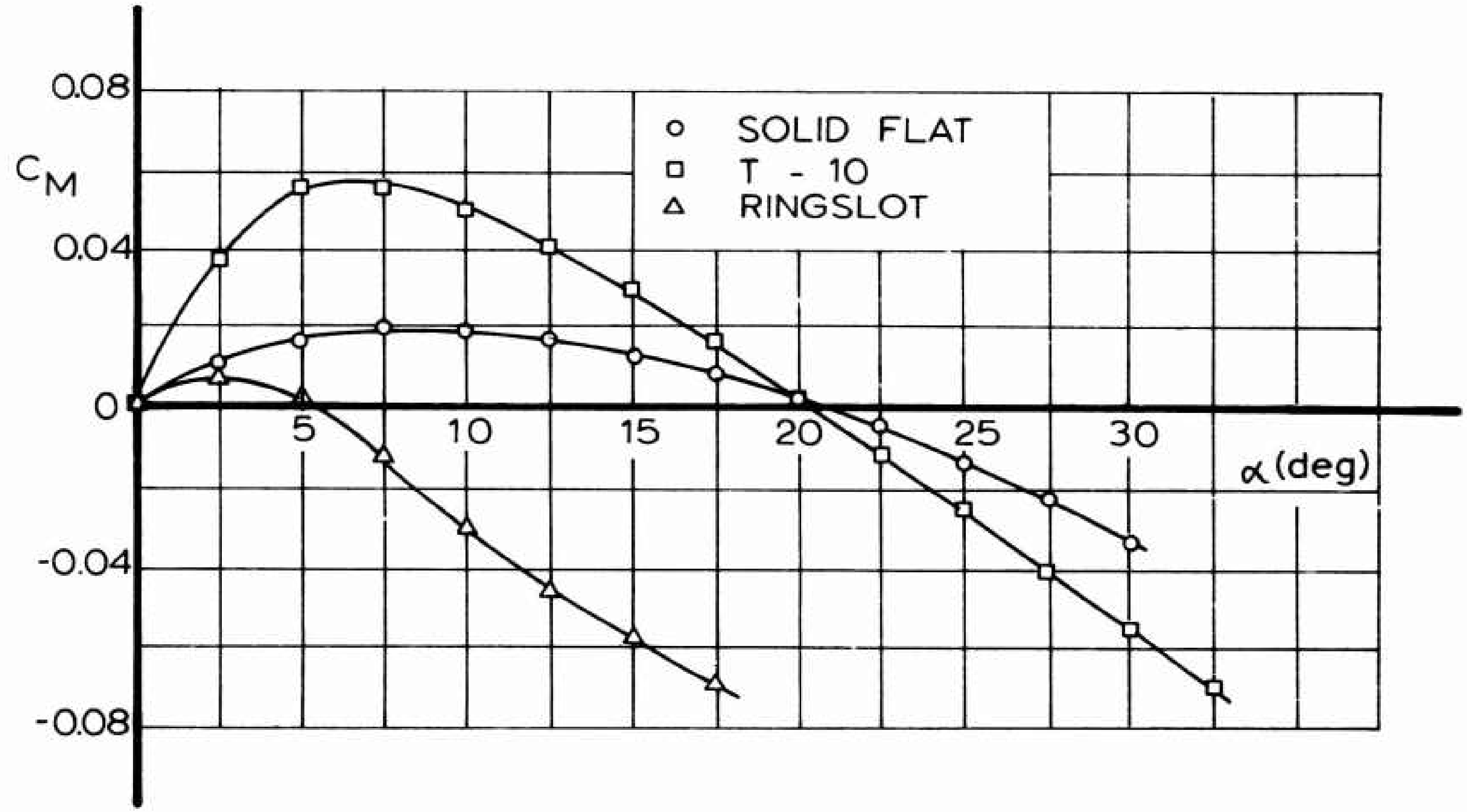

Fig 9 Moment Coefficients for the Standard Configurations

gives a means to compare the standard configurations to other configurations on the basis of L_C. Since the coefficients have been symmetrized, only the positive angles are shown. A tangent force coefficient at a negative angle is equal to that at the same positive angle; normal force and moment coefficients however change sign, the value of C_N and C_M at a negative angle are obtained from the value at the same positive angle by multiplying this value with -1.

The portions of the C_T curves in Fig 7 for the solid flat circular and T-10 parachute models which deviate from the data points indicate the authors' opinion about the values in this section. The deviating data points probably reflect the effect of the violent model vibrations at or near zero angle of attack. The ringslot model did not vibrate in this manner. The tabulated values shown in Table II and in the Appendix are from the curves, whereas the measured data points are shown on the figures in the Appendix. The C_T values at the trim angles, α_T, are results obtained under stable conditions and compare more favorably with values to be expected in full scale drop tests (Ref 3).

None of the three standard configurations was stable at $\alpha = 0$. Consistent with the observed vibrations, the solid flat circular and T-10 models were highly unstable at $\alpha = 0$, while the ringslot was only mildly unstable. The standard configurations achieved stable behavior at trim angles of 20.8^o for the solid flat circular, 20.4^o for the T-10, and 5.6^o for the ringslot. The T-10 had the most stable C_M and the solid flat circular the least stable, with about half the C_{M_α} of the T-10.

No direct comparison of the present results is made with those of Ref 1 because of differences in model construction and design, and force measurements. There are no

fundamental differences between the two, and in general, there is broad agreement of the results. Any differences in the C_T data can be reasonably attributed to increases in drag due to longer suspension lines, decreased porosity, and varying stiffness, but these factors have not been analyzed to the point where a quantitative comparison can be made.

Since confluence point normal forces were not measured in Ref 1, C_N and C_M data cannot be compared. The confluence point normal force results are not presented separately. However, the confluence point force is significant, since the normal forces at the confluence point and at the vent are roughly of the same magnitude, with the confluence point force generally less than the vent force.

C. <u>Configurations with Centerline.</u>

1. Tangent Force Coefficients.

Figures 10, 11, and 12 show the effects of centerlines on the C_T values for the solid flat circular, T-10, and ringslot parachute models respectively. The tangent force coefficient ratios shown in the figures were selected to suitably non-dimensionalize the effect of the centerline. The symbol $C_{T_T}^*$ represents the ratio of the total tangent force coefficient, C_T, of a centerline configuration to the C_T' value at a defined angle of attack. The symbol $C_{T_C}^*$ stands for the ratio of the centerline force coefficient, C_{T_C} to the C_T' value at a defined angle of attack. Thus four groups of data are shown as ratios: C_T and C_{T_C}, both at $\alpha = 0^o$ and at $\alpha = \alpha_T$. To form the $C_{T_T}^*$ and $C_{T_C}^*$ ratios for $\alpha = 0^o$, all values were taken at

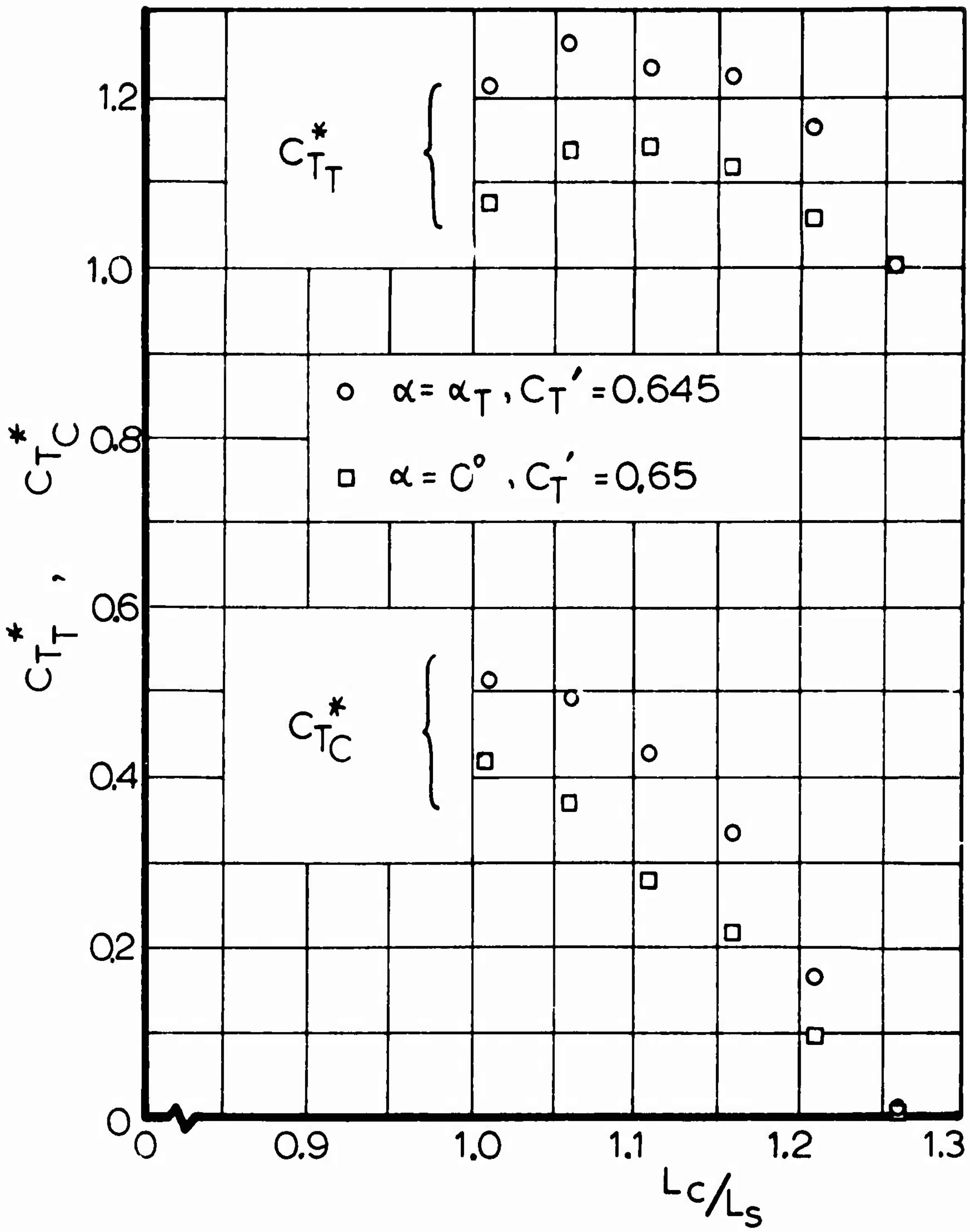

Fig 10 Normalized Tangent Force Coefficients for the Solid Flat Circular Parachute Model

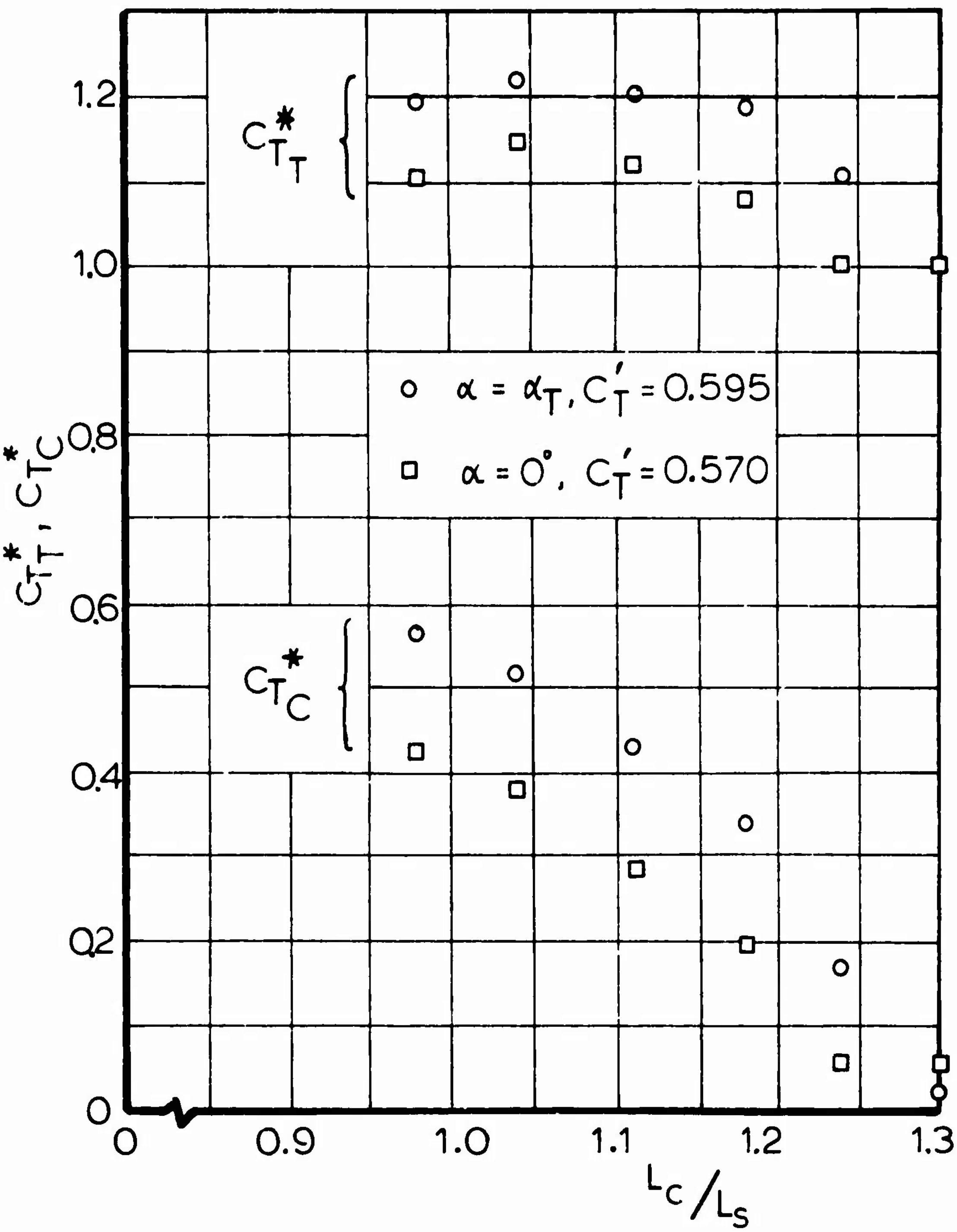

Fig 11 Normalized Tangent Force Coefficients for the T - 10 Parachute Model

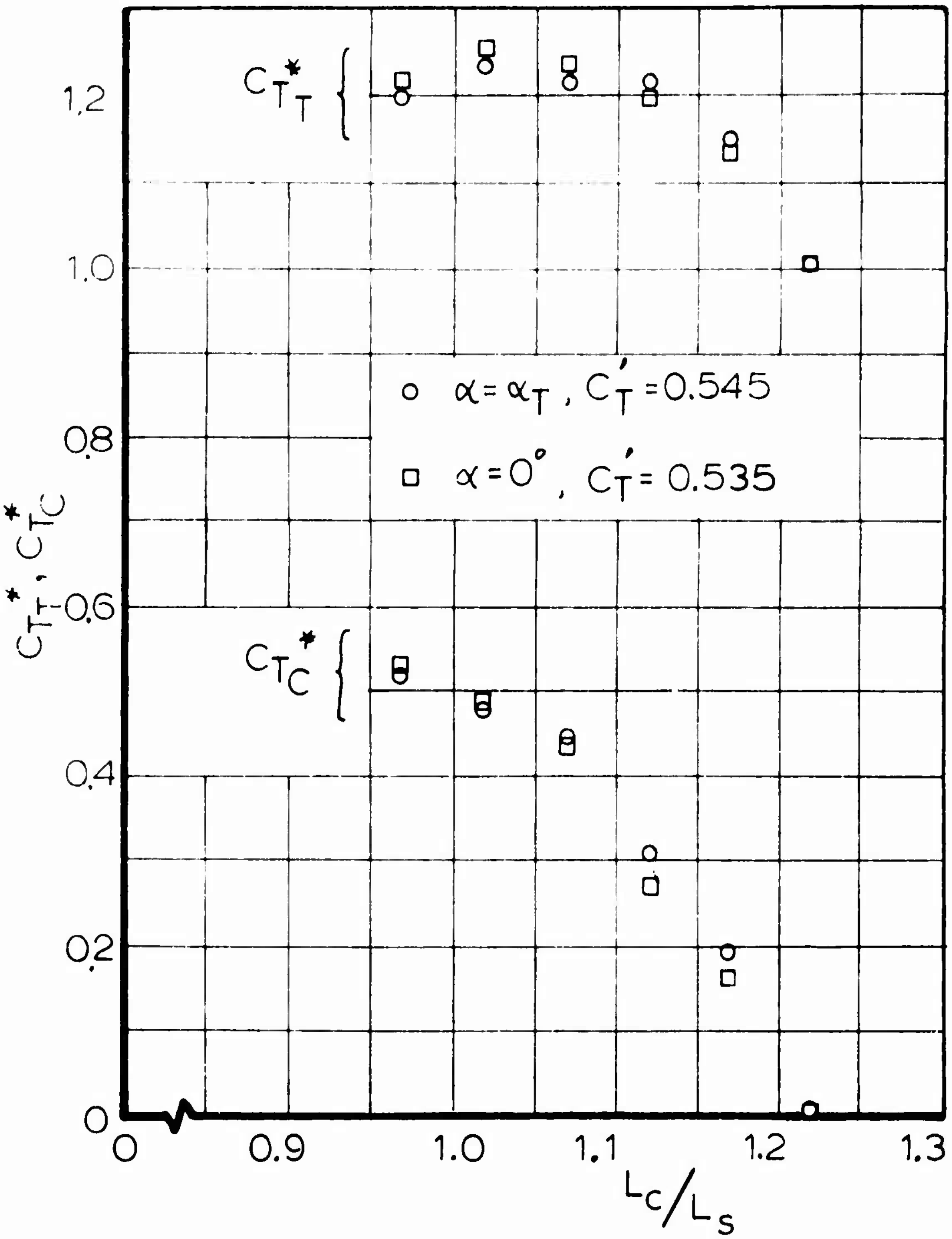

Fig 12 Normalized Tangent Force Coefficients for the Ringslot Parachute Model

$\alpha = 0^{\circ}$; for the ratios at $\alpha = \alpha_T$, values were taken at the α_T of the particular configuration, so the C_T and C_{T_C} values are not from a fixed angle of attack.

The results shown in the figures agree with the previous experience with centerlines, namely substantial increases in drag but with often large forces in the centerline. At the configuration trim angle, the solid flat circular model shows the greatest tangent force increase of 26%, the ringslot next with 23%, and the T-10 with 21%. The solid flat circular and T-10 models have clearly larger increases at the trim angle than at $\alpha = 0^{\circ}$, whereas the ringslot increases are much closer, with the trim angle increases less than those at $\alpha = 0$. This same behavior is seen in the centerline forces, higher percentages of total at trim angle for solid flat circular and T-10 models.

The similarity of the general behavior of the three different models can be seen from these figures. Maximum force increases are obtained with centerline lengths equal to or a few percent longer than the suspension line length. Centerline lengths of less than the suspension line length give tangent force increases less than maximum. The forces in the centerline increase as it is shortened, reaching about half of the total tangent force at a length equal to the suspension line length.

2. Trim Angle and $C^*_{M_\alpha}$

Figures 13, 14, and 15 show the effects of a centerline on the stability of the solid flat circular, T-10, and ringslot parachute models. The upper portions of the figures show the variations in α_T with centerline length. The lower portion shows centerline configuration characteristics again

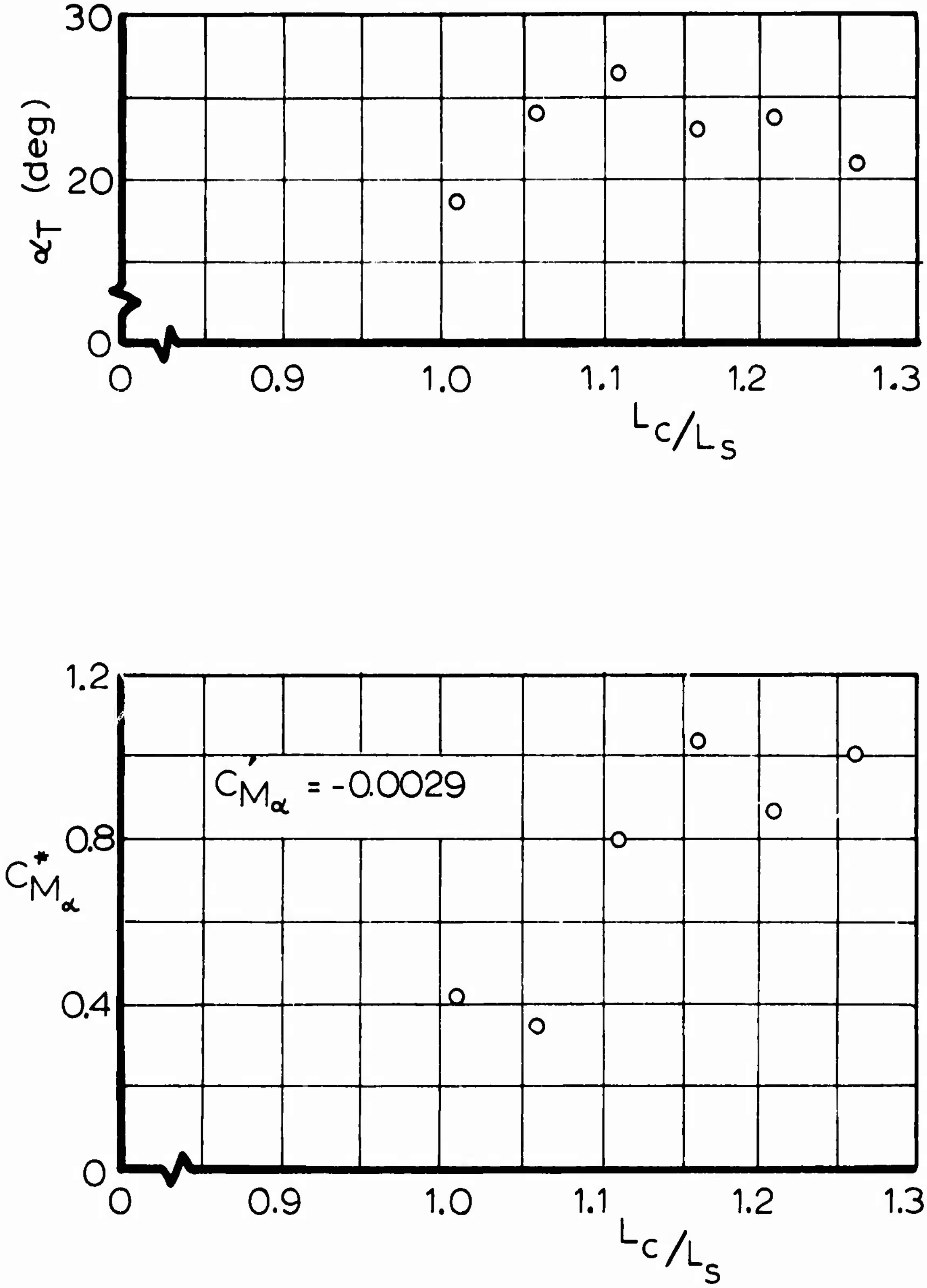

Fig 13 Stability Characteristics of the Solid Flat Circular Parachute Model

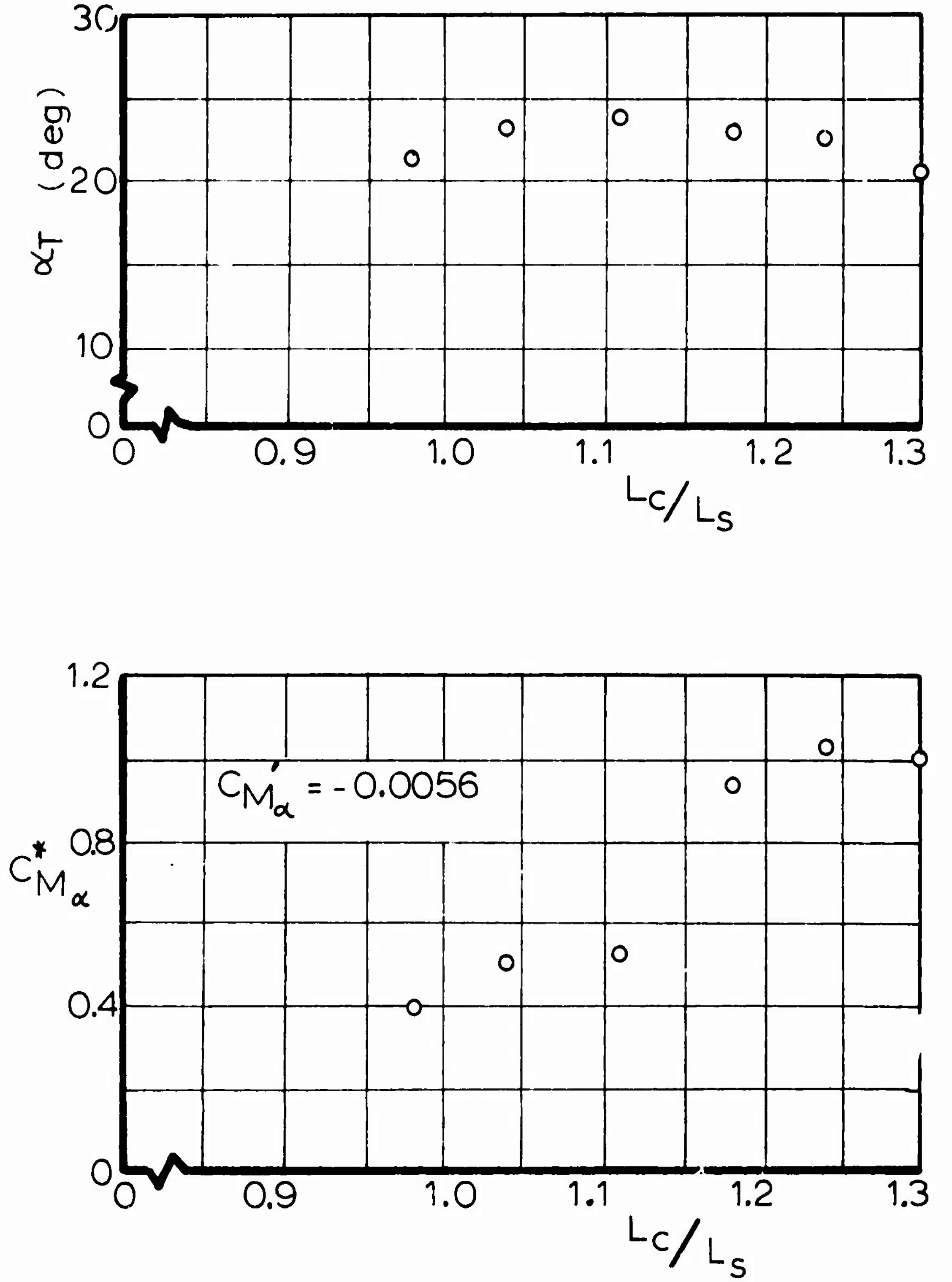

Fig 14 Stability Characteristics of the T-10 Parachute Model

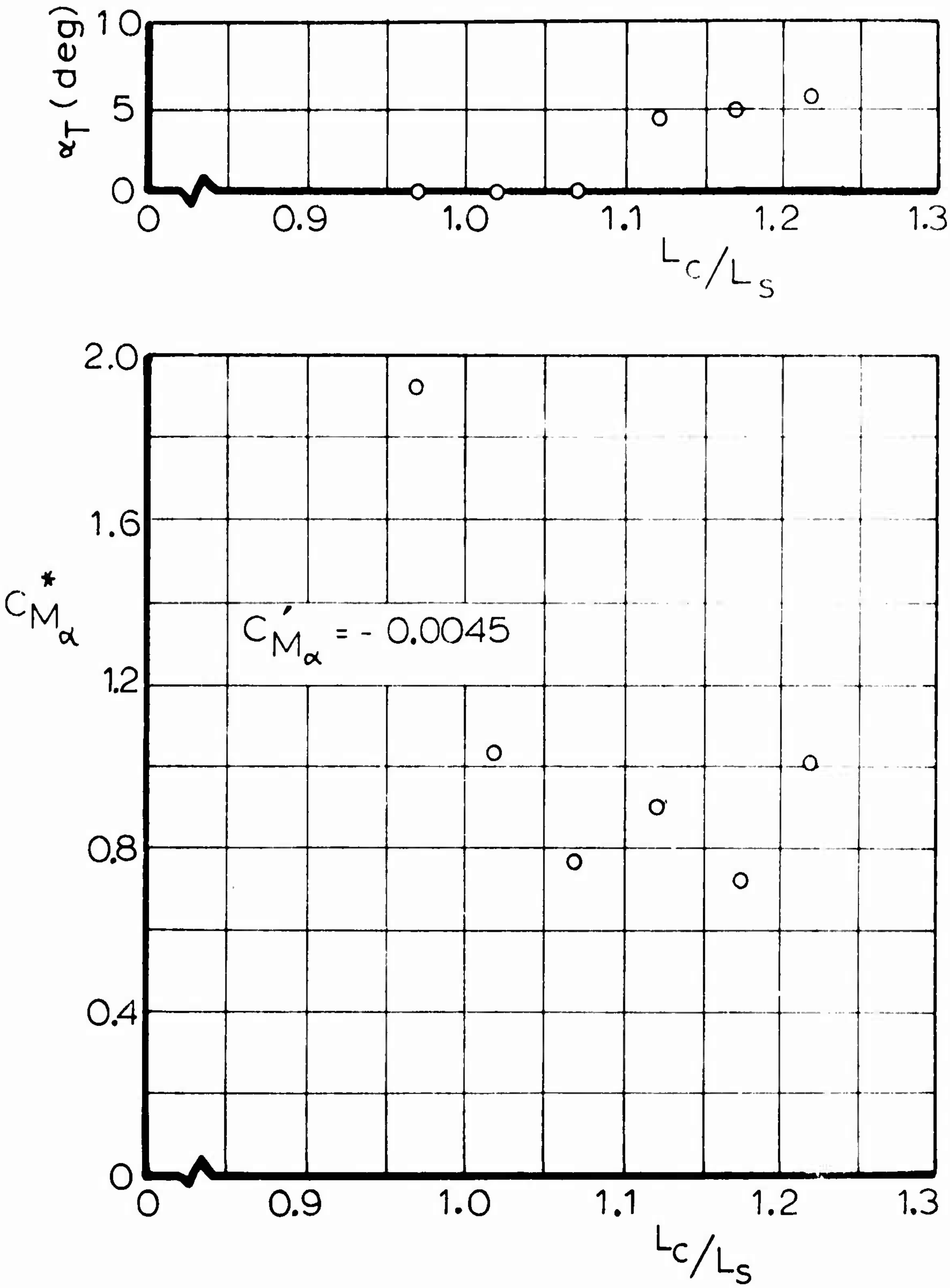

Fig 15 Stability Characteristics of the Ringslot Parachute Model

ratioed to standard configurations. The quantities ratioed in these figures are the slopes of the moment coefficient curves, $C_{M\alpha}$, at the trim angle. Thus $C_{M\alpha}^{*}$ is the ratio of the slope of the moment curve at α_T for a centerline configuration to $C_{M\alpha}'$ at α_T. The determination of these characteristics is difficult since they are functions of exactly where and how the moment curve is drawn. Thus a certain amount of scatter in the data points is unavoidable, and basic trends should get primary attention.

The solid flat circular and T-10 models show an initial increase in α_T and then a decrease as the centerline is shortened, with the magnitude of change less on the T-10 than the solid flat circular. The ringslot shows first a very small decrease in α_T and then a change to $\alpha_T = 0^o$ for centerlines of $L_C/L_S < 1.1$.

In the stability slope ratios $C_{M\alpha}^{*}$ results, the solid flat circular and T-10 models both show strong decreases in slope at the shorter centerline lengths. At centerline lengths of $L_C/L_S > 1.1$ the data scatter makes it difficult to differentiate between a mild decrease or little change. The stability behavior of the ringslot model was markedly different from the other two models. The ringslot $C_{M\alpha}^{*}$ decreases slightly as the centerline is shortened, but then the slope ratio increases with further shortening up to 1.9 for a centerline length of 0.9, L_S.

VI. SUMMARY

The aerodynamic force coefficients for solid flat circular, T-10, and ringslot parachute models with centerlines were measured. The design of the wind tunnel balance and the related equipment was complicated by the requirements of measuring normal forces at the confluence point and preserving model geometry. Measurements with the satisfactory wind tunnel apparatus showed that a suspension line confluence point had to be formed, axial sting sizes had to be less than 3% of the nominal diameter, and that the confluence point normal forces were significant, being about the same magnitude as the vent normal forces.

General similarities in the effects of a centerline on the various models were found. Tangent force increases of 20% to 26% can be obtained at centerline lengths equal to or a few percent longer than the suspension line length. At this centerline length, the force in the centerline was approximately one-half of the total tangent force of the configuration. The stability behavior of the models varied with the length of the centerline. For the solid flat and T-10 parachute models at the centerline lengths which provided the greatest tangent force increase, the angle of trim increased slightly while the slope $C_{M\alpha}$ decreased. This may be considered to be a general decrease in stability. For the ringslot parachute the two longest centerlines reduced the trim angle slightly, whereas the three shorter lines gave trim angles of zero degrees. The effort of the four longer centerlines upon the stability slope is relatively small, however the centerline with $L_C/L_S = 0.97$ provided a stability slope 1.9 times the slope of the standard configuration.

REFERENCES

1. Heinrich, H. G., Haak, E. L., Stability and Drag of Parachutes With Varying Effective Porosity, AFFDL-TR-71-58, February 1971.

2. Heinrich, H. G., Hektner, T. R., Flexibility as Parameter of Model Parachute Performance, AFFDL-TR-70-53, August 1970.

3. Performance of and Design Criteria for Deployable Aerodynamic Decelerators, ASD-TR-61-579 December 1963, AD 429 971.

APPENDIX

This appendix contains the complete coefficient results in graphs and tables. Least squares polynomial curve fits are shown on the graphs for the standard configurations.

TABLE III

AERODYNAMIC COEFFICIENTS FOR THE SOLID FLAT CIRCULAR PARACHUTE MODEL WITH L_C/L_S = 1.26 (STANDARD CONFIGURATION)

α^{o}	C_T	C_{T_C}	C_N	C_M
0*	.65	0.0	0.0	0.0
2.5*	.65	0.0	.013	.010
5.0*	.66	.001	.020	.015
7.5*	.67	.001	.026	.019
10.0	.69	.002	.026	.018
12.5	.69	.002	.023	.016
15.0	.68	.002	.017	.012
17.5	.66	.002	.011	.008
20.0	.65	.003	.003	.002
22.5	.64	.003	-.005	-.005
25.0	.63	.003	-.014	-.014
27.5	.62	.003	-.027	-.023
30.0	.62	.004	-.041	-.034

* Values From Curves

TABLE IV

AERODYNAMIC COEFFICIENTS FOR THE SOLID FLAT CIRCULAR PARACHUTE MODEL WITH $L_C/L_S = 1.21$

α°	C_T	C_{T_C}	C_N	C_M
0*	.69	.06	0.0	0.0
2.5*	.70	.07	.014	.010
5.0*	.71	.09	.022	.015
7.5*	.75	.10	.023	.019
10.0	.75	.11	.029	.019
12.5	.76	.12	.027	.018
15.0	.76	.12	.023	.016
17.5	.76	.12	.018	.012
20.0	.76	.12	.012	.007
22.5	.73	.11	.007	.003
25.0	.71	.10	-.004	-.003
27.5	.69	.10	-.015	-.012
30.0	.69	.10	-.028	-.022

* Values From Curves

TABLE V

AERODYNAMIC COEFFICIENTS FOR THE SOLID FLAT CIRCULAR PARACHUTE MODEL WITH $L_C/L_S = 1.16$

$\alpha°$	C_T	C_{T_C}	C_N	C_M
0*	.73	.14	0.0	0.0
2.5*	.73	.15	.018	.012
5.0*	.74	.17	.029	.019
7.5*	.76	.19	.034	.022
10.0	.78	.20	.035	.022
12.5	.79	.20	.033	.021
15.0	.80	.21	.030	.018
17.5	.80	.21	.026	.015
20.0	.80	.21	.016	.008
22.5	.79	.21	.005	.001
25.0	.77	.21	-.003	-.006
27.5	.75	.20	-.015	-.015
30.0	.74	.20	-.027	-.025

* Values From Curves

TABLE VI

AERODYNAMIC COEFFICIENTS FOR THE SOLID FLAT CIRCULAR PARACHUTE MODEL WITH $L_C/L_S = 1.11$

α^o	C_T	C_{T_C}	C_N	C_M
0*	.74	.18	0.0	0.0
2.5*	.75	.19	.010	.006
5.0*	.76	.21	.016	.010
7.5*	.78	.24	.020	.014
10.0	.80	.27	.022	.014
12.5	.81	.28	.025	.014
15.0	.82	.28	.025	.014
17.5	.82	.28	.023	.012
20.0	.82	.28	.020	.010
22.5	.82	.28	.016	.007
25.0	.81	.28	.011	.004
27.5	.78	.26	-.001	-.004
30.0	.76	.25	-.010	-.008

* Values From Curves

TABLE VII

AERODYNAMIC COEFFICIENTS FOR THE SOLID FLAT CIRCULAR PARACHUTE MODEL WITH $L_C/L_S = 1.06$

$\alpha°$	C_T	C_{T_C}	C_N	C_M
0*	.74	.24	0.0	0.0
2.5*	.75	.24	.011	.005
5.0*	.76	.26	.018	.009
7.5*	.78	.29	.021	.009
10.0	.80	.30	.022	.009
12.5	.81	.30	.023	.009
15.0	.81	.31	.022	.008
17.5	.82	.31	.019	.006
20.0	.82	.31	.016	.004
22.5	.82	.31	.012	.001
25.0	.81	.32	.006	-.001
27.5	.80	.31	-.001	-.004
30.0	.76	.30	-.007	-.007

* Values From Curves

TABLE VIII

AERODYNAMIC COEFFICIENTS FOR THE SOLID FLAT CIRCULAR PARACHUTE MODEL WITH $L_C/L_S = 1.01$

$\alpha°$	C_T	C_{T_C}	C_N	C_M
0*	.70	.27	0.0	0.0
2.5*	.71	.27	.006	0.0
5.0*	.72	.29	.009	0.0
7.5*	.75	.31	.010	.001
10.0	.76	.32	.012	.003
12.5	.77	.32	.012	.003
15.0	.77	.33	.011	.003
17.5	.78	.33	.007	.001
20.0	.78	.33	.002	-.002
22.5	.78	.33	-.003	-.006
25.0	.78	.33	-.010	-.011
27.5	.77	.33	-.018	-.018
30.0	.77	.31	-.028	-.025

* Values From Curves

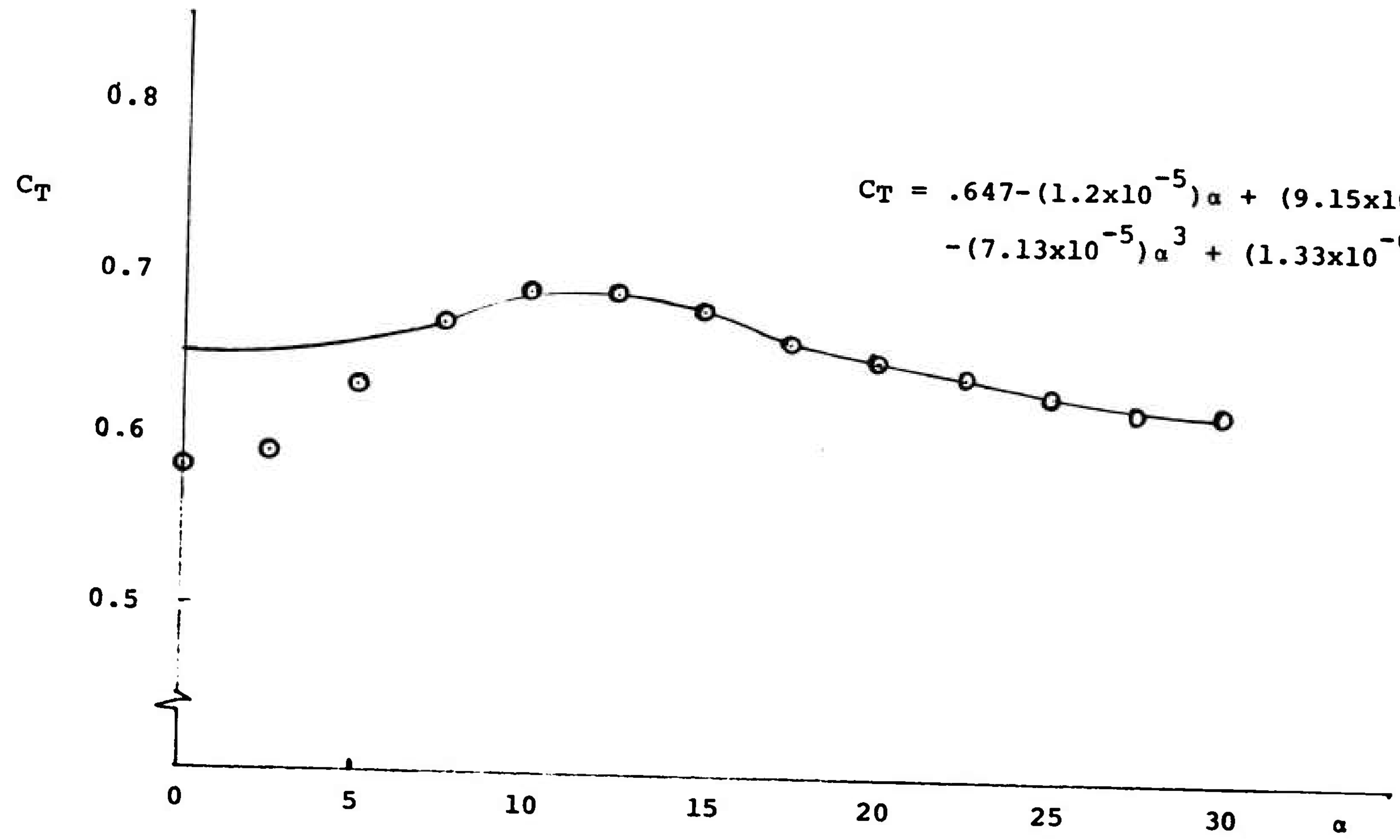

FIG. 16 C_T VALUES FOR THE SOLID FLAT CIRCULAR PARACHUTE MODEL AT $L_C/L_S = 1.26$ (STANDARD CONFIGURATION)

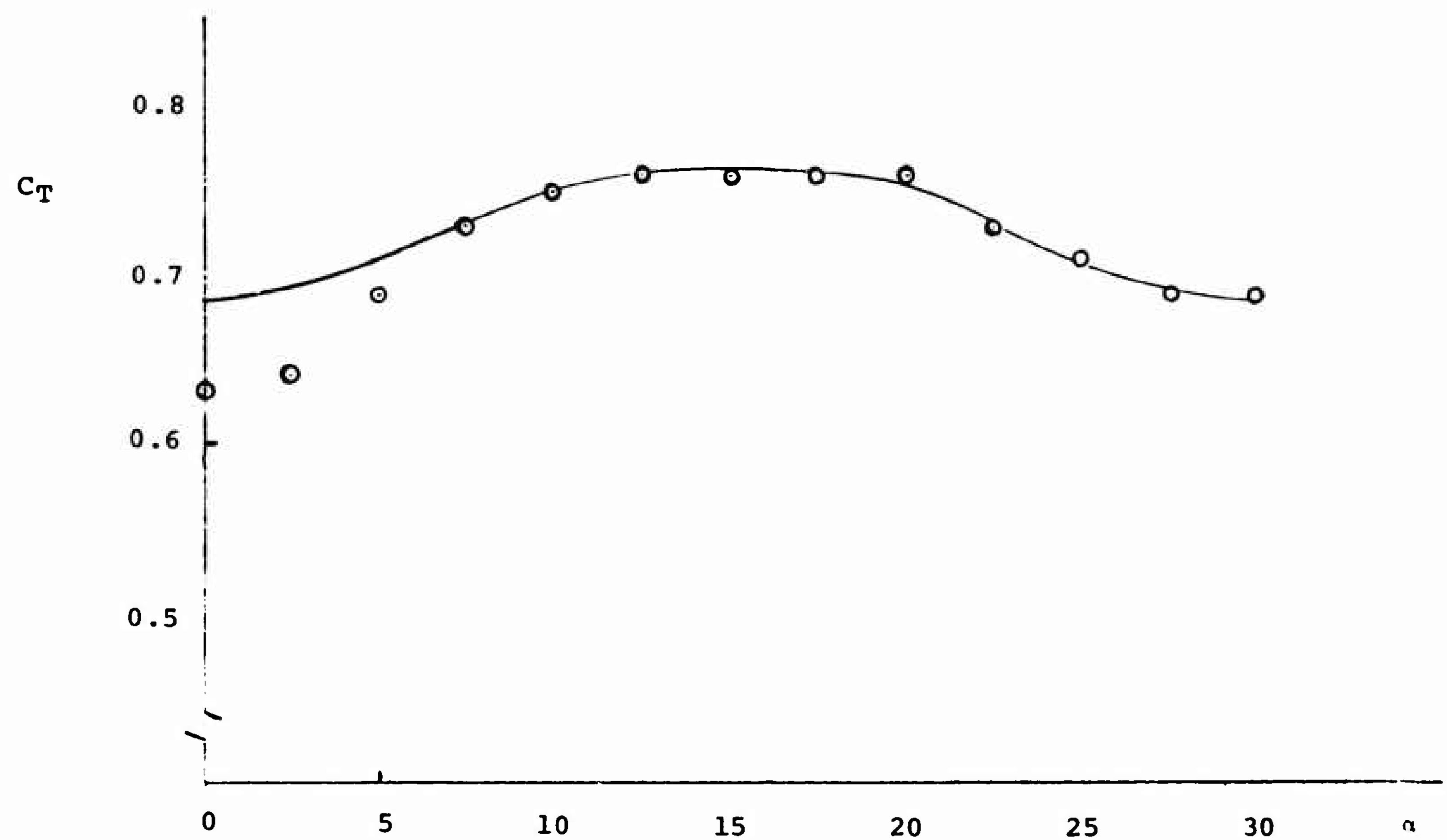

FIG. 17 C_T VALUES FOR THE SOLID FLAT CIRCULAR PARACHUTE MODEL AT $L_c/L_s = 1.21$

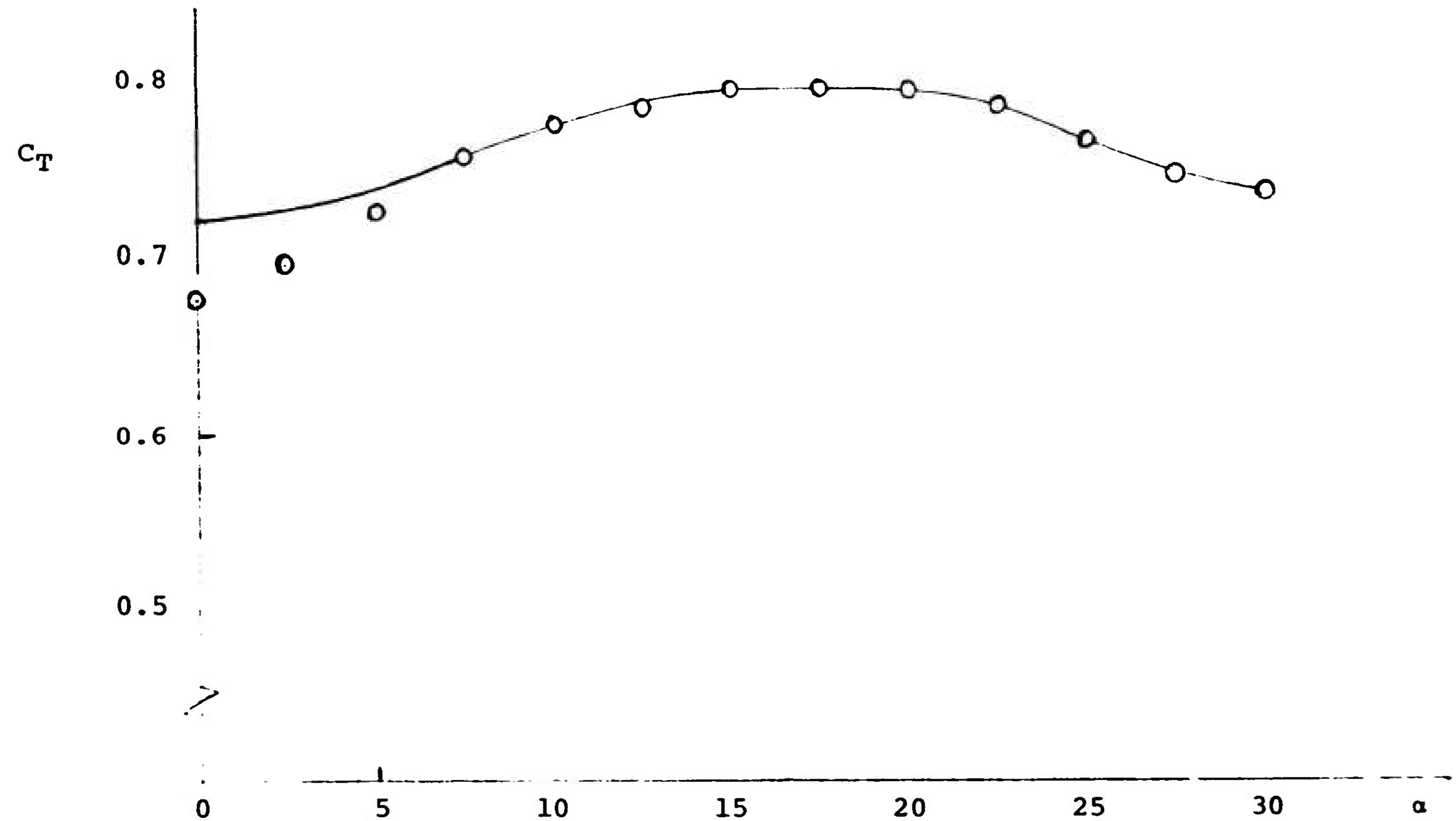

FIG. 18 C_T VALUES FOR THE SOLID FLAT CIRCULAR PARACHUTE MODEL AT L_C/L_S = 1.16

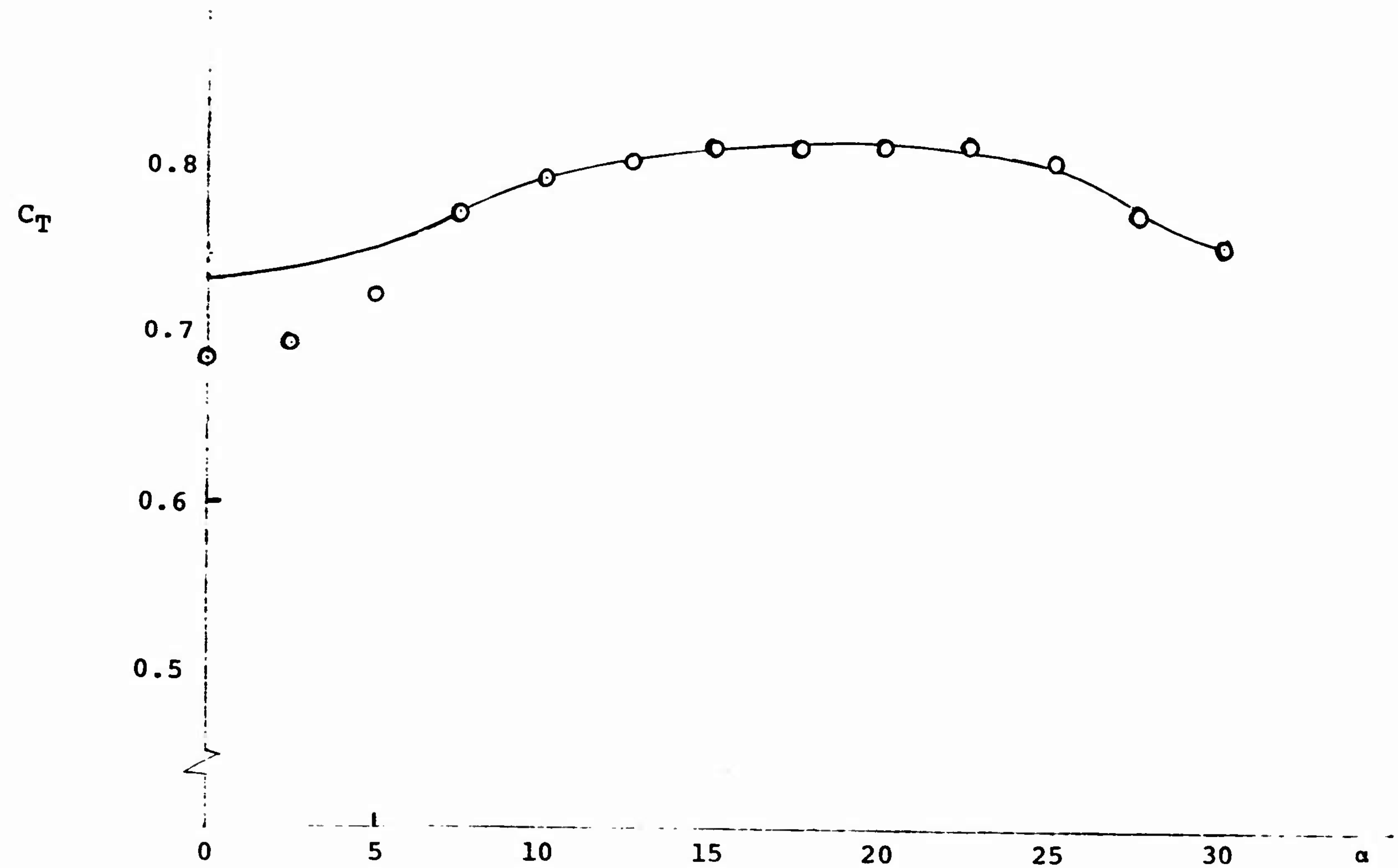

FIG. 19 C_T VALUES FOR THE SOLID FLAT CIRCULAR PARACHUTE MODEL AT L_C/L_S = 1.11

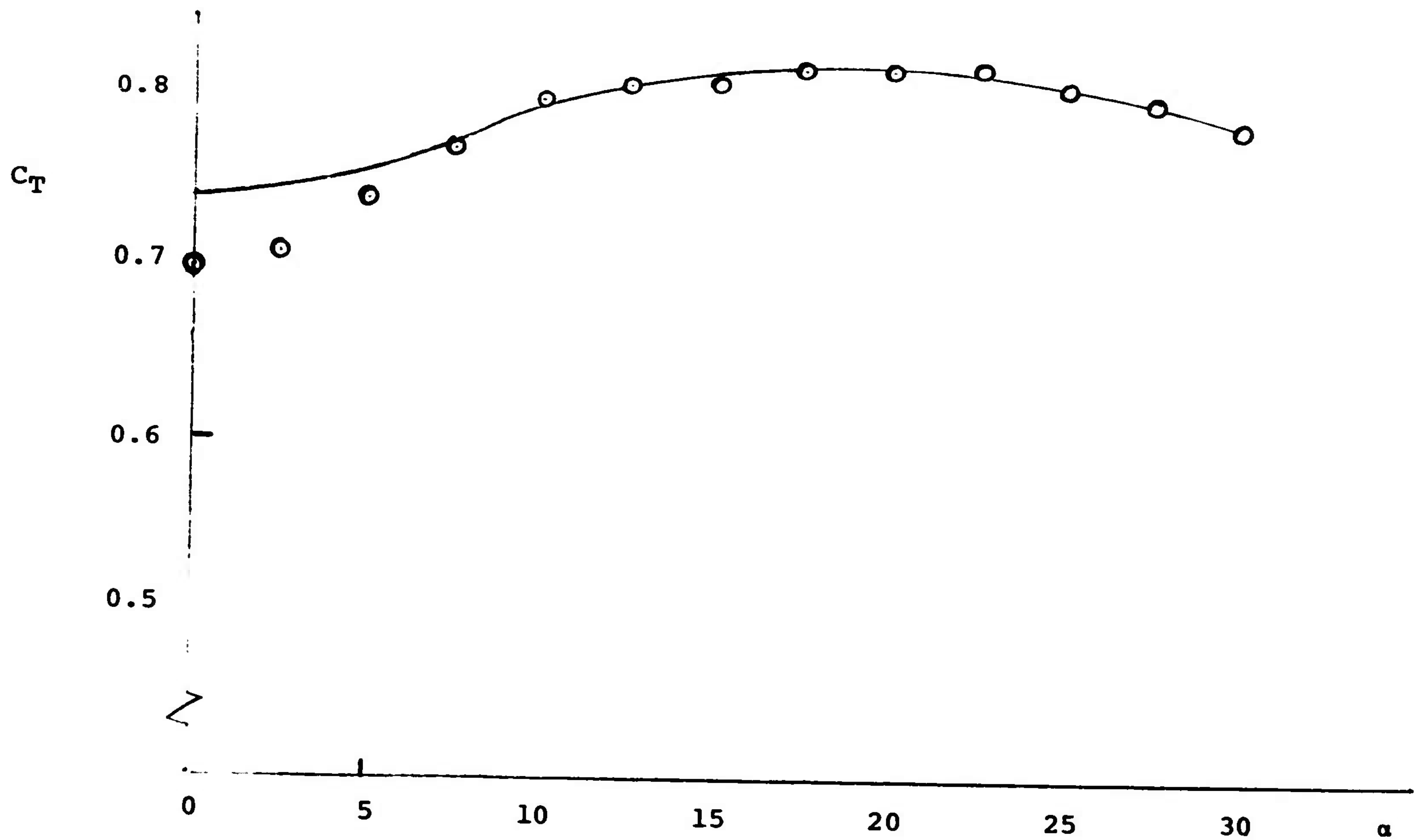

FIG. 20 C_T VALUES FOR THE SOLID FLAT CIRCULAR PARACHUTE MODEL AT $L_C/L_S = 1.06$

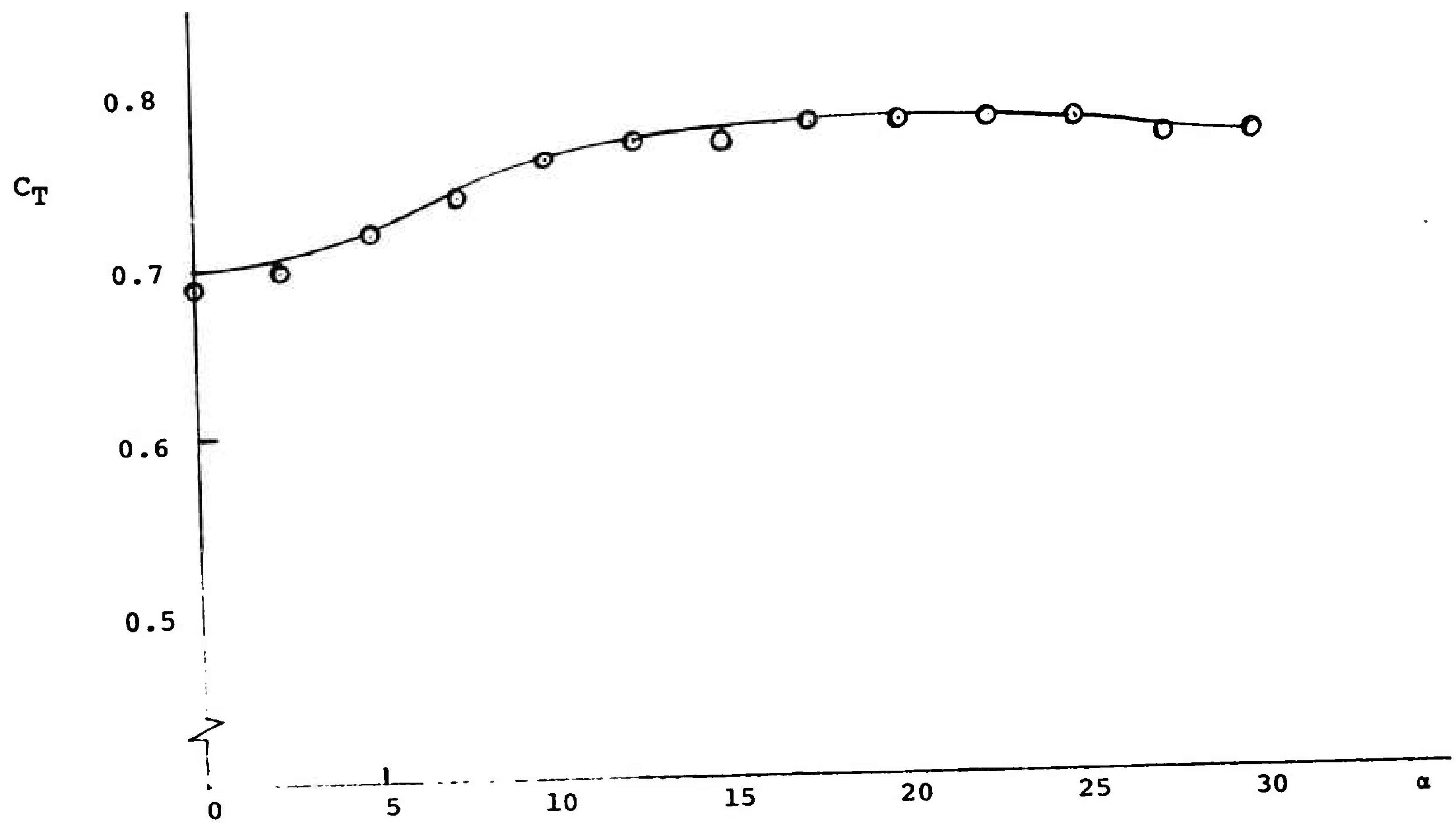

FIG. 21 C_T VALUES FOR THE SOLID FLAT CIRCULAR PARACHUTE MODEL AT $L_c/L_s = 1.01$

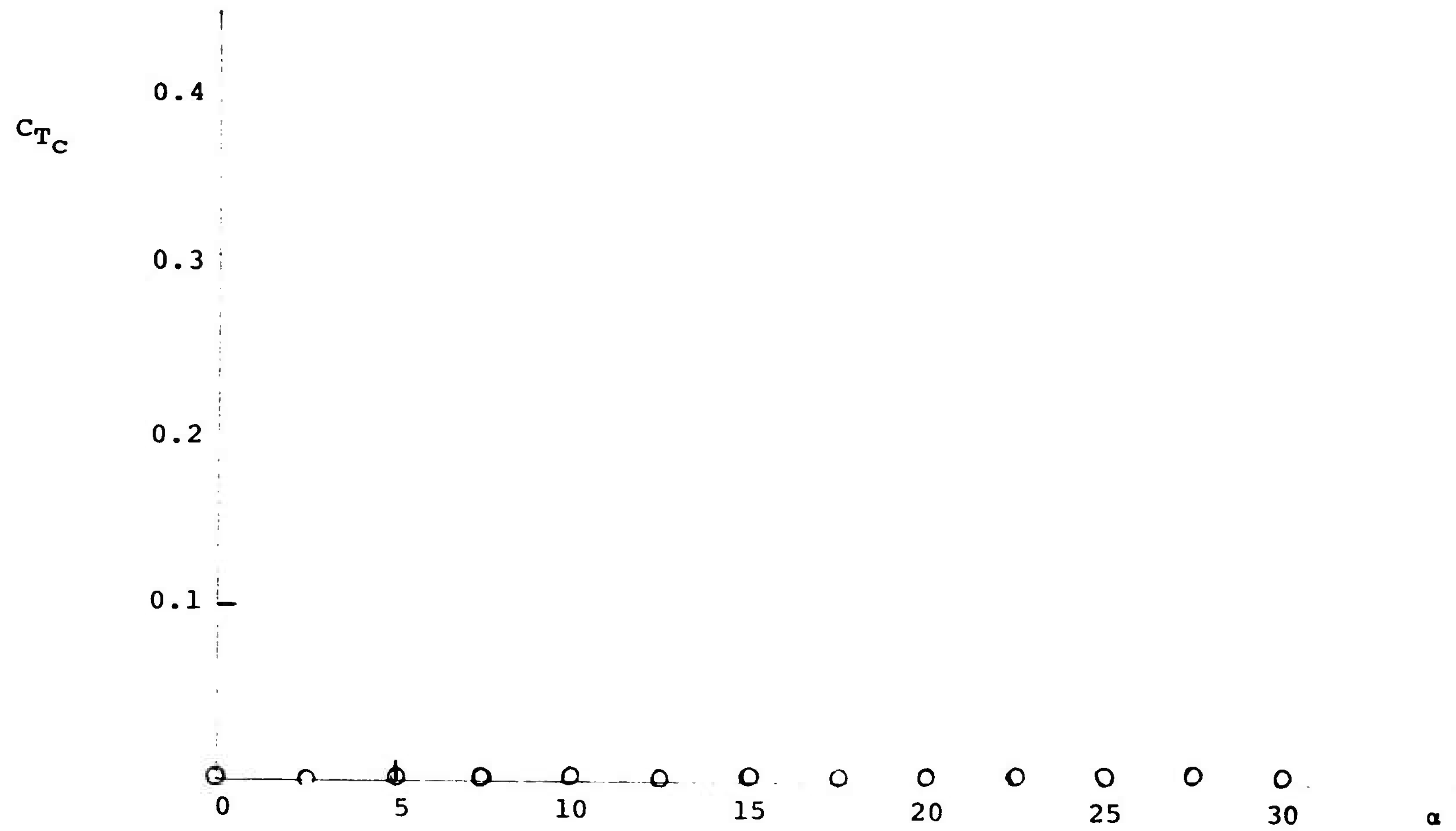

FIG. 22 C_{T_C} VALUES FOR THE SOLID FLAT CIRCULAR PARACHUTE MODEL AT L_C/L_S = 1.26 (STANDARD CONFIGURATION)

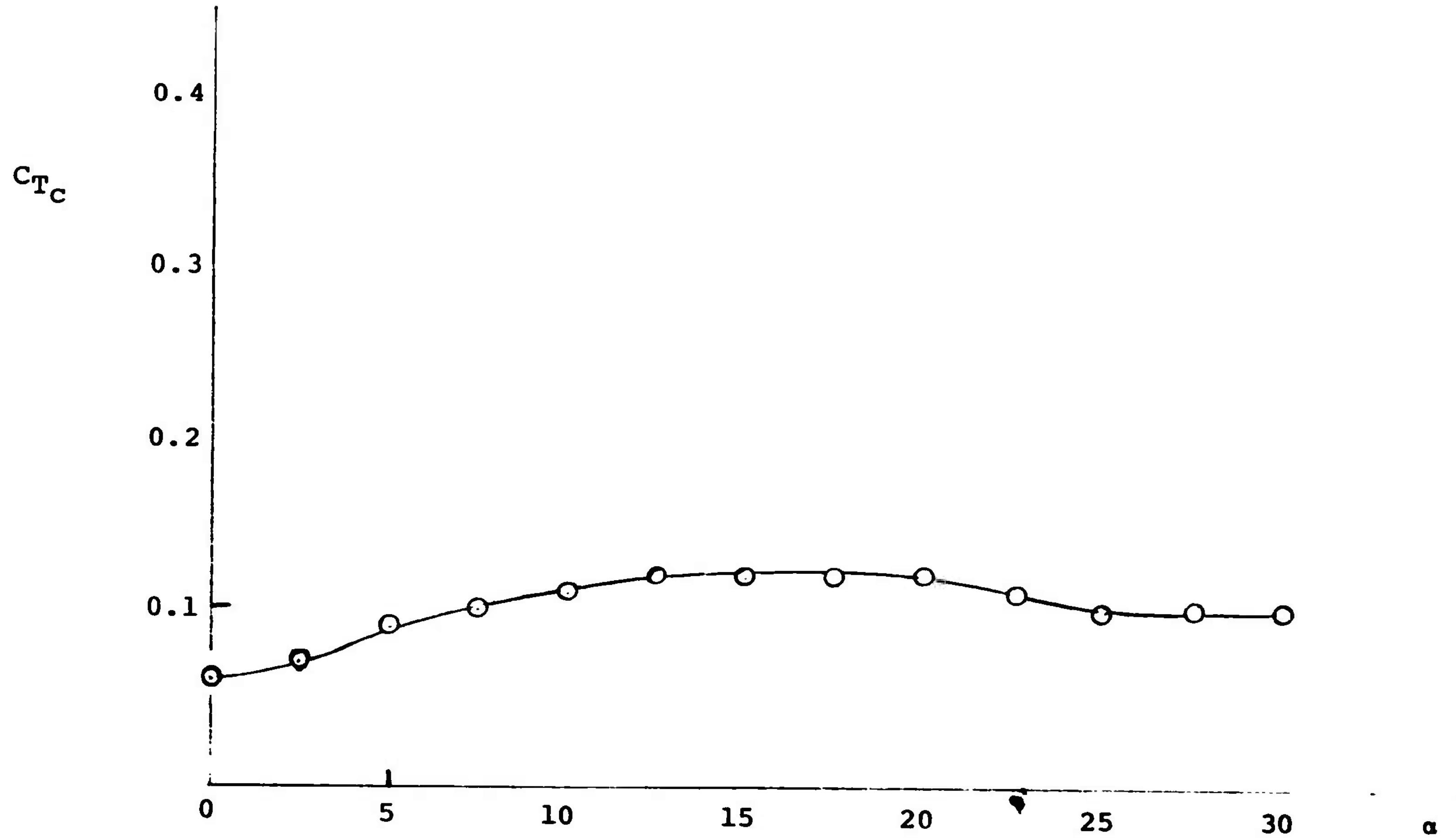

FIG. 23 C_{T_C} VALUES FOR THE SOLID FLAT CIRCULAR PARACHUTE MODEL AT $L_C/L_S = 1.21$

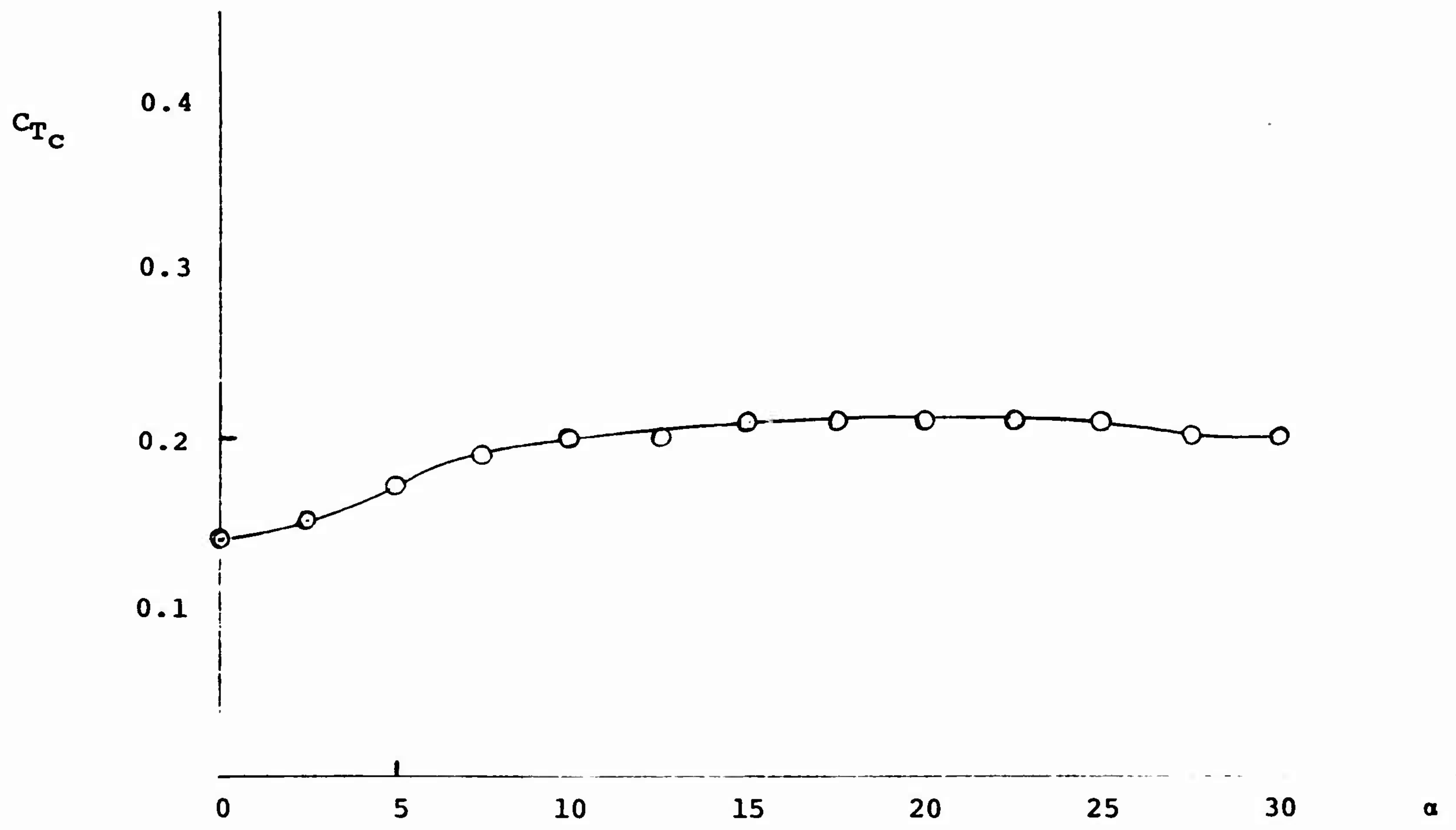

FIG. 24 C_{T_C} VALUES FOR THE SOLID FLAT CIRCULAR PARACHUTE MODEL AT $L_C/L_S = 1.16$

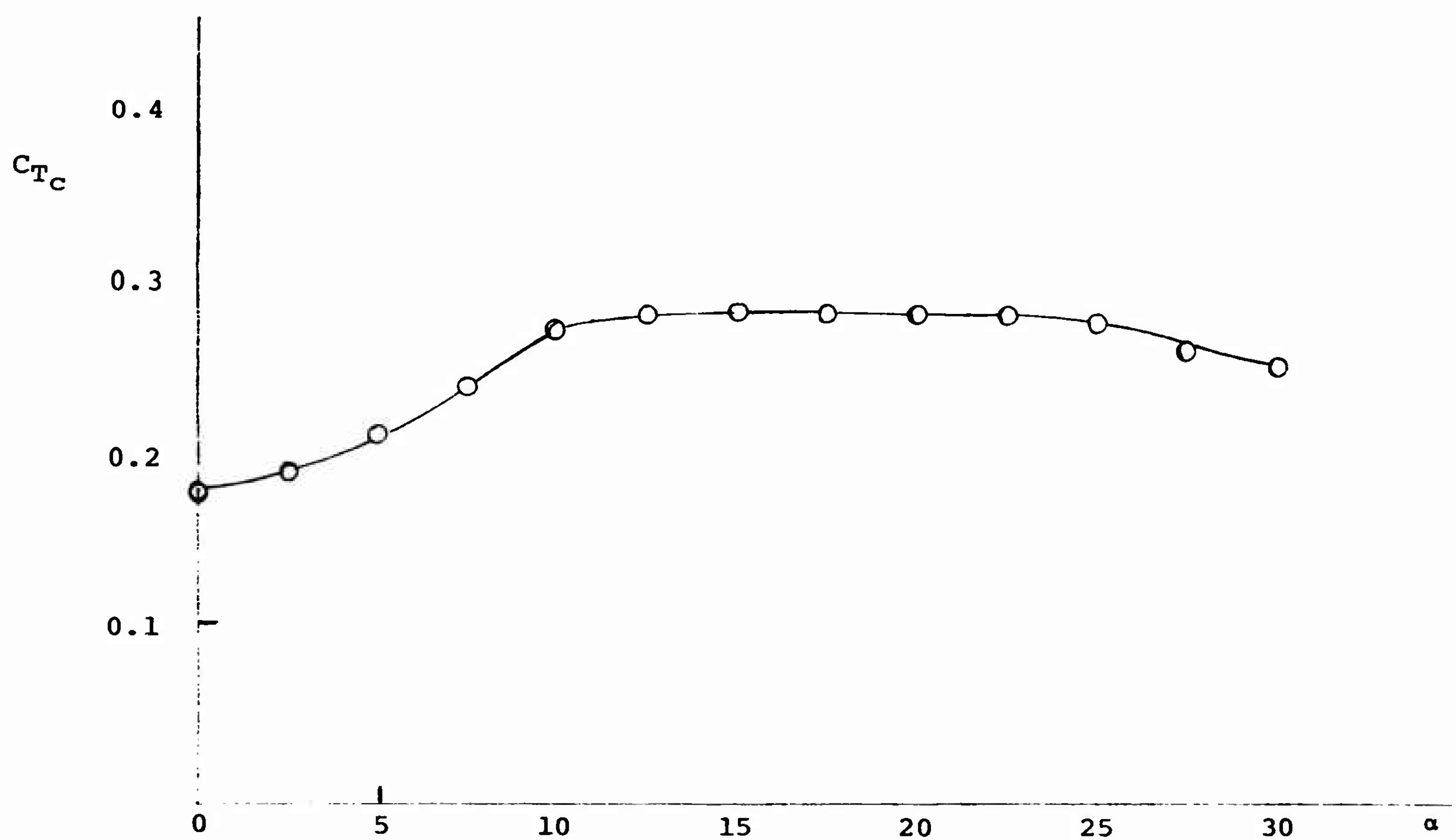

FIG. 25 C_{T_C} VALUES FOR THE SOLID FLAT CIRCULAR PARACHUTE MODEL AT $L_C/L_S = 1.11$

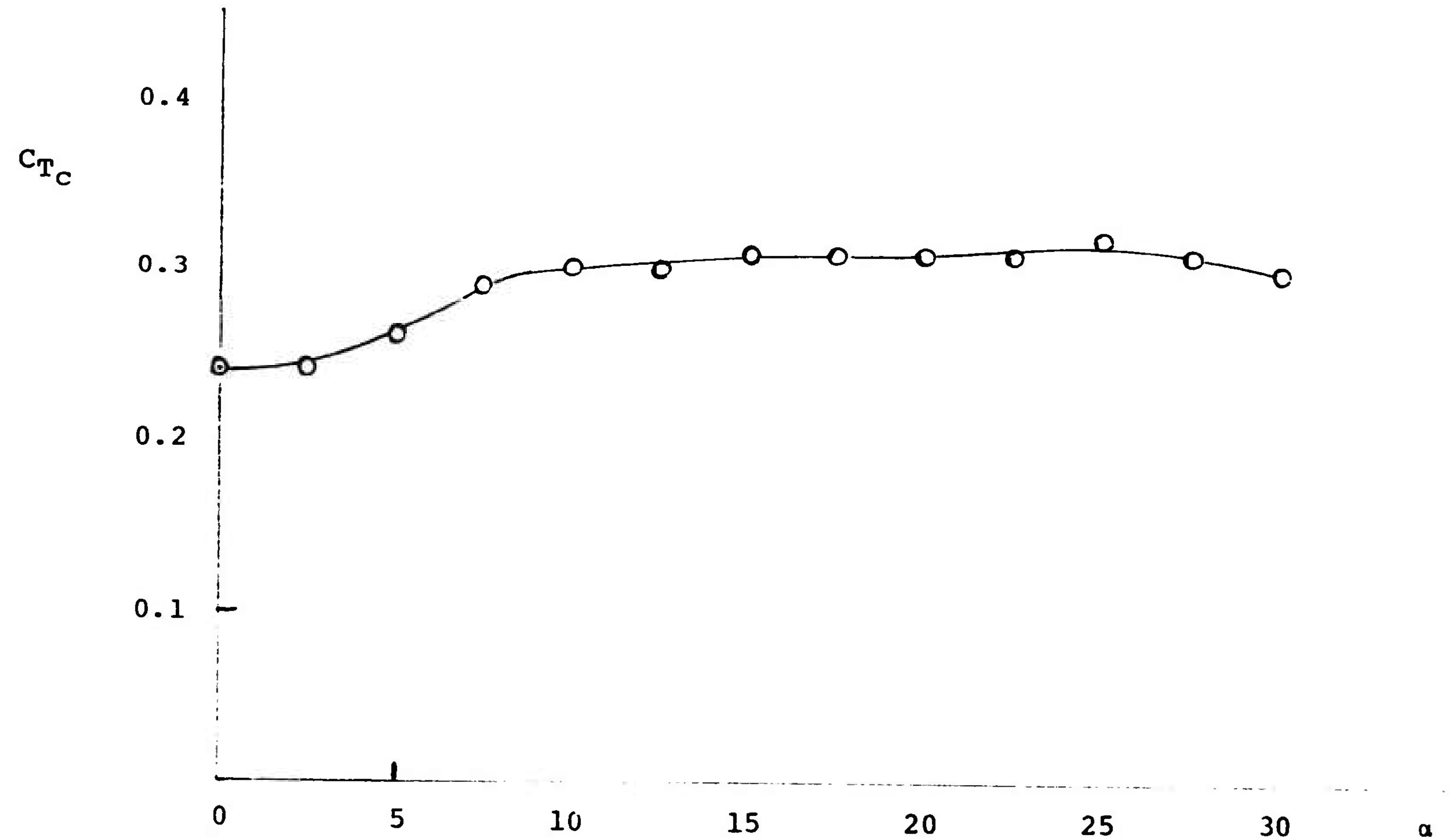

FIG. 26 C_{T_C} VALUES FOR THE SOLID FLAT CIRCULAR PARACHUTE MODEL AT $L_C/L_S = 1.06$

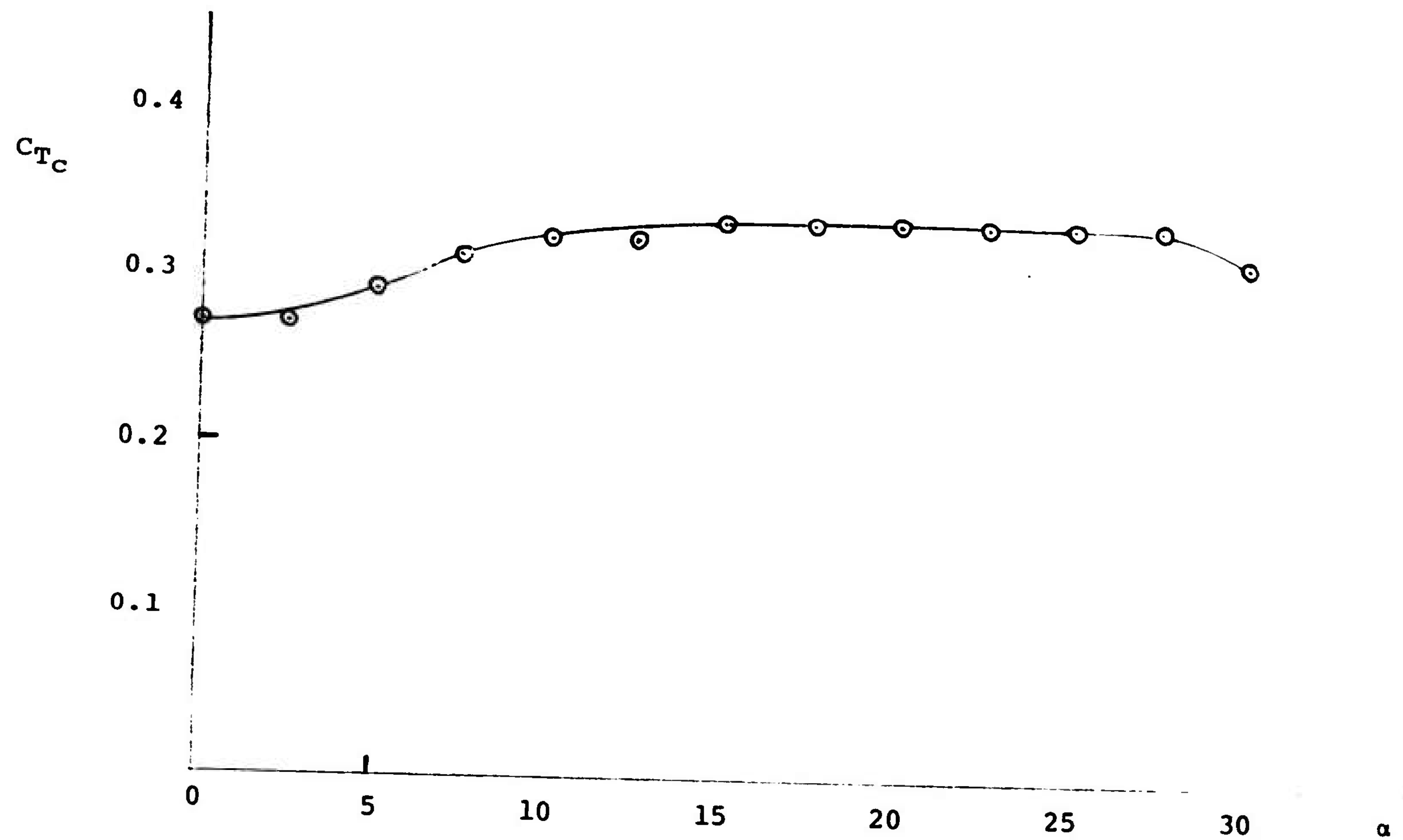

FIG. 27 C_{T_C} VALUES FOR THE SOLID FLAT CIRCULAR PARACHUTE MODEL AT L_C/L_S = 1.01

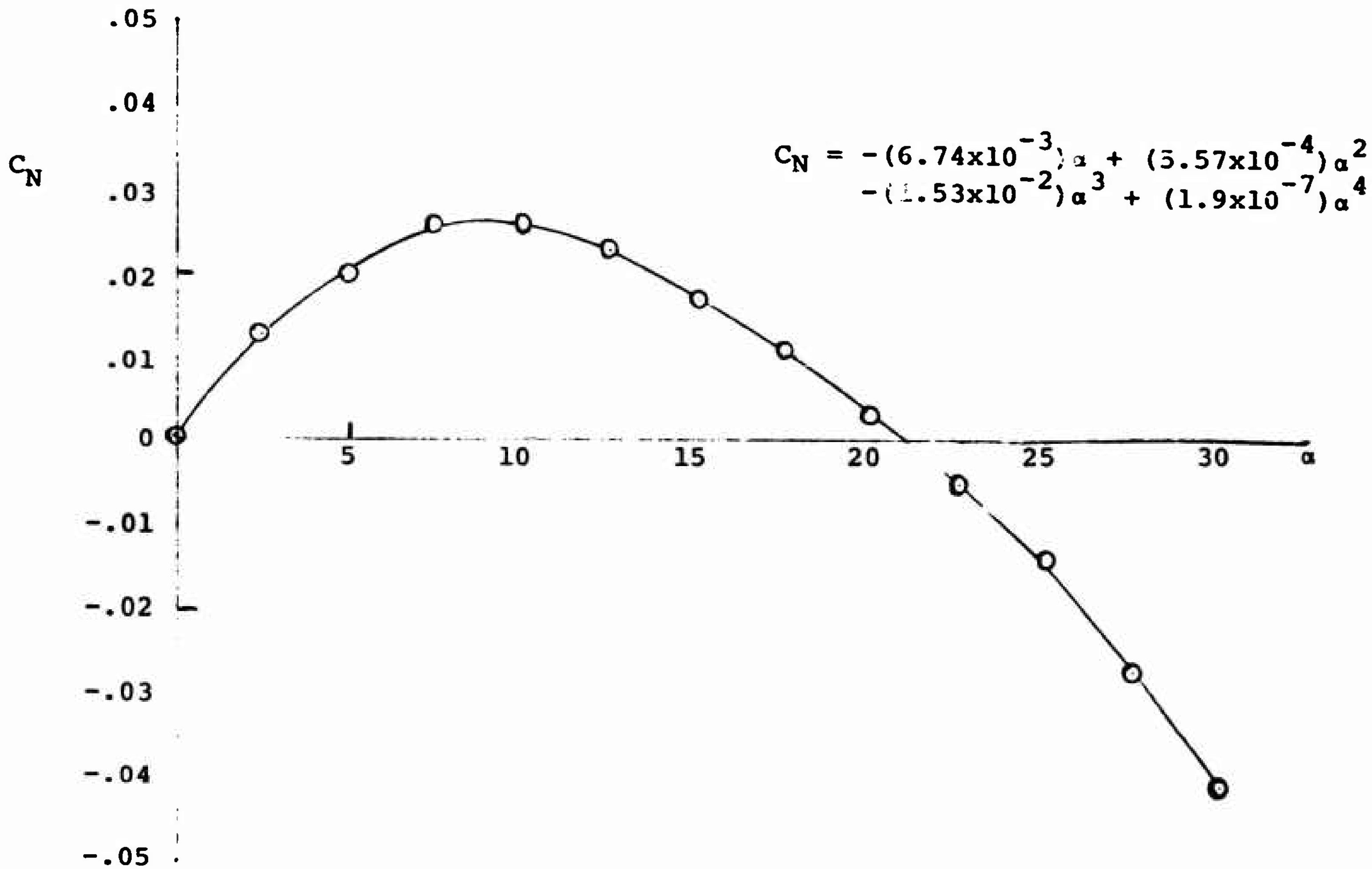

FIG. 28 C_N VALUES FOR THE SOLID FLAT CIRCULAR PARACHUTE MODEL AT L_C/L_S = 1.26 (STANDARD CONFIGURATION)

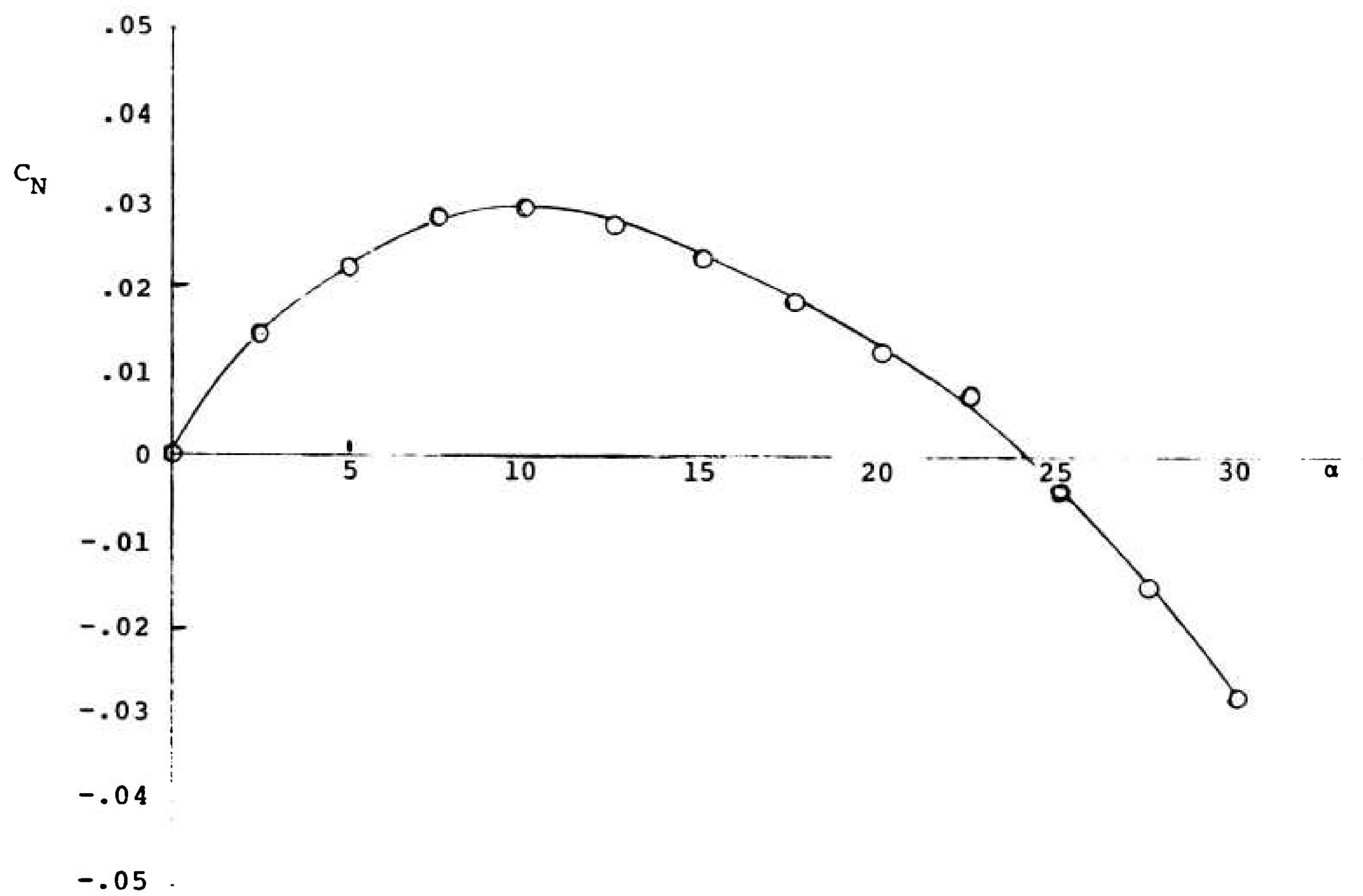

FIG. 29 C_N VALUES FOR THE SOLID FLAT CIRCULAR PARACHUTE MODEL AT $L_c/L_s = 1.21$

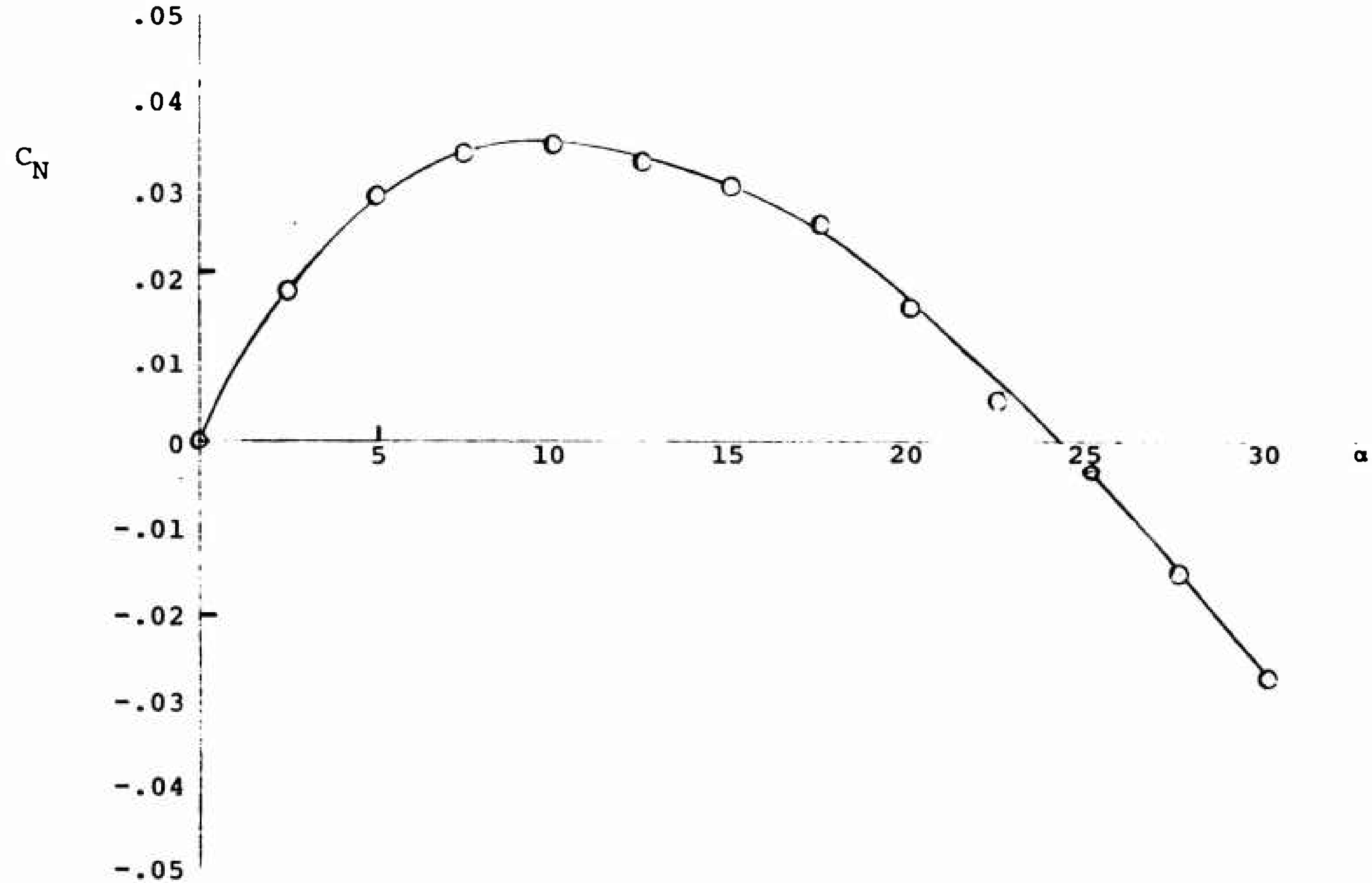

FIG. 30 C_N VALUES FOR THE SOLID FLAT CIRCULAR PARACHUTE MODEL AT $L_c/L_s = 1.16$

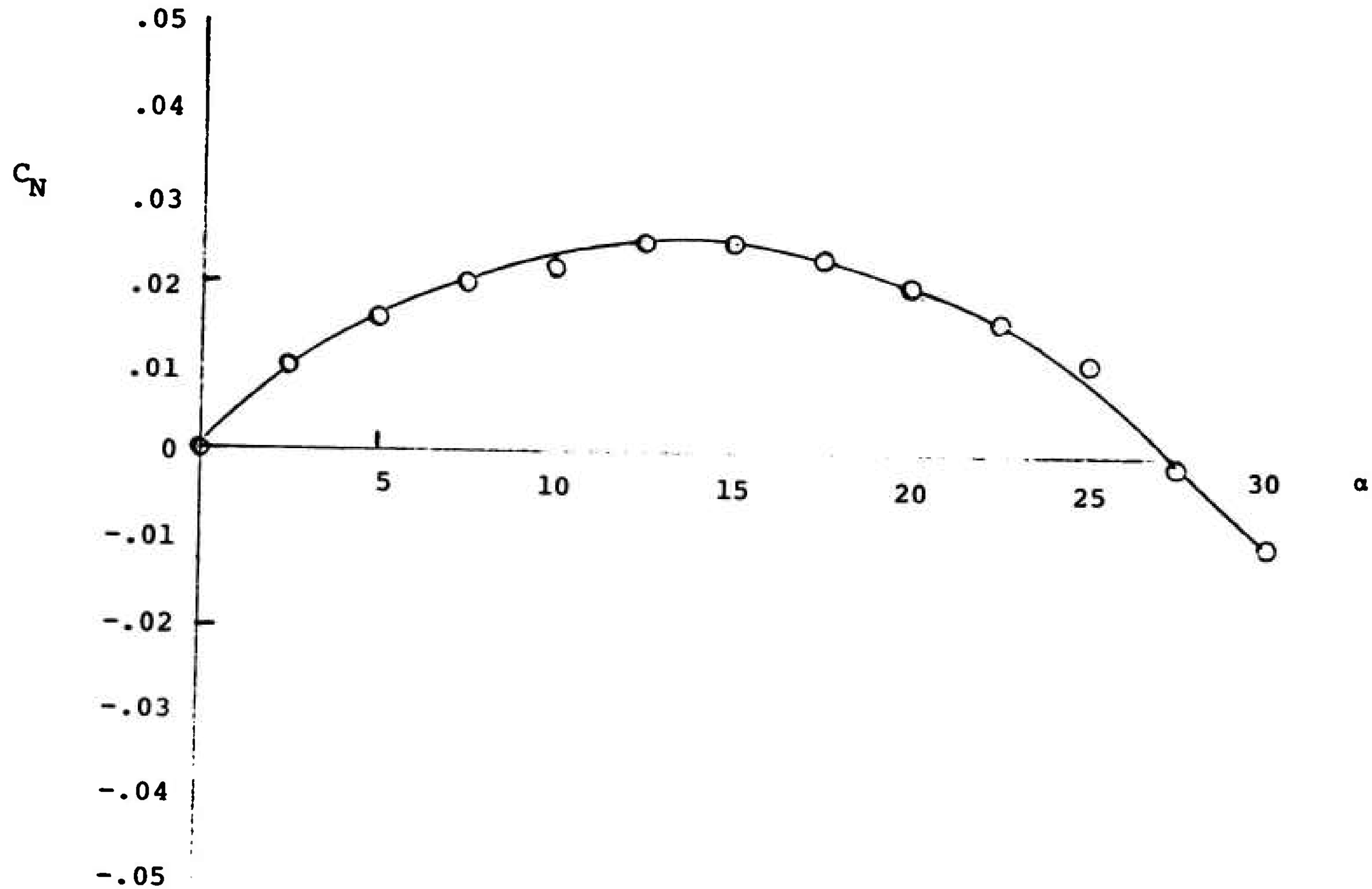

FIG. 31 C_N VALUES FOR THE SOLID FLAT CIRCULAR PARACHUTE MODEL AT $L_c/L_s = 1.11$

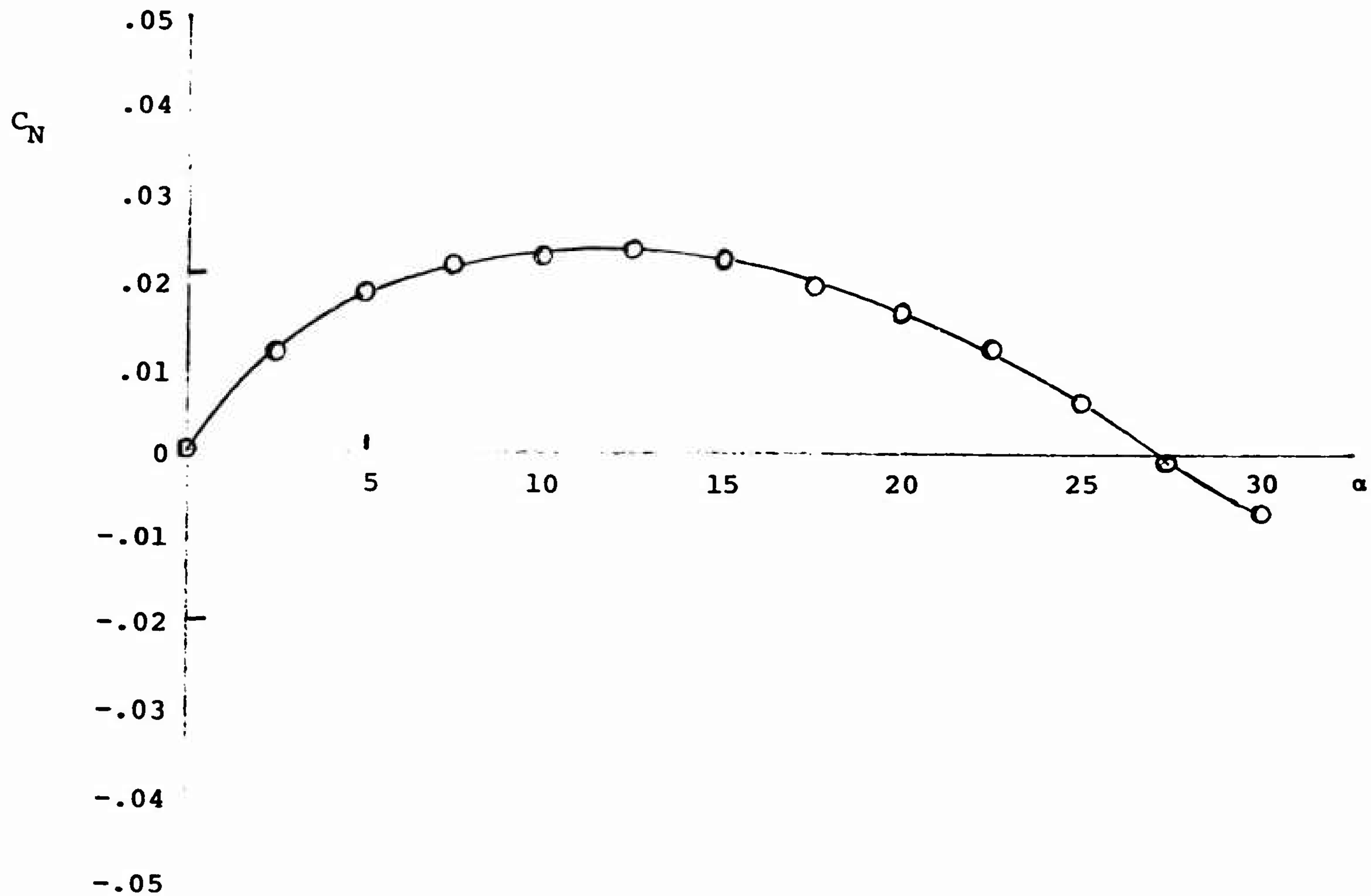

FIG. 32 C_N VALUES FOR THE SOLID FLAT CIRCULAR PARACHUTE MODEL AT $L_C/L_S = 1.06$

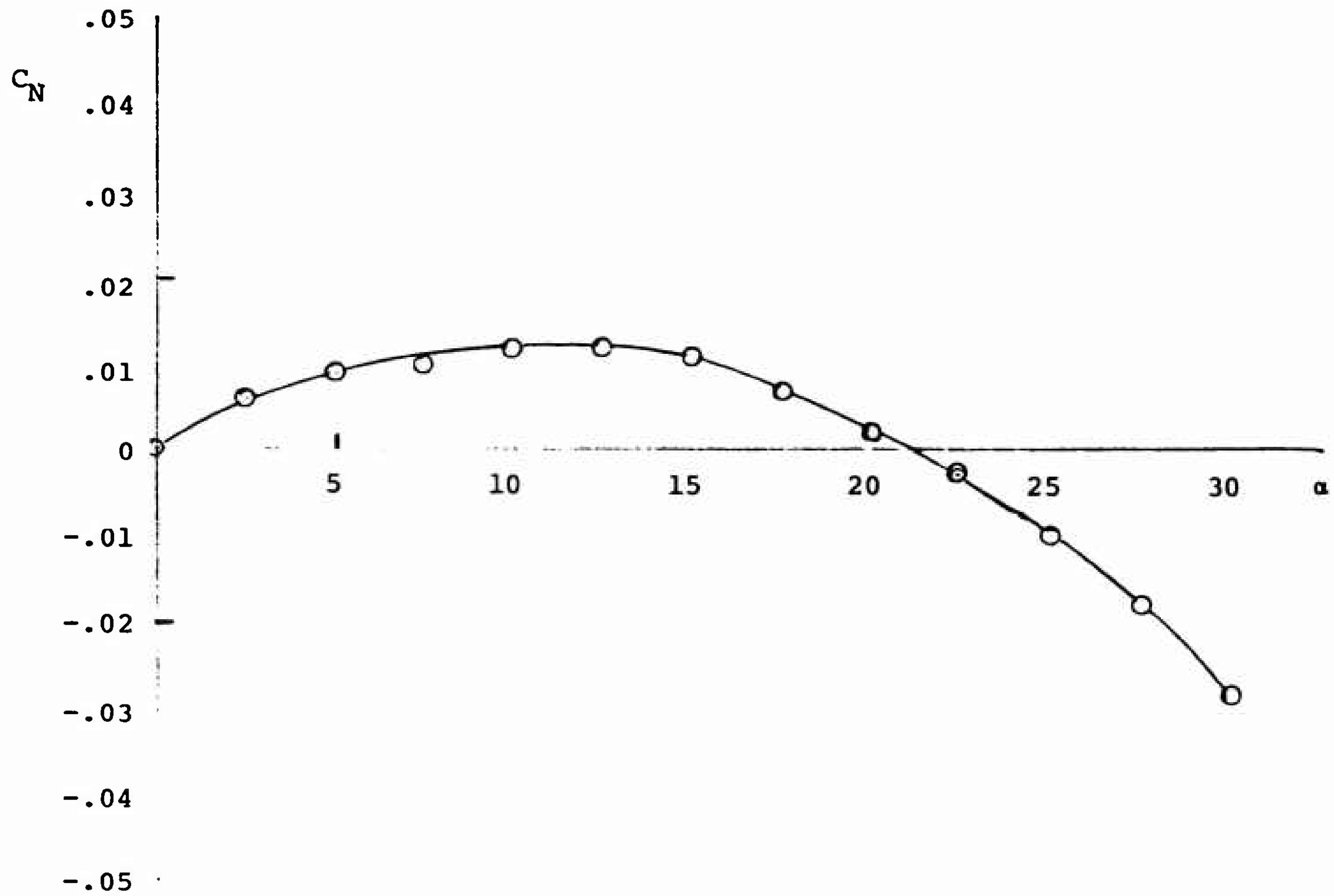

FIG. 33 C_N VALUES FOR THE SOLID FLAT CIRCULAR PARACHUTE MODEL AT $L_c/L_s = 1.01$

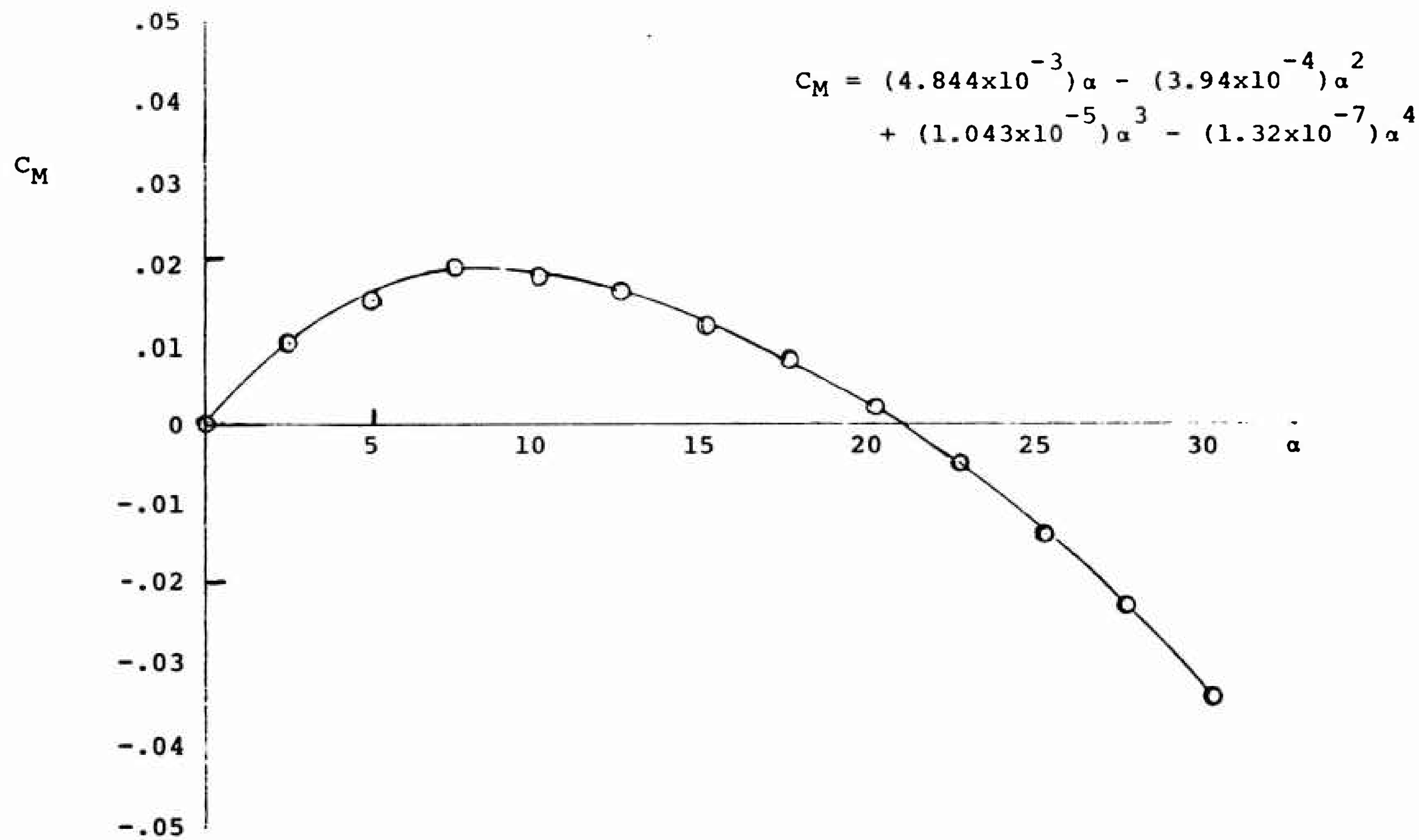

FIG. 34 C_M VALUES FOR THE SOLID FLAT CIRCULAR PARACHUTE MODEL AT $L_C/L_S = 1.26$ (STANDARD CONFIGURATION)

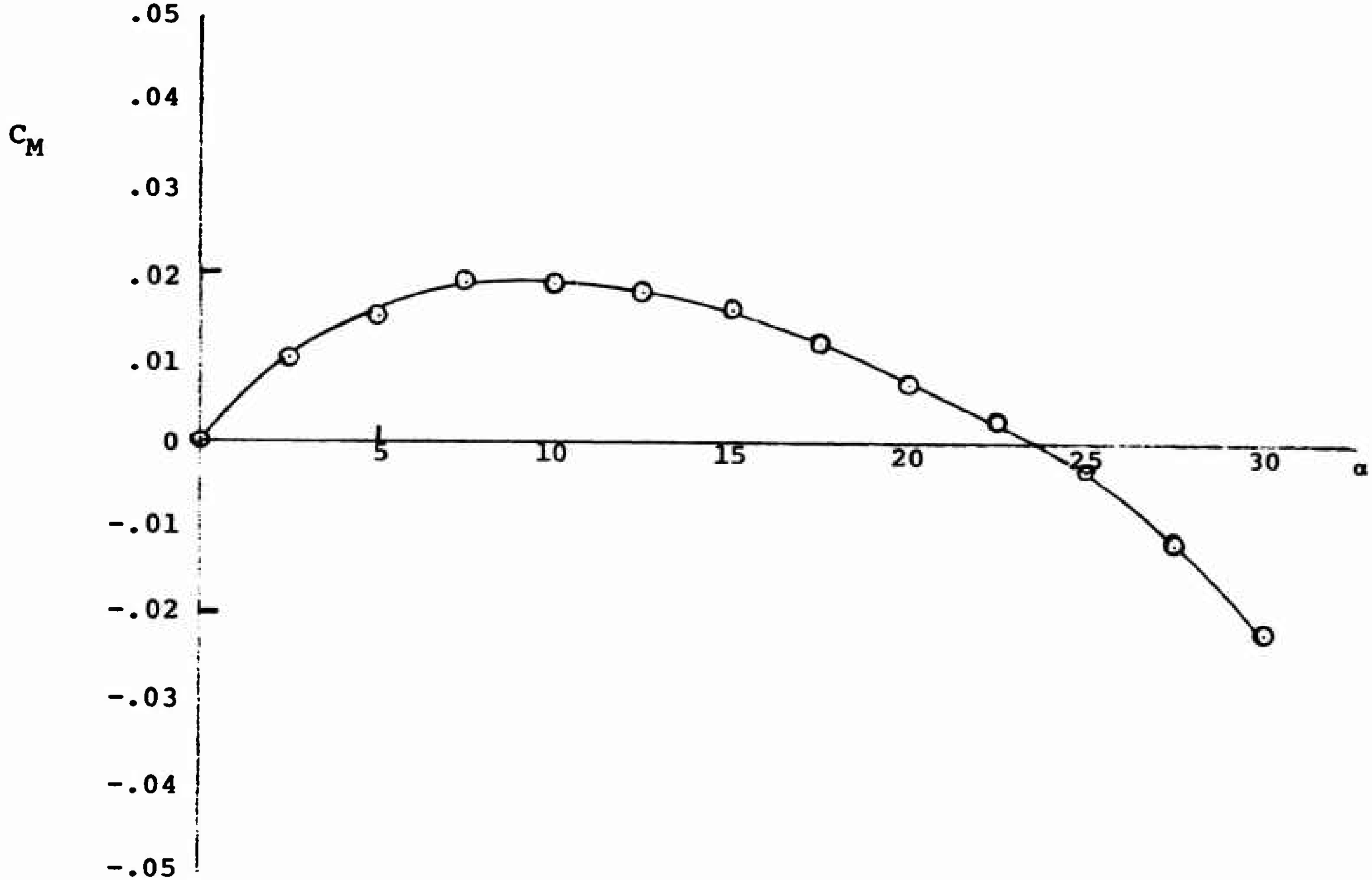

FIG. 35 C_M VALUES FOR THE SOLID FLAT CIRCULAR PARACHUTE MODEL AT $L_C/L_S = 1.21$

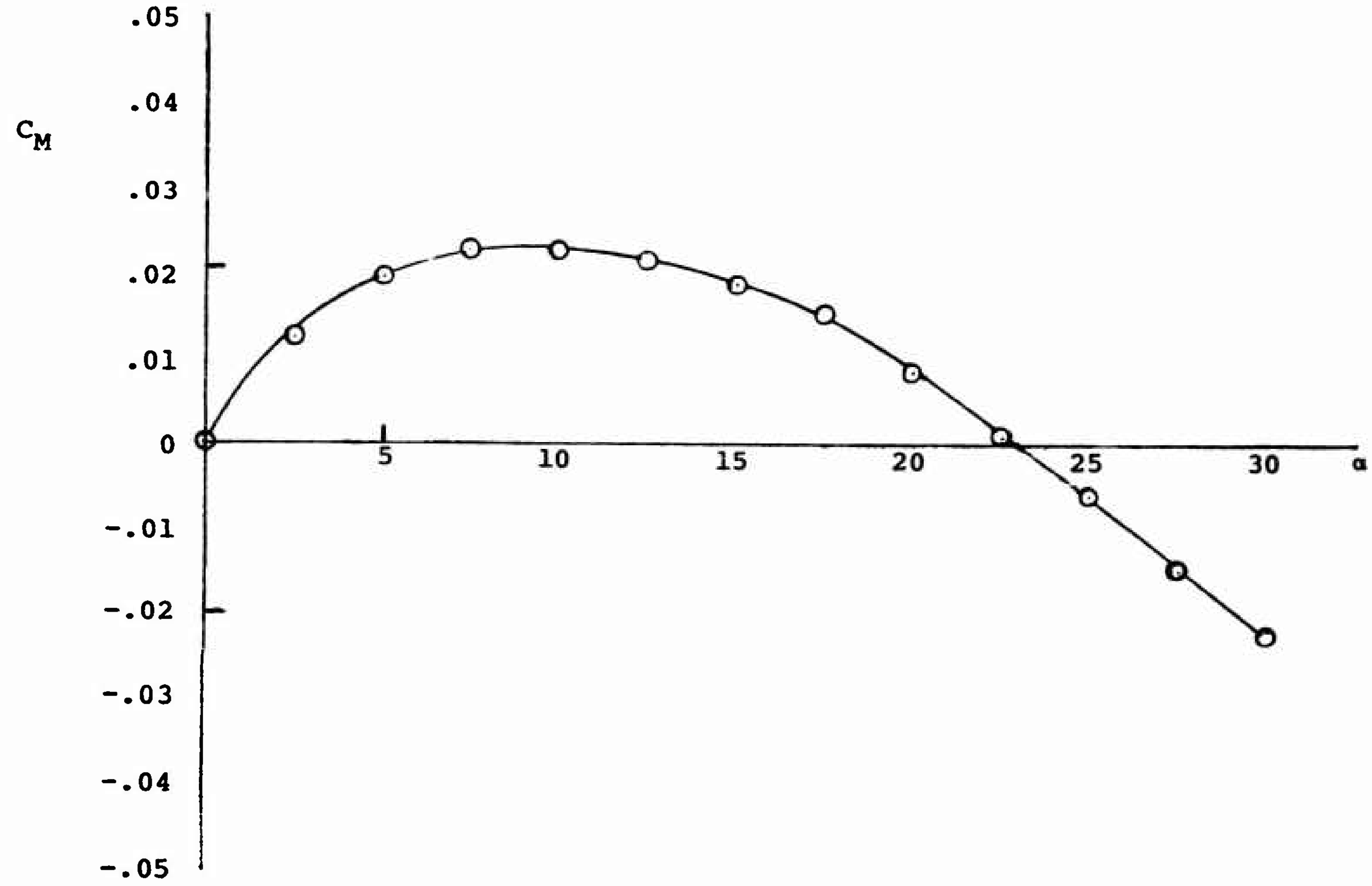

FIG. 36 C_M VALUES FOR THE SOLID FLAT CIRCULAR PARACHUTE MODEL AT $L_C/L_S = 1.16$

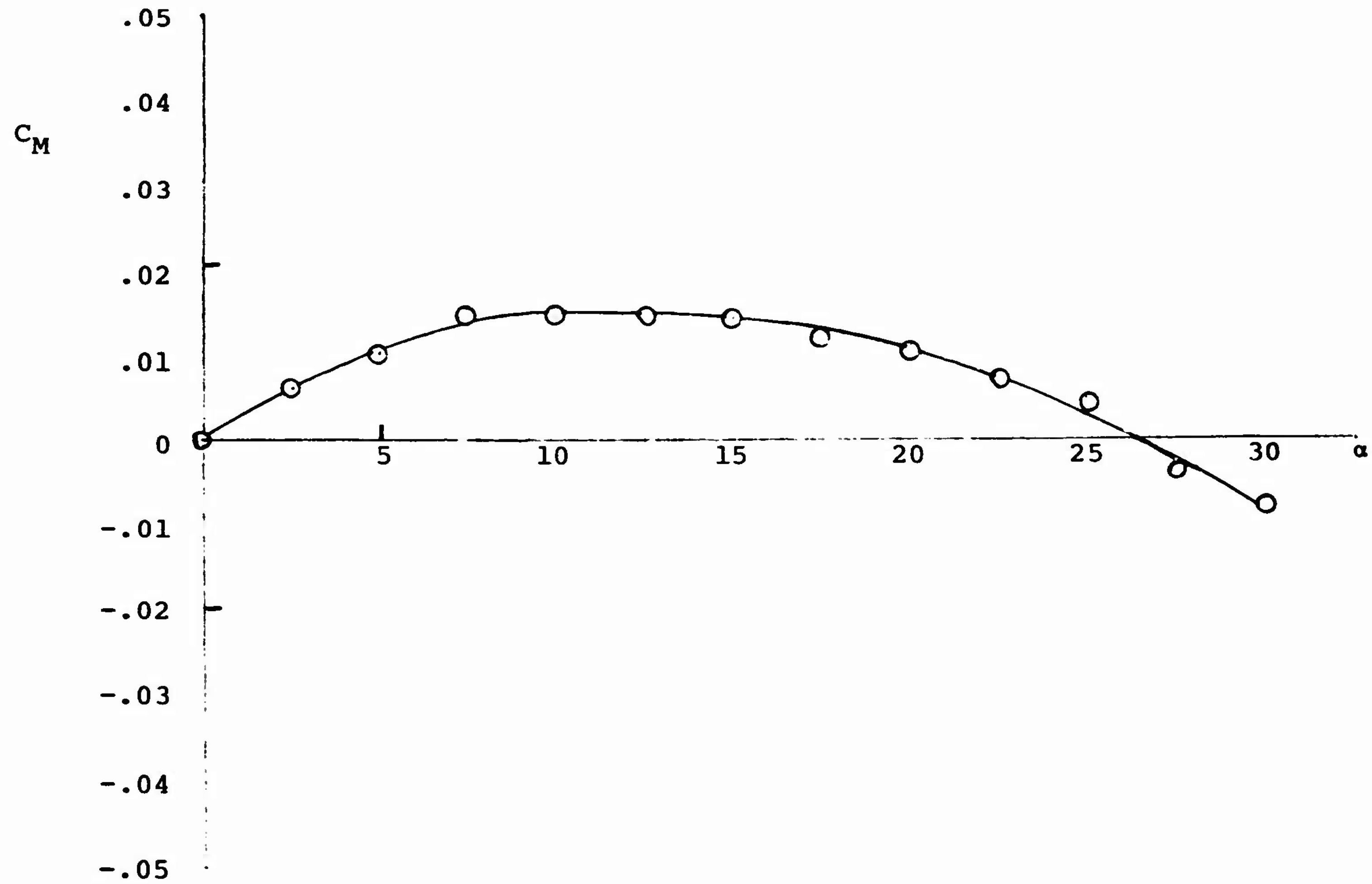

FIG. 37 C_M VALUES FOR THE SOLID FLAT CIRCULAR PARACHUTE MODEL AT $L_c/L_s = 1.11$

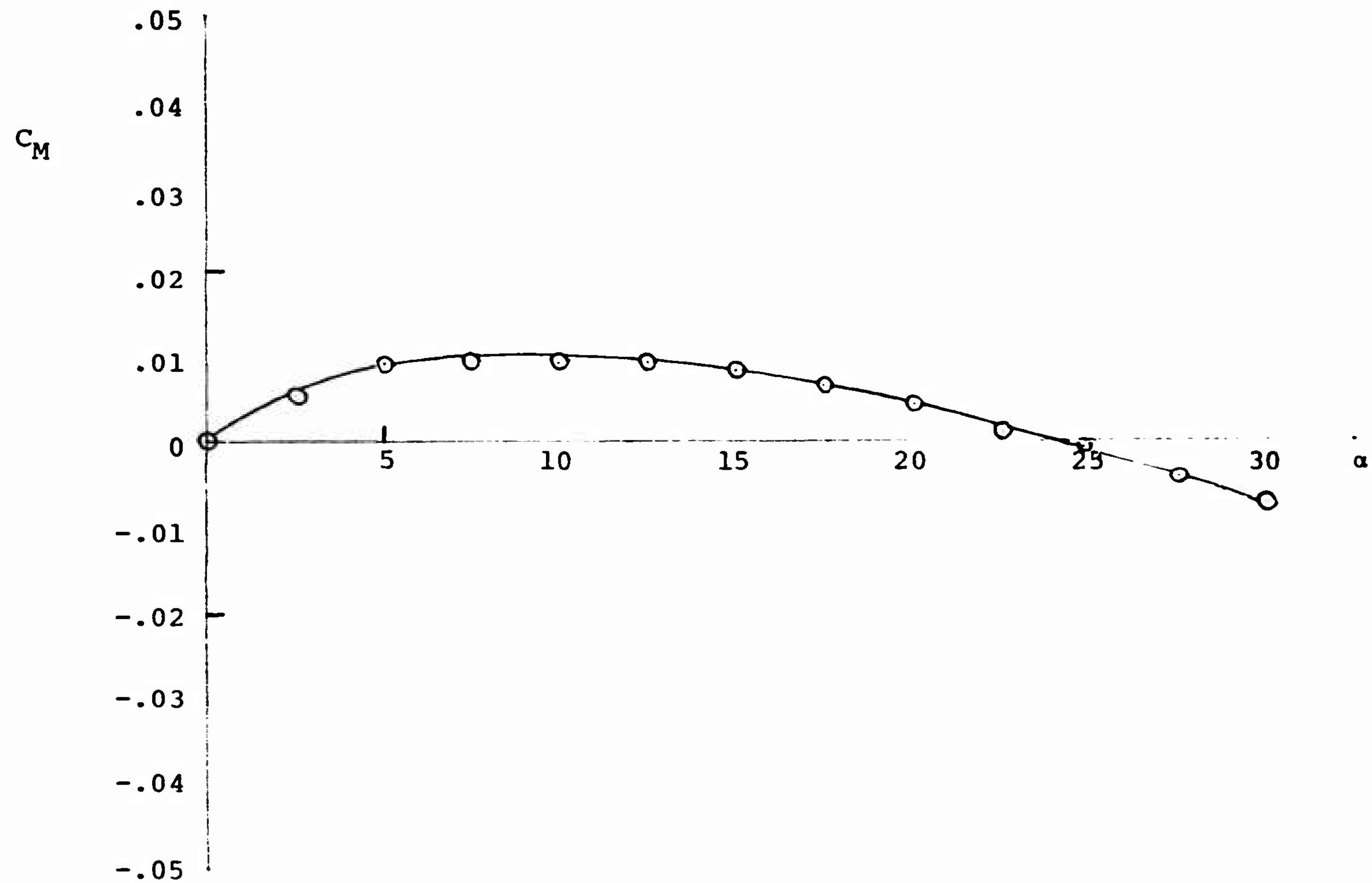

FIG. 38 C_M VALUES FOR THE SOLID FLAT CIRCULAR PARACHUTE MODEL AT $L_C/L_S = 1.06$

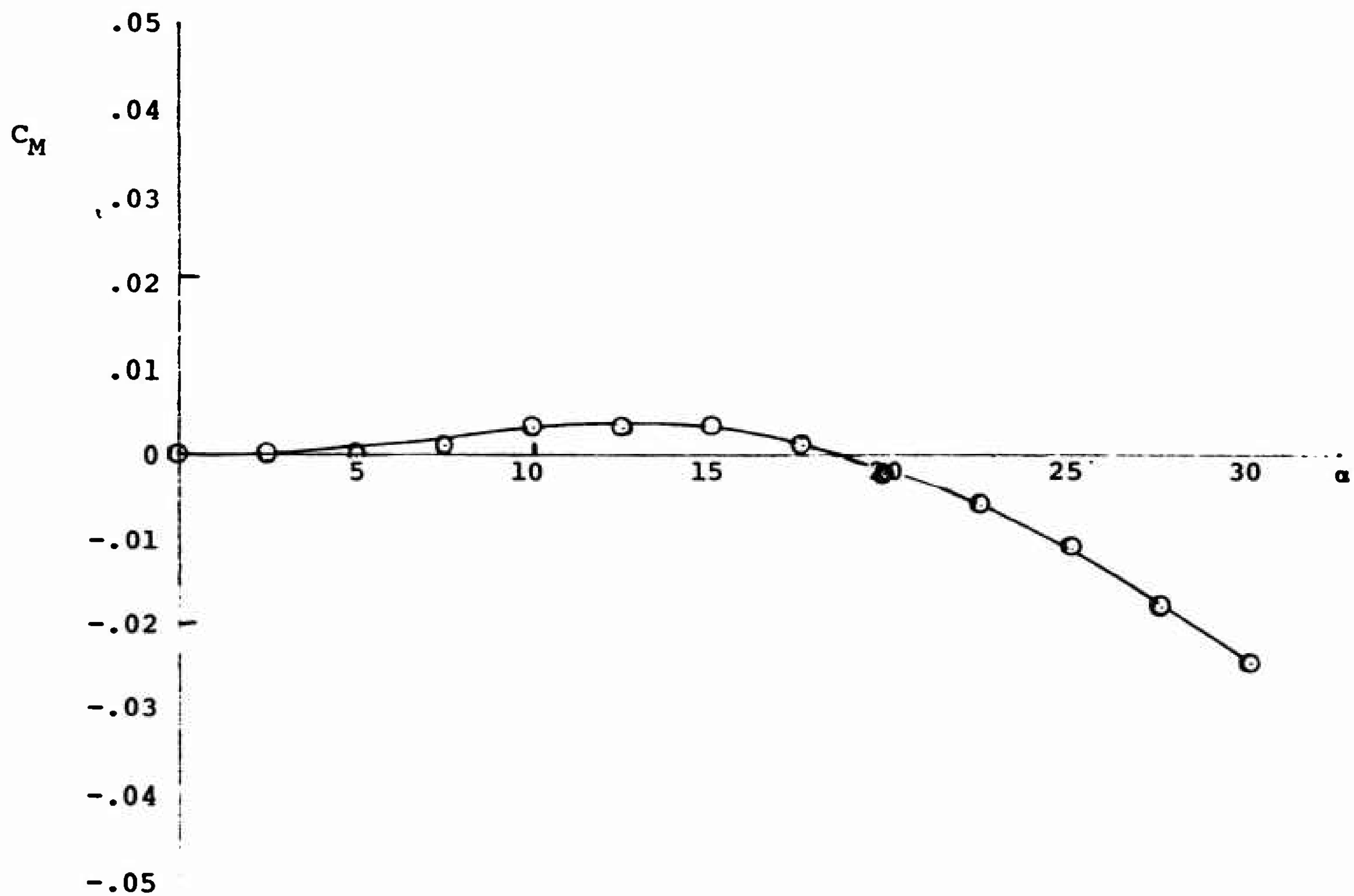

FIG. 39 C_M VALUES FOR THE SOLID FLAT CIRCULAR PARACHUTE MODEL AT $L_C/L_S = 1.01$

TABLE IX

AERODYNAMIC COEFFICIENTS FOR THE T-10 PARACHUTE
(MODEL WITH $L_C/L_S = 1.30$ (STANDARD CONFIGURATION)

$\alpha°$	C_T	C_{T_C}	C_N	C_M
0*	.570	.032	0.0	0.0
2.5*	.572	.020	.0445	.036
5.0*	.578	.012	.0641	.053
7.5*	.587	.009	.0664	.055
10.0	.605	.009	.0606	.049
12.5	.614	.009	.0481	.039
15.0	.615	.009	.0345	.028
17.5	.610	.009	.0190	.016
20.0	.599	.009	.0029	.002
22.5	.587	.009	-.0130	-.012
25.0	.569	.009	-.0291	-.026
27.5	.563	.009	-.0463	-.041
30.0	.554	.009	-.0636	-.056

* Values From Curves

TABLE X

AERODYNAMIC COEFFICIENTS FOR THE T-10 PARACHUTE MODEL WITH $L_C/L_S = 1.24$

$\alpha°$	C_T	C_{T_C}	C_N	C_M
0*	.570	.030	0.0	0.0
2.5*	.580	.036	.0274	.019
5.0*	.605	.045	.0433	.032
7.5*	.627	.059	.0504	.037
10.0	.651	.073	.0510	.038
12.5	.668	.083	.0469	.036
15.0	.680	.092	.0404	.032
17.5	.683	.099	.0314	.025
20.0	.675	.100	.0172	.013
22.5	.657	.098	.0012	-.001
25.0	.629	.096	-.0172	-.017
27.5	.611	.097	-.0339	-.031
30.0	.606	.100	-.0546	-.050

* Values From Curves

TABLE XI

AERODYNAMIC COEFFICIENTS FOR THE T-10 PARACHUTE MODEL WITH $L_C/L_S = 1.18$

α°	C_T	C_{T_C}	C_N	C_M
0*	[illegible]	.115	0.0	0.0
2.5*	.624	.122	.0232	.017
5.0*	.644	.135	.0386	.028
7.5*	.670	.153	.0469	.035
10.0	.703	.171	.0481	.037
12.5	.721	.184	.0445	.034
15.0	.731	.196	.0373	.028
17.5	.733	.203	.0297	.022
20.0	.726	.205	.0190	.014
22.5	.711	.202	.0054	.002
25.0	.690	.192	-.0107	-.011
27.5	.667	.186	-.0285	-.026
30.0	.652	.183	-.0463	-.041

* Values From Curves

TABLE XII

AERODYNAMIC COEFFICIENTS FOR THE T-10 PARACHUTE MODEL WITH $L_C/L_S = 1.11$

$\alpha°$	C_T	C_{T_C}	C_N	C_M
0*	.637	.168	0.0	0.0
2.5*	.647	.178	.0196	.014
5.0*	.662	.199	.0320	.022
7.5*	.679	.217	.0386	.027
10.0	.705	.235	.0386	.027
12.5	.722	.247	.0356	.024
15.0	.733	.256	.0309	.020
17.5	.736	.266	.0243	.017
20.0	.733	.266	.0155	.010
22.5	.722	.257	.0059	.004
25.0	.708	.253	-.0059	-.005
27.5	.691	.249	-.0136	-.009
30.0	.673	.245	-.0274	-.010

* Values From Curves

TABLE XIII

AERODYNAMIC COEFFICIENTS FOR THE T-10 PARACHUTE MODEL WITH $L_C/L_S = 1.04$

α^o	C_T	C_{T_C}	C_N	C_M
0*	.650	.227	0.0	0.0
2.5*	.659	.236	.0155	.010
5.0*	.672	.254	.025	.017
7.5*	.688	.277	.030	.019
10.0	.711	.294	.030	.020
12.5	.728	.306	.027	.018
15.0	.738	.312	.022	.015
17.5	.741	.318	.019	.013
20.0	.737	.312	.0125	.008
22.5	.727	.307	.0036	.002
25.0	.711	.304	-.0059	-.005
27.5	.696	.299	-.0161	-.013
30.0	.680	.294	-.0255	-.024

* Values From Curves

TABLE XIV

AERODYNAMIC COEFFICIENTS FOR THE T-10 PARACHUTE MODEL WITH $L_C/L_S = 0.98$

$\alpha°$	C_T	C_{T_C}	C_N	C_M
0*	.630	.254	0.0	0.0
2.5*	.633	.263	.0054	.003
5.0*	.642	.285	.0095	.006
7.5*	.655	.305	.0136	.008
10.0	.675	.318	.0172	.010
12.5	.693	.327	.0190	.012
15.0	.703	.330	.0184	.011
17.5	.709	.333	.0148	.009
20.0	.710	.334	.0089	.003
22.5	.709	.334	.0018	-.002
25.0	.703	.331	-.0054	-.008
27.5	.692	.326	-.0148	-.015
30.0	.666	.315	-.0261	-.023

* Values From Curves

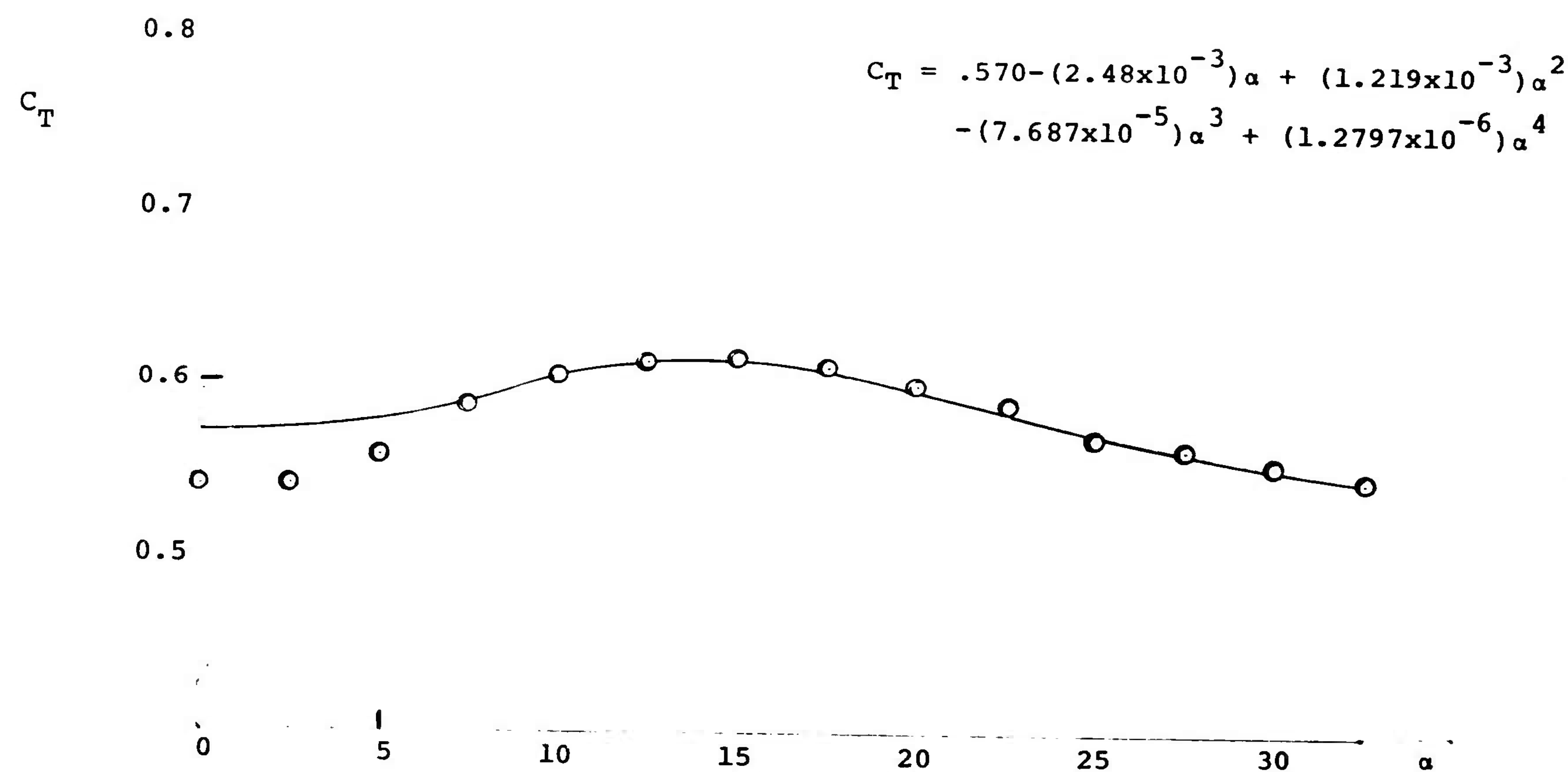

FIG. 40 C_T VALUES FOR THE T-10 PARACHUTE MODEL AT L_C/L_S = 1.30 (STANDARD CONFIGURATION)

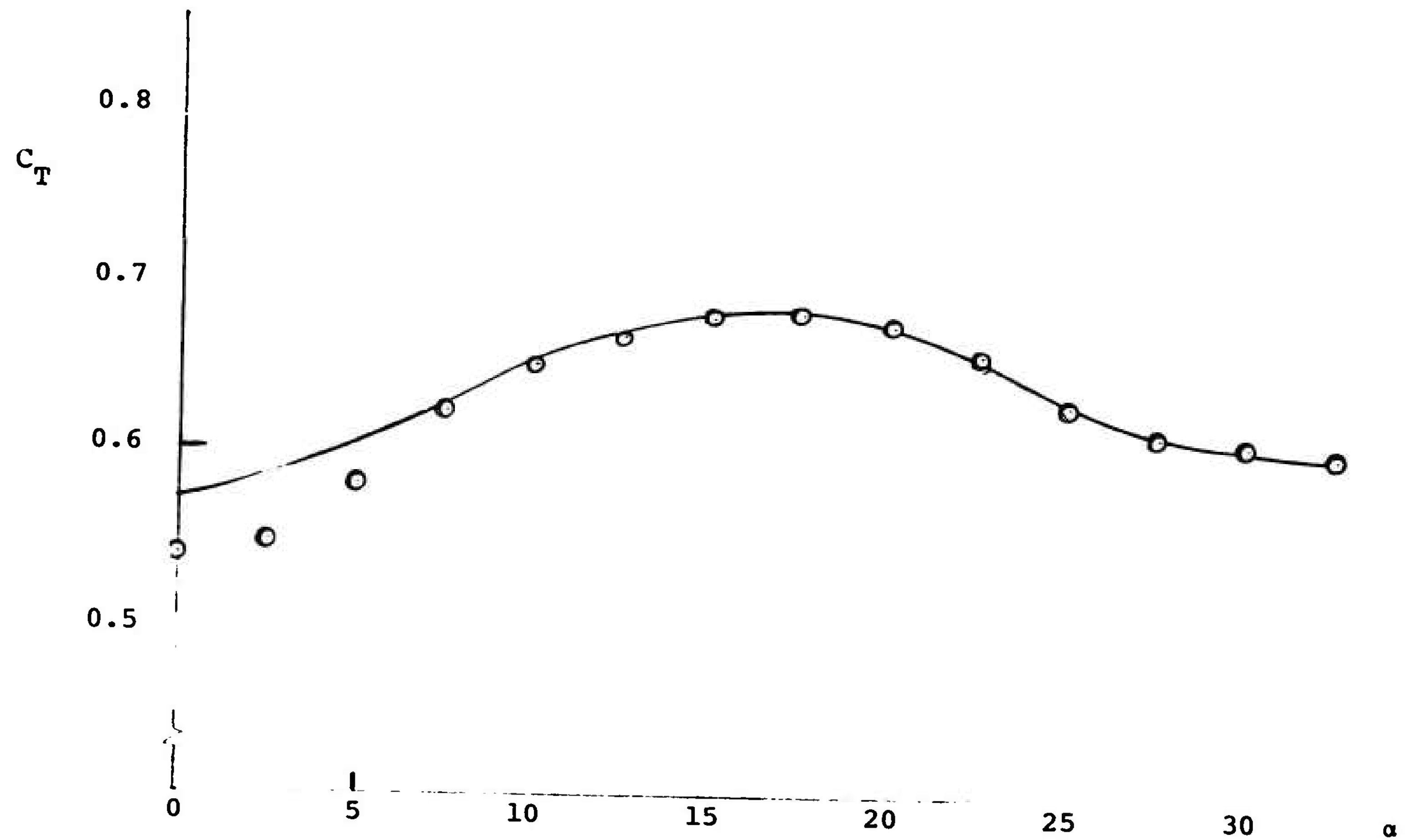

FIG. 41 C_T VALUES FOR THE T-10 PARACHUTE MODEL AT $L_C/L_S = 1.24$

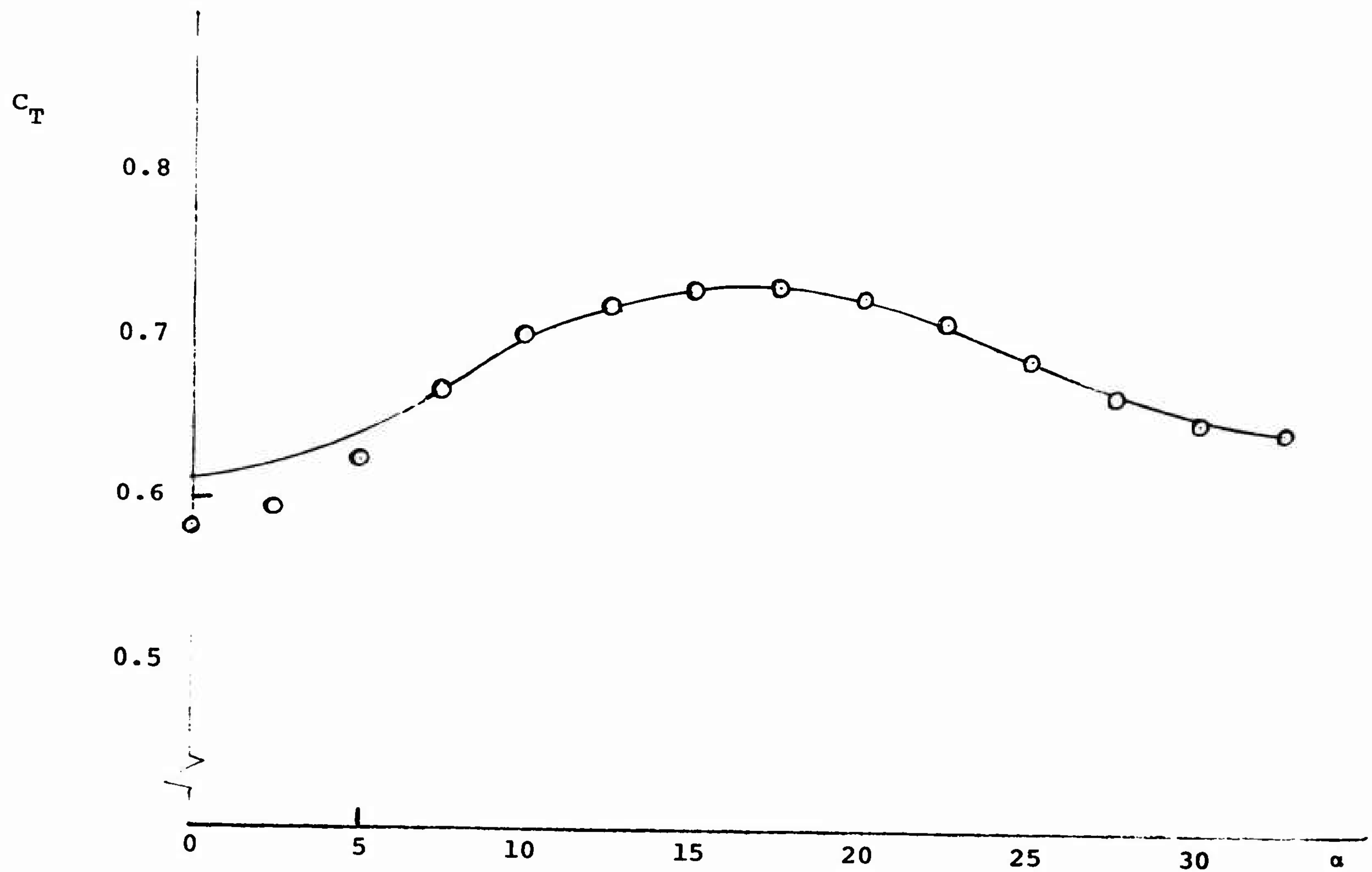

FIG. 42 C_T VALUES FOR THE T-10 PARACHUTE MODEL AT L_C/L_S = 1.18

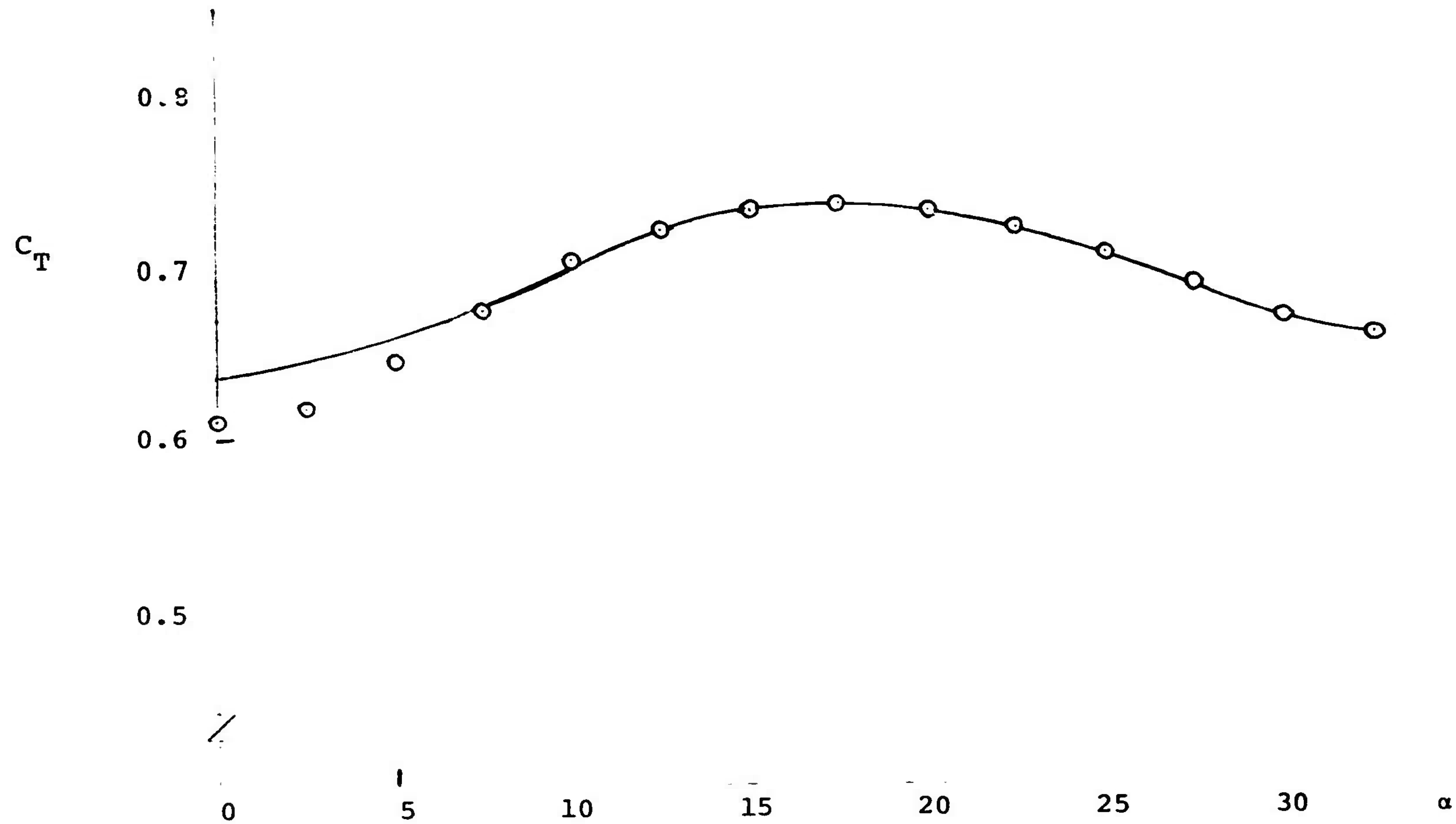

FIG. 43 C_T VALUES FOR THE T-10 PARACHUTE MODEL AT $L_C/L_S = 1.11$

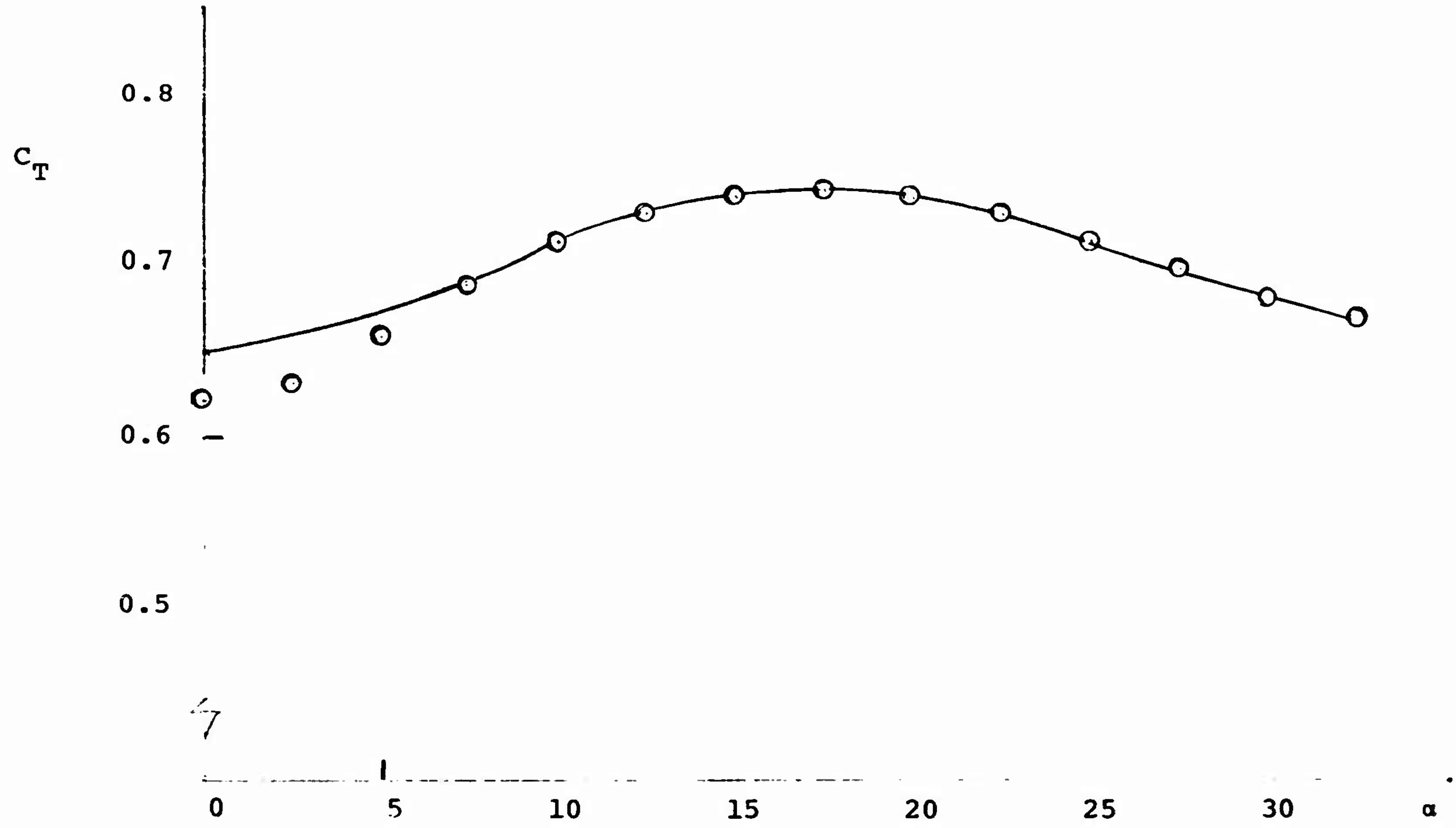

FIG. 44 C_T VALUES FOR THE T-10 PARACHUTE MODEL AT $L_C/L_S = 1.04$

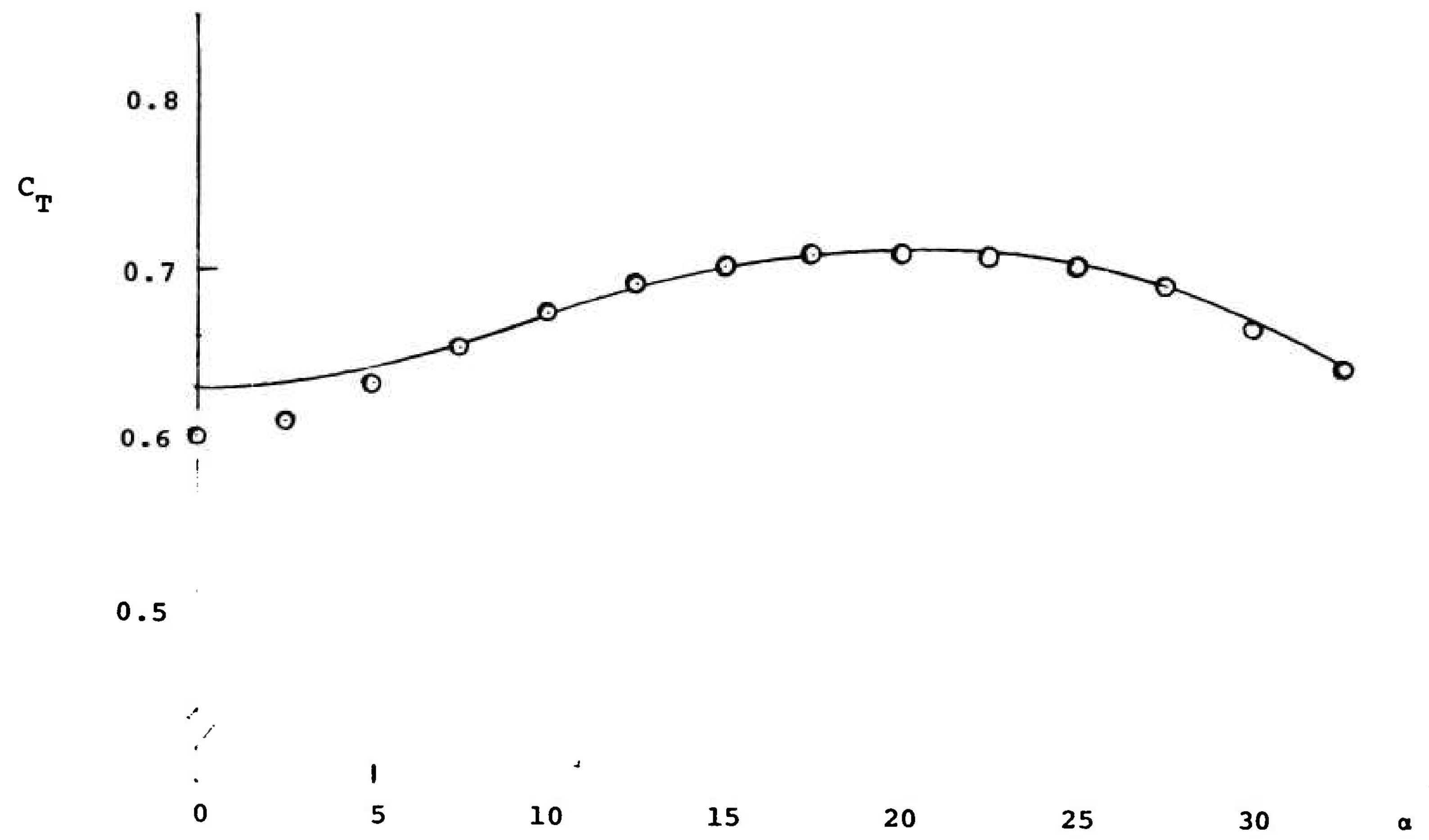

FIG. 45 C_T VALUES FOR THE T-10 PARACHUTE MODEL AT L_C/L_S = .98

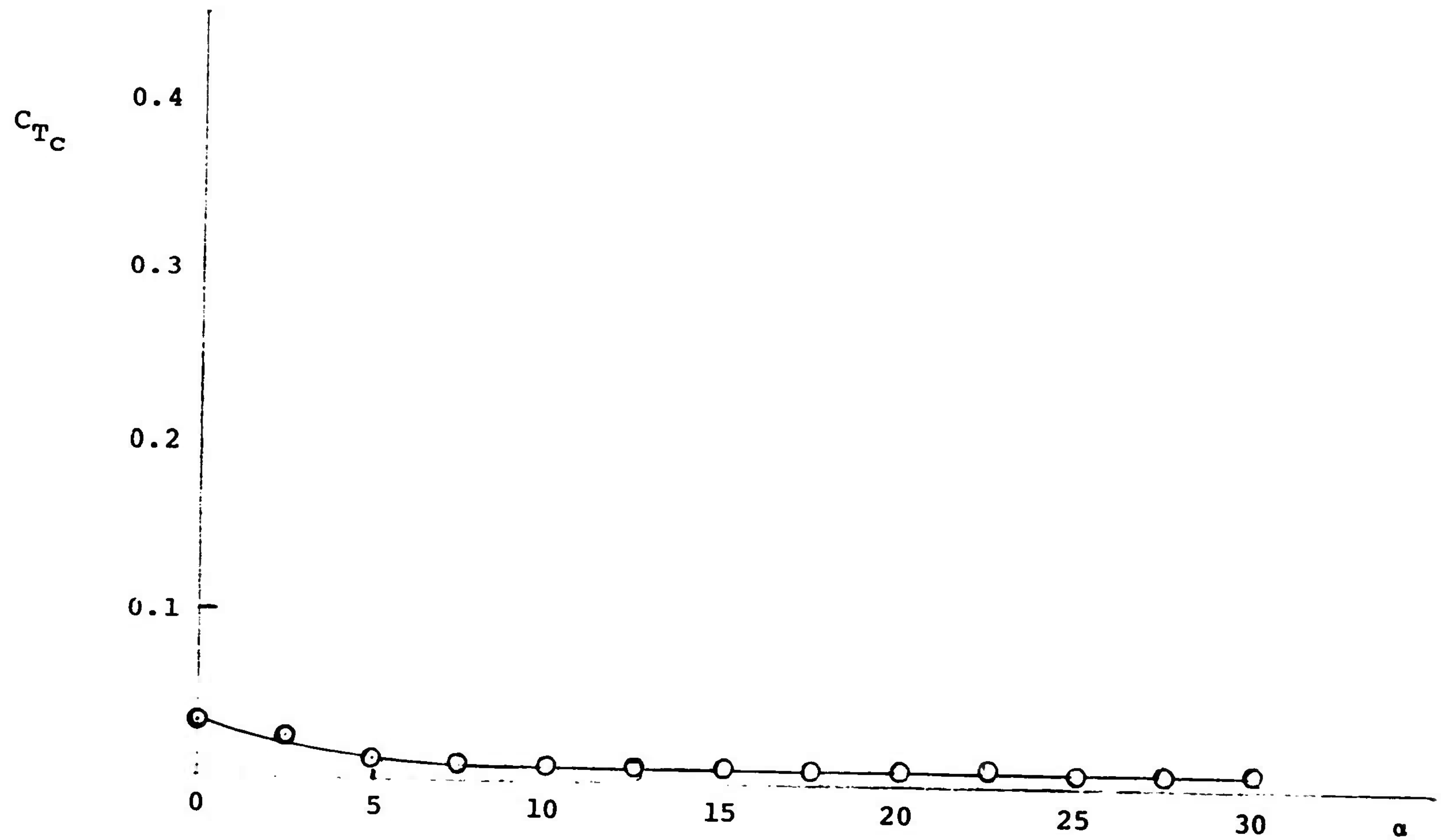

FIG. 46 C_{T_C} VALUES FOR THE T-10 PARACHUTE MODEL AT $L_C/L_S = 1.30$ (STANDARD CONFIGURATION)

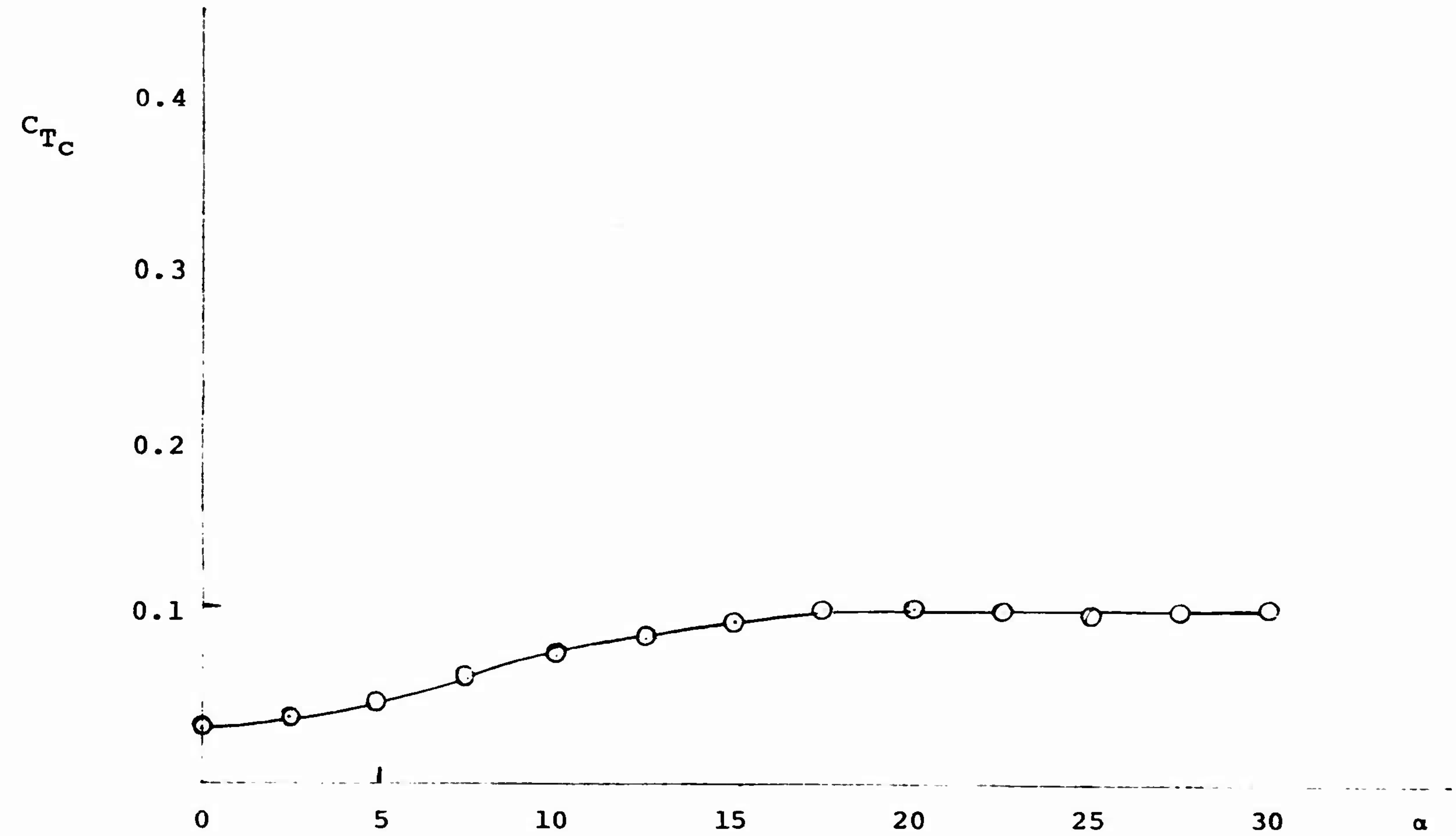

FIG. 47 C_{T_C} VALUES [illegible] THE T-10 PARACHUTE MODEL AT $L_c/L_s = 1$

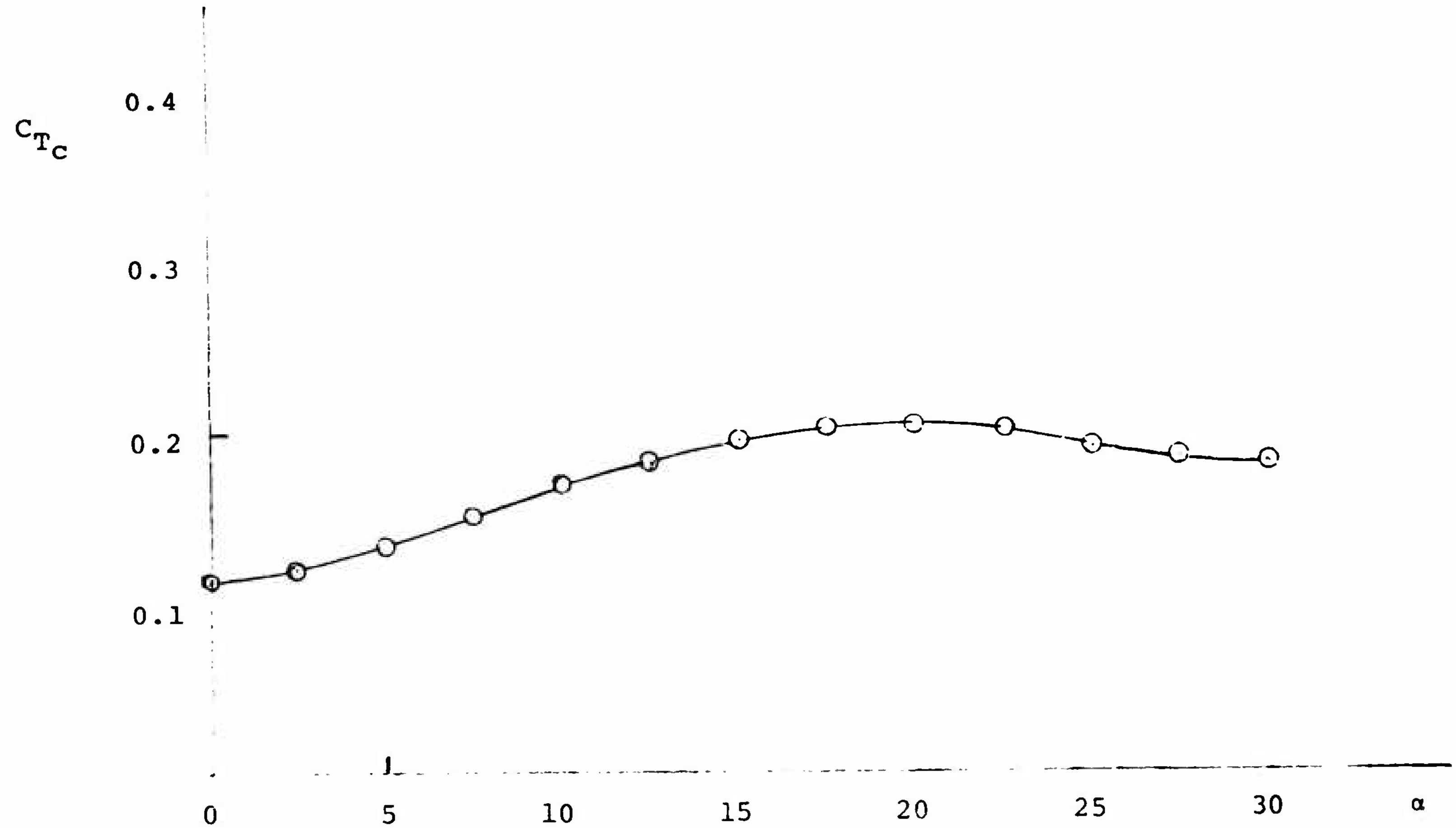

FIG. 48 C_{T_C} VALUES FOR THE T-10 PARACHUTE MODEL AT $L_C/L_S = 1.18$

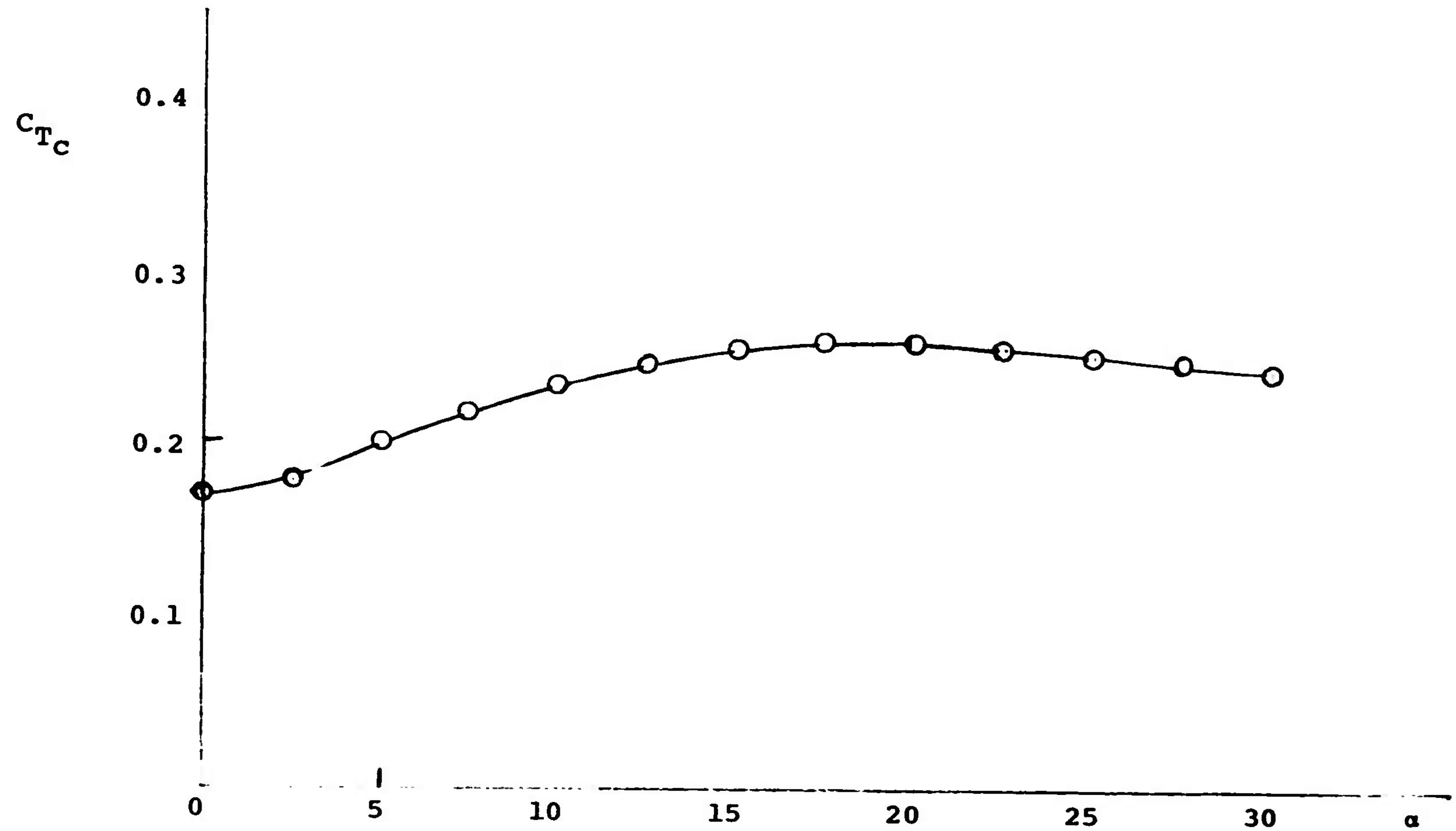

FIG. 49 C_{T_C} VALUES FOR THE T-10 PARACHUTE MODEL AT $L_C/L_S = 1.11$

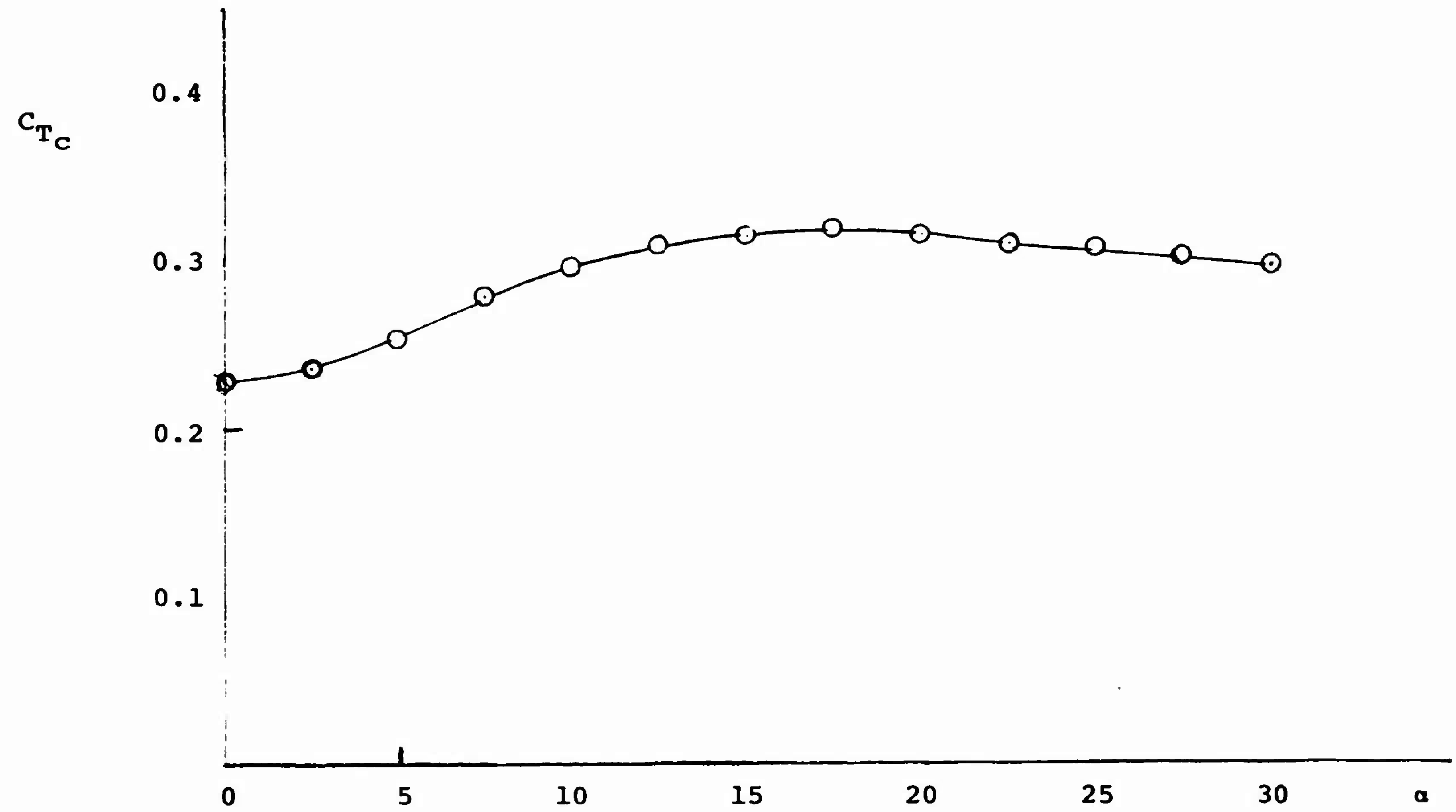

FIG. 50 C_{T_C} VALUES FOR THE T-10 PARACHUTE MODEL AT $L_C/L_S = 1.04$

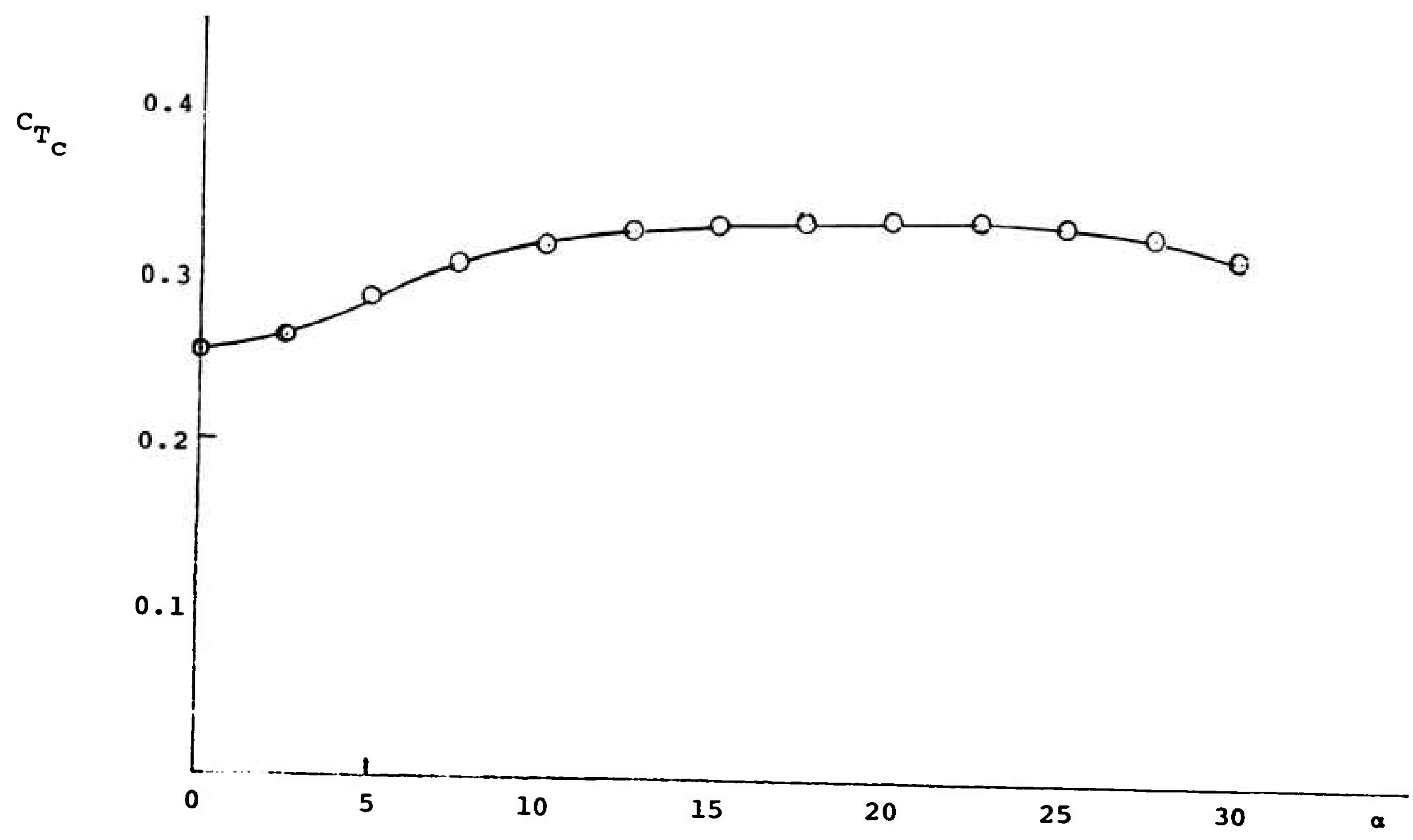

FIG. 51 C_{T_C} VALUES FOR THE T-10 PARACHUTE MODEL AT L_C/L_S = .98

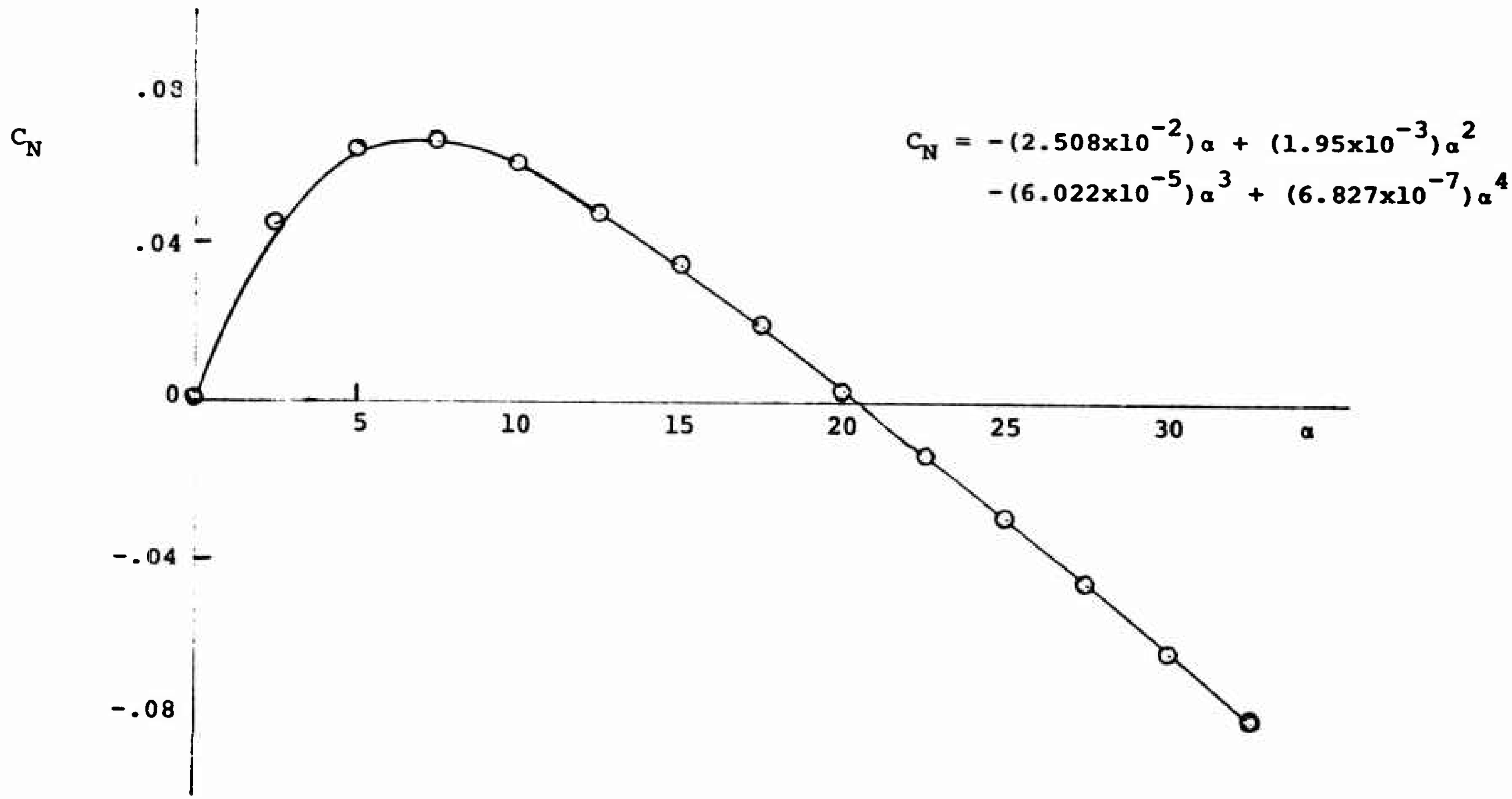

FIG. 52 C_N VALUES FOR THE T-10 PARACHUTE MODEL AT L_C/L_S = 1.30 (STANDARD CONFIGURATION)

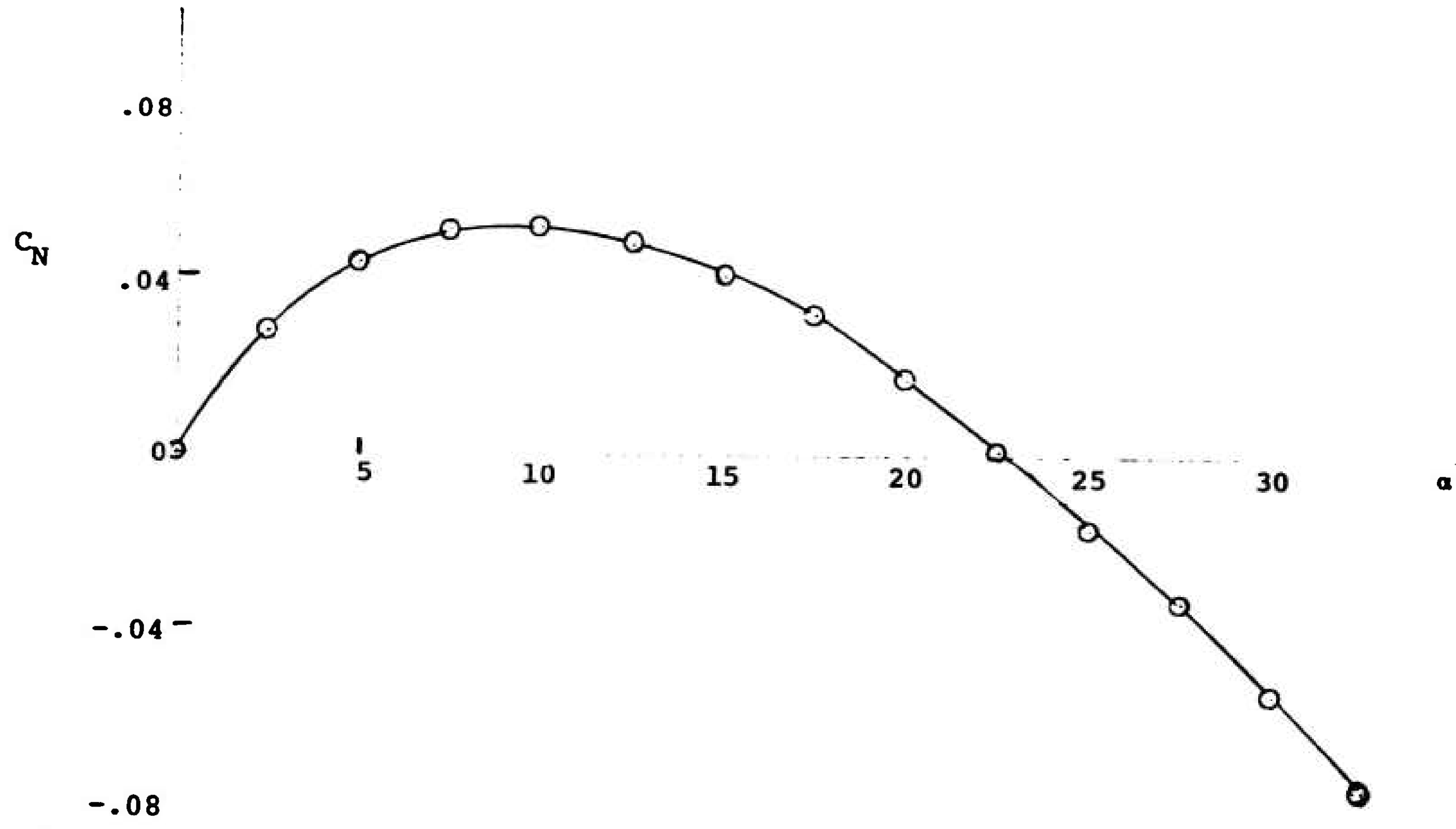

FIG. 53 C_N VALUES FOR THE T-10 PARACHUTE MODEL AT $L_C/L_S = 1.24$

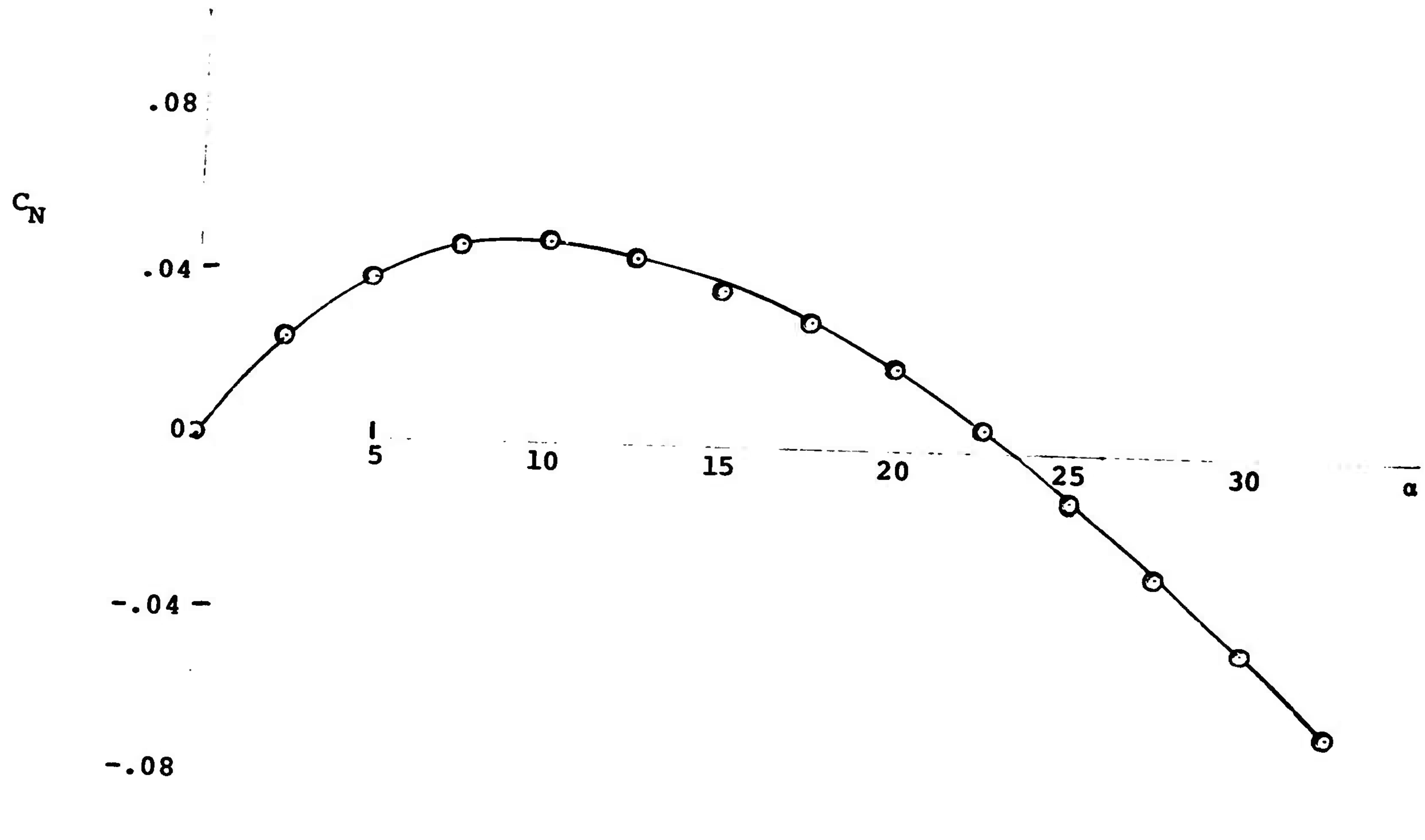

FIG. 54 C_N VALUES FOR THE T-10 PARACHUTE MODEL AT $L_C/L_S = 1.18$

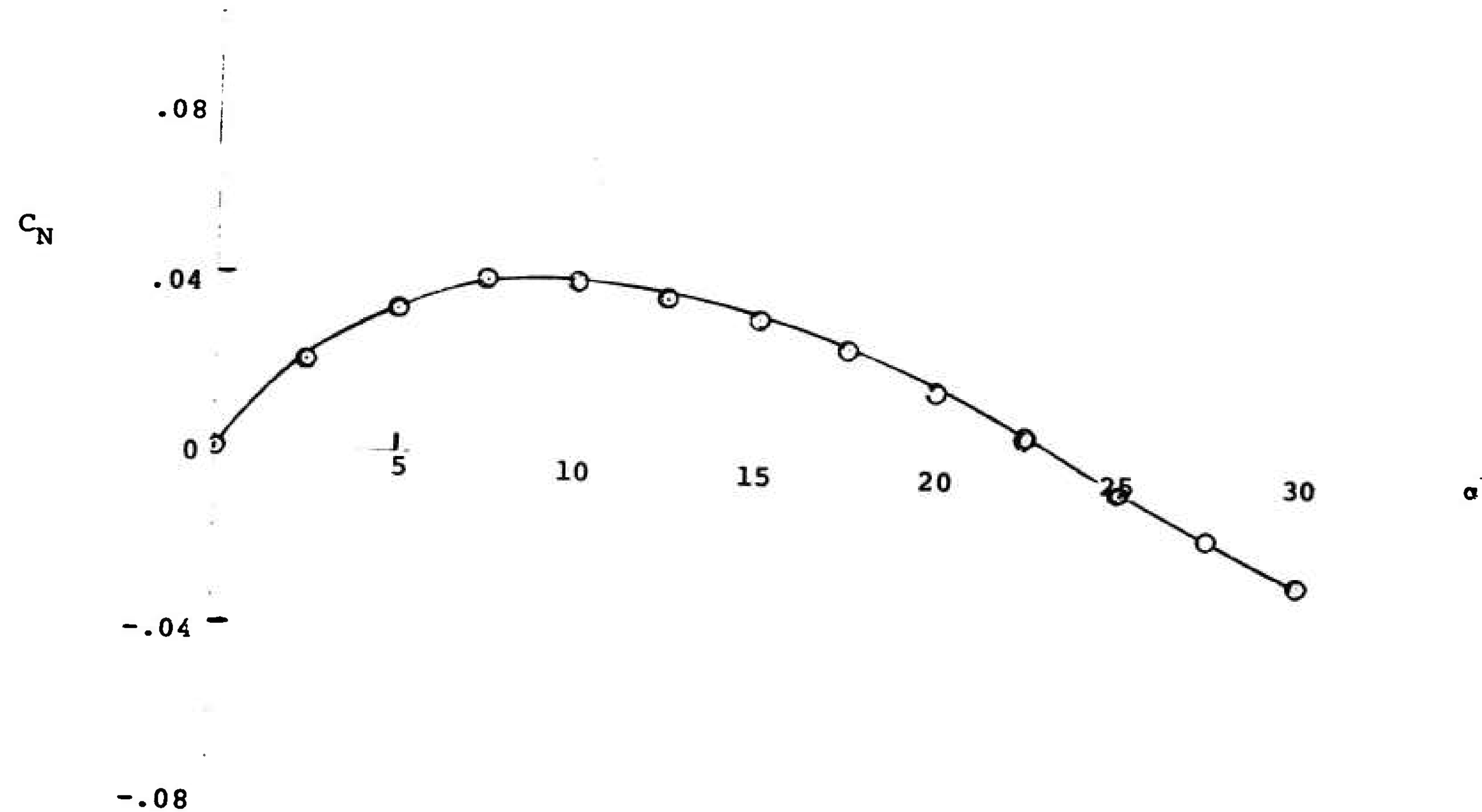

FIG. 55 C_N VALUES FOR THE T-10 PARACHUTE MODEL AT $L_C/L_S = 1.11$

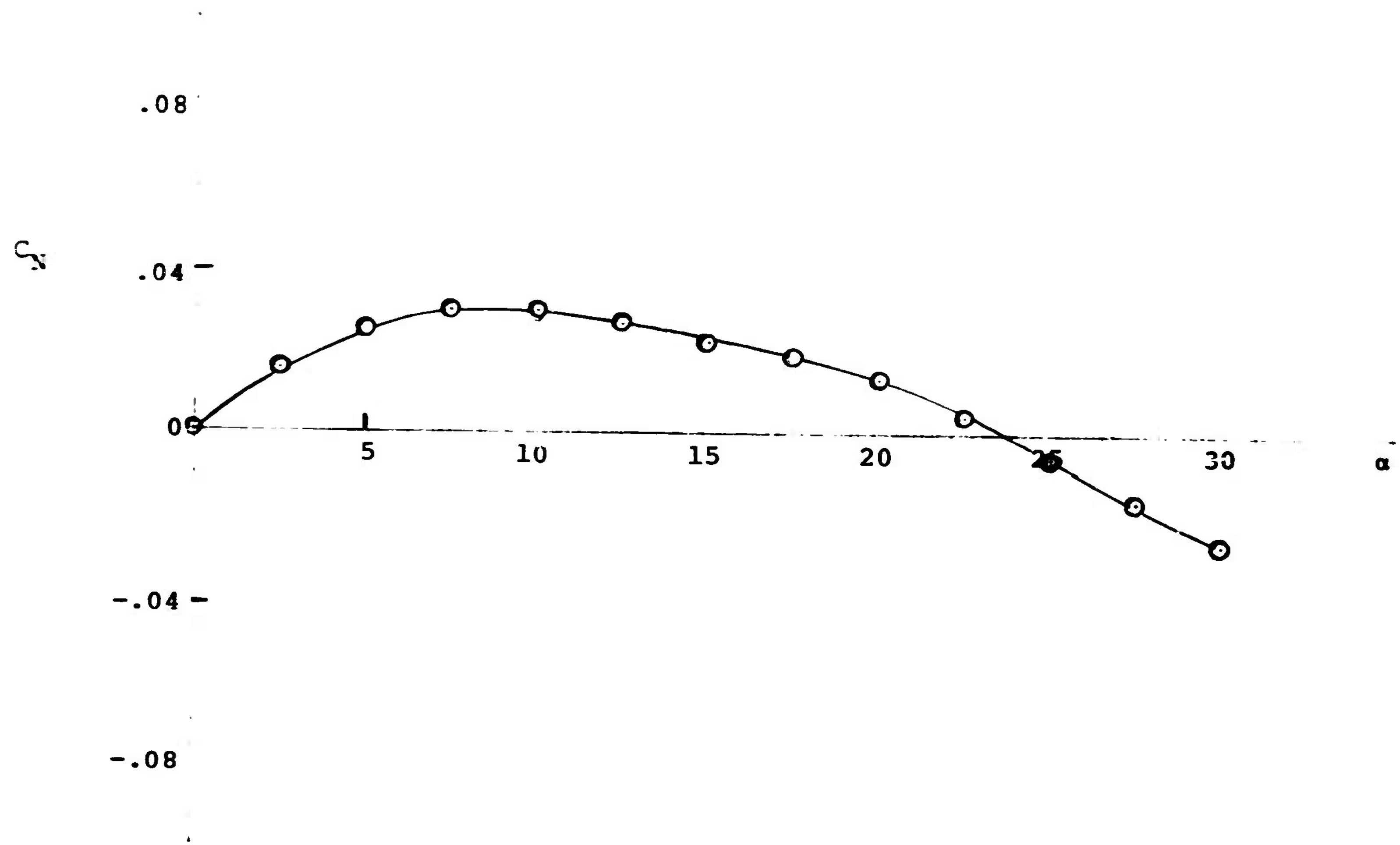

FIG. 56 C_N VALUES FOR THE T-10 PARACHUTE MODEL AT $L_c/L_s = 1.04$

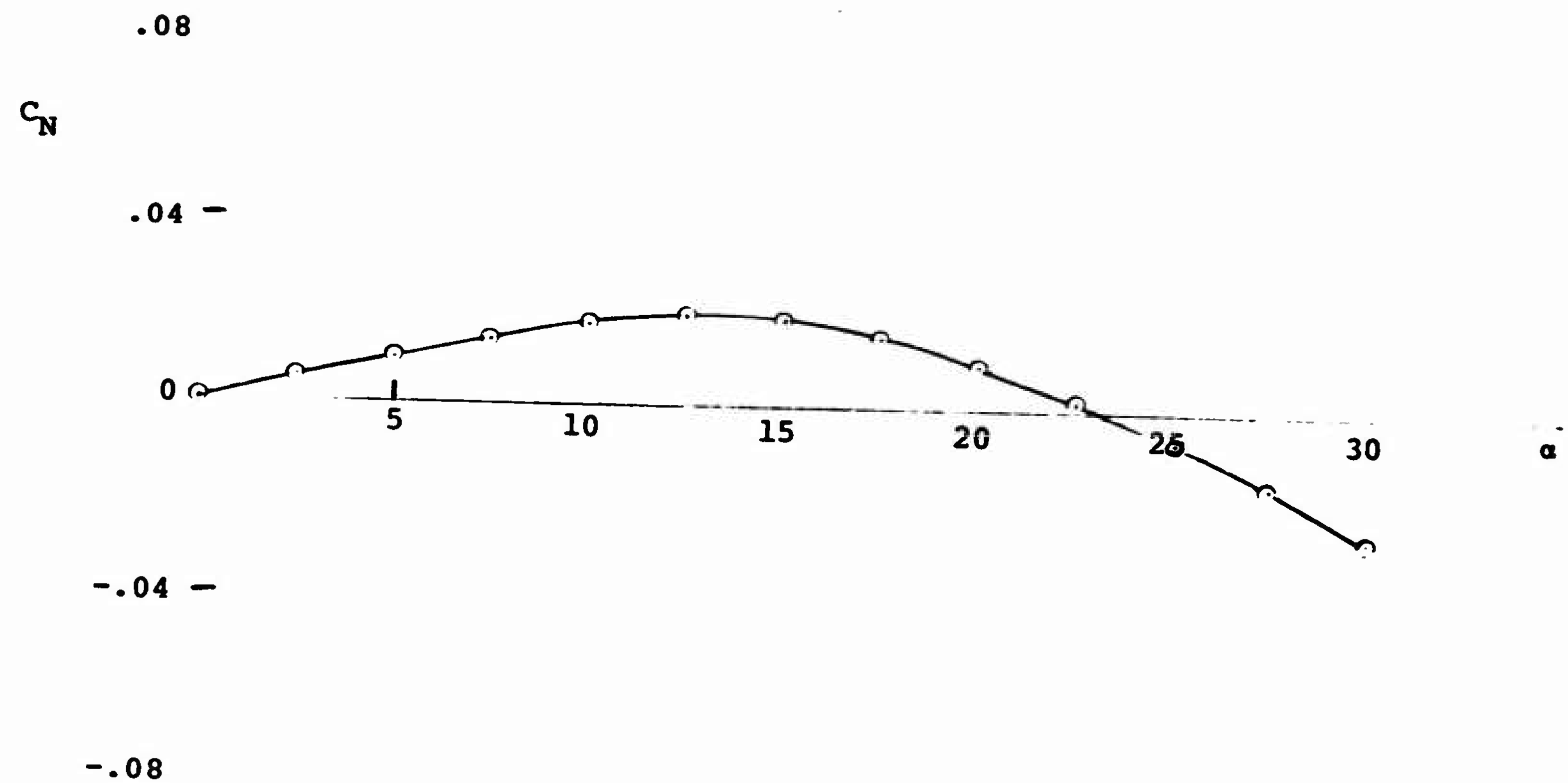

FIG. 57 C_N VALUES FOR THE T-10 PARACHUTE MODEL AT $L_C/L_S = .98$

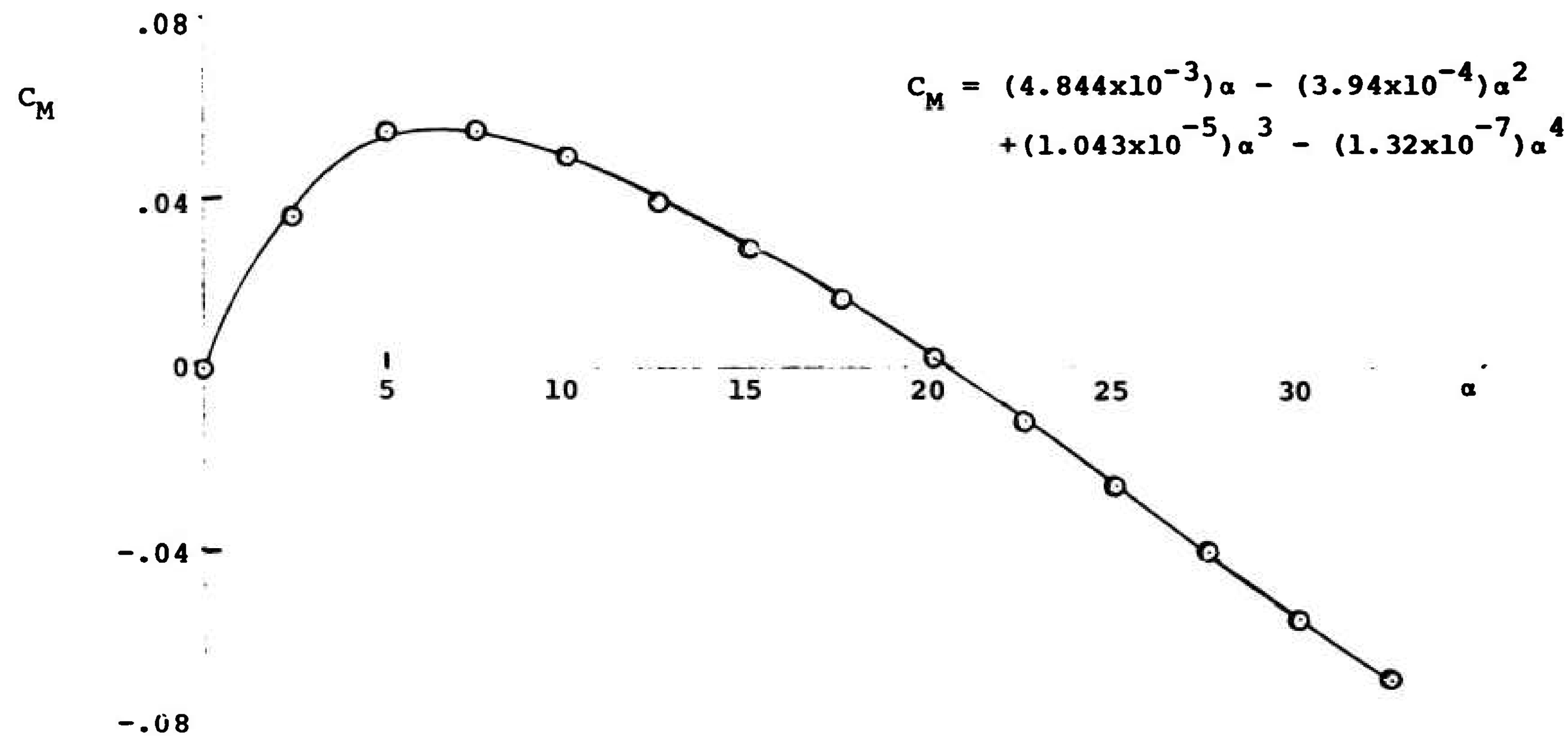

FIG. 58 C_M VALUES FOR THE T-10 PARACHUTE MODEL AT $L_C/L_S = 1.30$ (STANDARD CONFIGURATION)

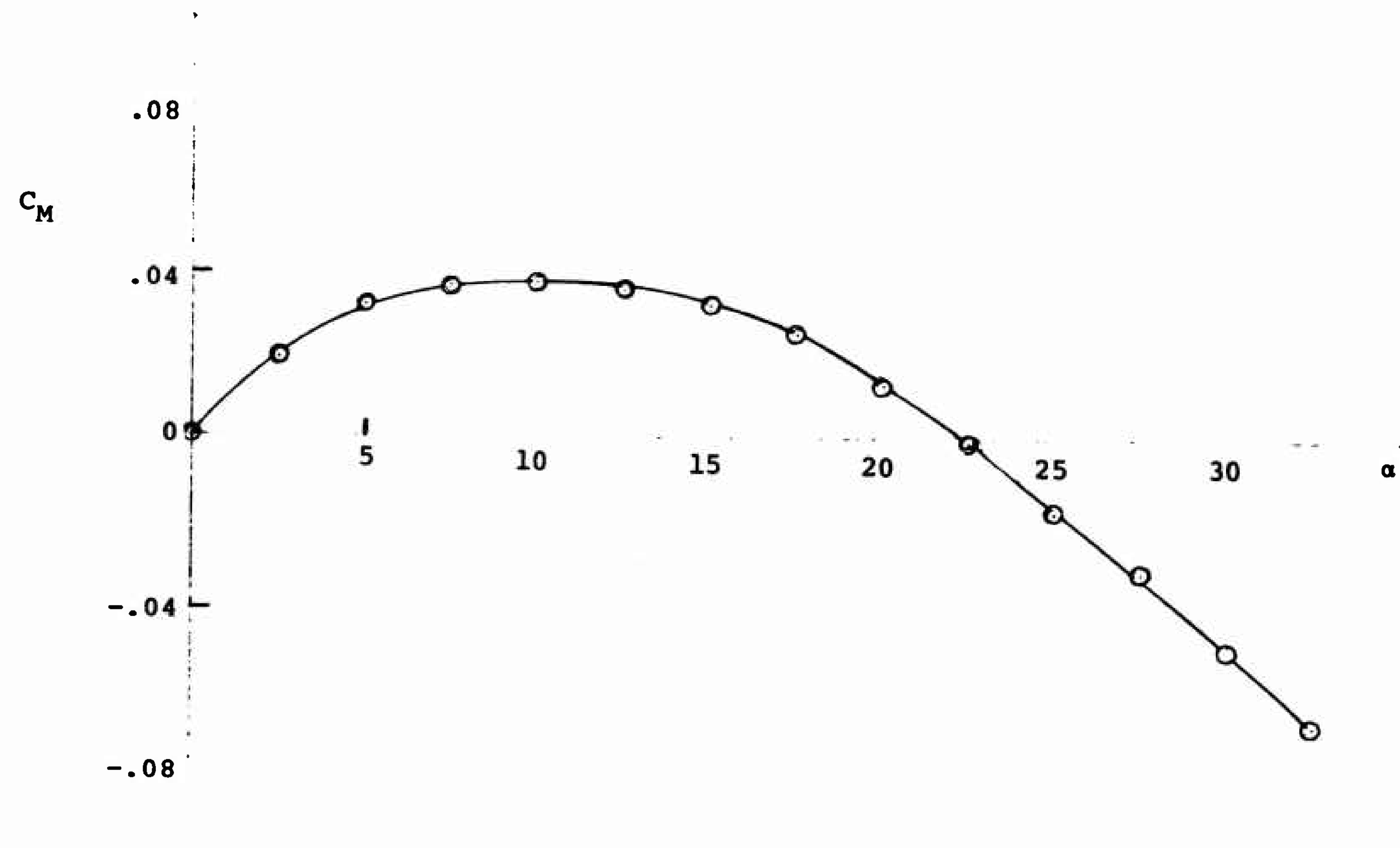

FIG. 59 C_M VALUES FOR THE T-10 PARACHUTE MODEL AT L_C/L_S = 1.24

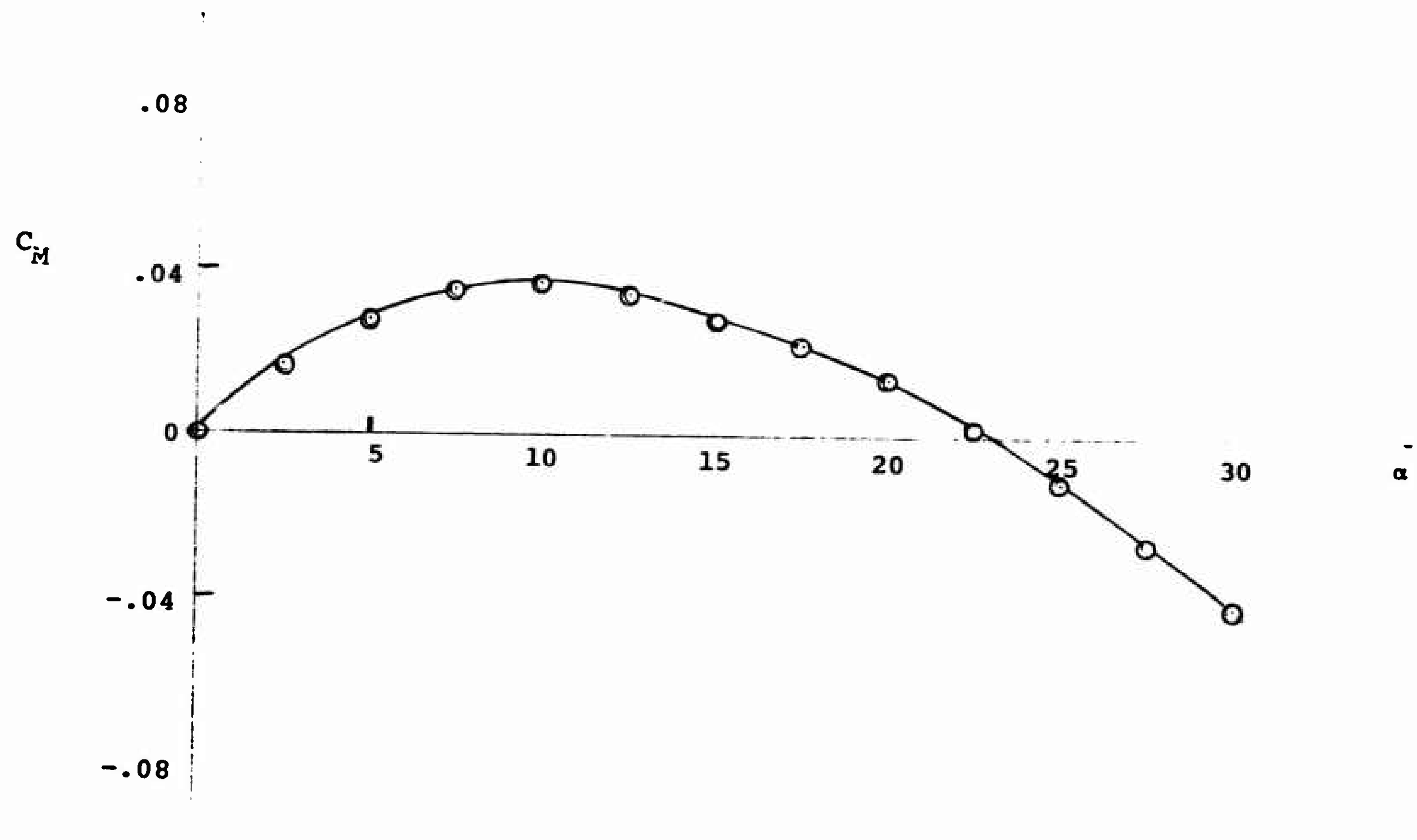

FIG. 60 C_M VALUES FOR THE T-10 PARACHUTE MODEL AT L_C/L_S = 1.18

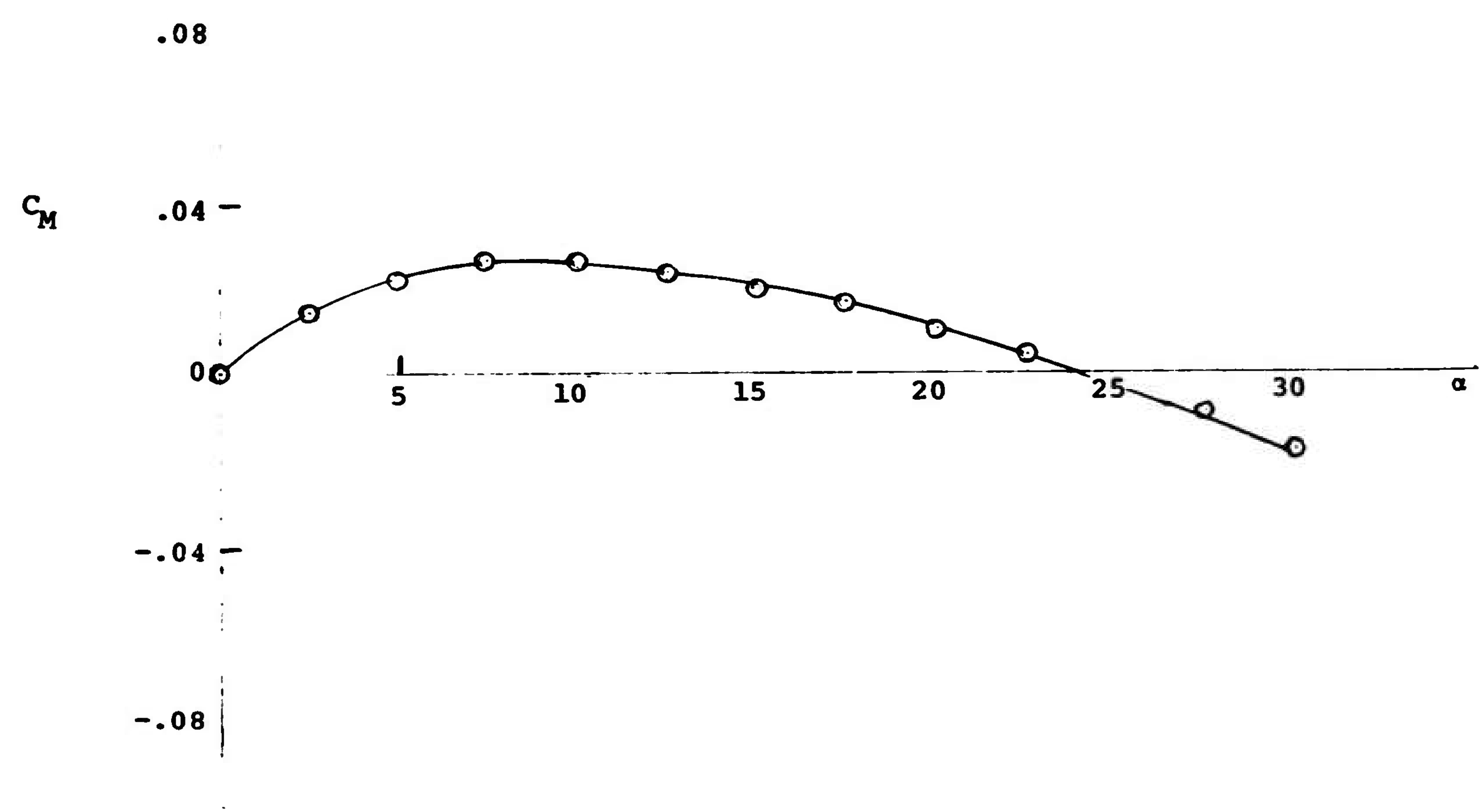

FIG. 61 C_M VALUES FOR THE T-10 PARACHUTE MODEL AT $L_C/L_S = 1.11$

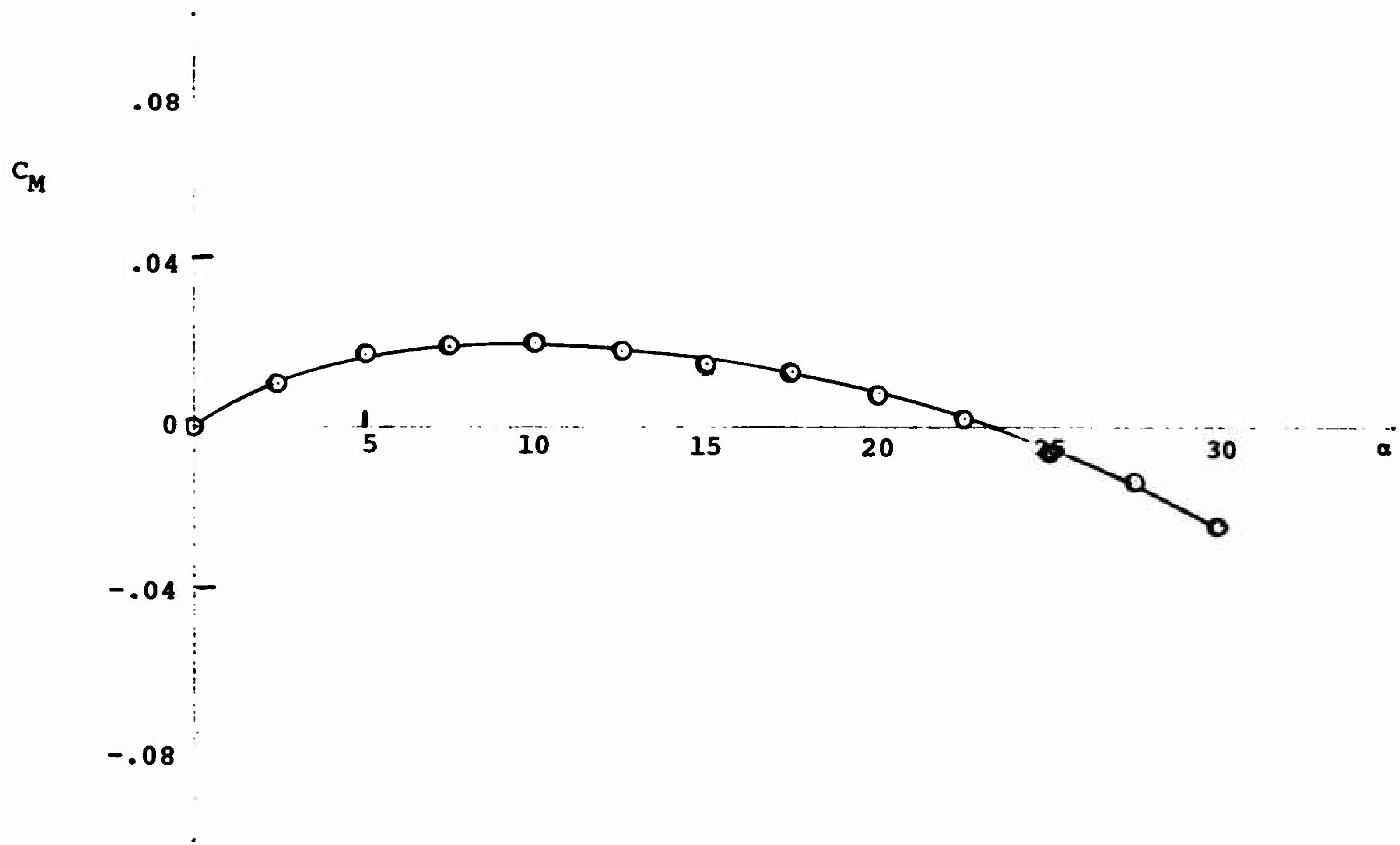

FIG. 62 C_M VALUES FOR THE T-10 PARACHUTE MODEL AT $L_C/L_S = 1.04$

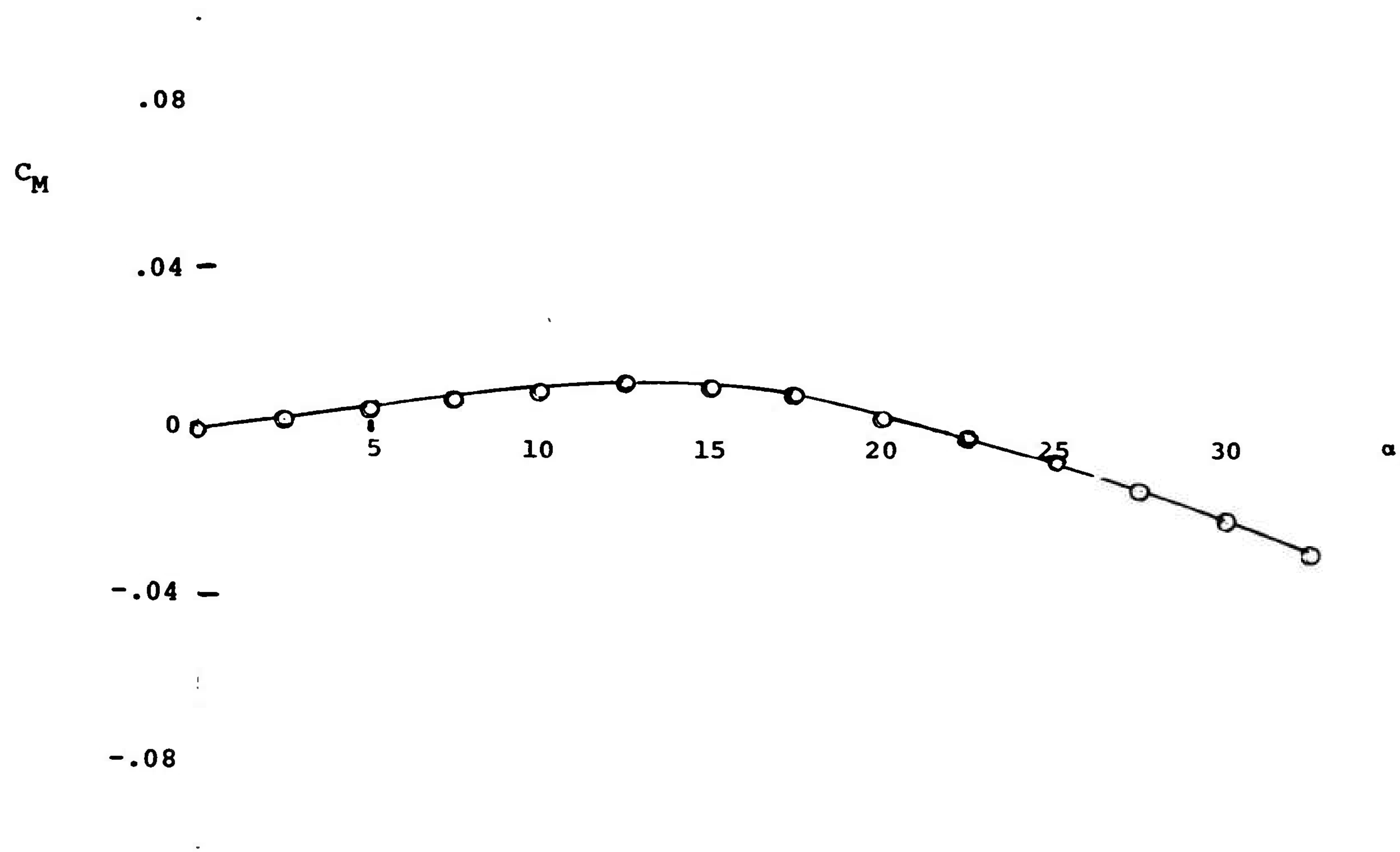

FIG. 63 C_M VALUES FOR THE T-10 PARACHUTE MODEL AT $L_C/L_S = .98$

TABLE XV

AERODYNAMIC COEFFICIENTS FOR THE RINGSLOT PARACHUTE MODEL WITH $L_C/L_S = 1.22$ (STANDARD CONFIGURATION)

$\alpha°$	C_T	C_{T_C}	C_N	C_M
0	.535	0.0	0.0	0.0
2.5	.539	.005	.0138	.007
5.0	.543	.008	.0110	.002
7.5	.557	.010	-.0049	-.013
10.0	.570	.012	-.0248	-.030
12.5	.572	.013	-.0442	-.046
15.0	.571	.016	-.0594	-.058
17.5	.566	.017	-.0718	-.070

TABLE XVI

AERODYNAMIC COEFFICIENTS FOR THE RINGSLOT PARACHUTE MODEL WITH $L_C/L_S = 1.17$

$\alpha°$	C_T	C_{T_C}	C_N	C_M
0	.605	.078	0.0	0.0
2.5	.615	.090	.0103	.005
5.0	.629	.105	.0076	-.001
7.5	.645	.120	-.0042	-.010
10.0	.657	.123	-.0214	-.023
12.5	.659	.123	-.0387	-.037
15.0	.658	.123	-.0518	-.048
17.5	.652	.124	-.0649	-.058

TABLE XVII

AERODYNAMIC COEFFICIENTS FOR THE RINGSLOT PARACHUTE MODEL WITH $L_C/L_S = 1.12$

$\alpha°$	C_T	C_{T_C}	C_N	C_M
0	.639	.143	0.0	0.0
2.5	.650	.156	.0103	.004
5.0	.666	.172	.0056	-.003
7.5	.680	.185	-.0062	-.013
10.0	.694	.193	-.0228	-.023
12.5	.697	.194	-.0387	-.034
15.0	.695	.193	-.0511	-.044
17.5	.670	.193	-.0635	-.056

TABLE XVIII

AERODYNAMIC COEFFICIENTS FOR THE RINGSLOT PARACHUTE MODEL WITH $L_C/L_S = 1.07$

α°	C_T	C_{T_C}	C_N	C_M
0	.662	.203	0.0	0.0
2.5	.674	.218	-.0020	-.008
5.0	.680	.230	-.0062	-.013
7.5	.688	.242	-.0138	-.018
10.0	.703	.253	-.0255	-.024
12.5	.709	.256	-.0387	-.033
15.0	.705	.253	-.0578	-.044
17.5	.697	.249	-.0663	-.055

TABLE XIX

AERODYNAMIC COEFFICIENTS FOR THE
RINGSLOT PARACHUTE MODEL WITH L_C/L_S = 1.02

α°	C_T	C_{T_C}	C_N	C_M
0	.672	.259	0.0	0.0
2.5	.677	.267	-.0076	-.012
5.0	.677	.279	-.0125	-.018
7.5	.683	.289	-.0179	-.021
10.0	.694	.296	-.0262	-.024
12.5	.699	.301	-.0366	-.032
15.0	.699	.301	-.0476	-.040
17.5	.694	.297	-.0601	-.049

TABLE XX

AERODYNAMIC COEFFICIENTS FOR THE
RINGSLOT PARACHUTE MODEL WITH $L_C/L_S = 0.$[illegible]7

$\alpha°$	C_T	C_{T_C}	C_N	C_M
0	.652	.280	0.0	0.0
2.5	.649	.283	-.0172	-.018
5.0	.642	.289	-.0235	-.023
7.5	.647	.296	-.0235	-.023
10.0	.654	.301	-.0290	-.026
12.5	.656	.301	-.0393	-.032
15.0	.651	.298	-.0504	-.039
17.5	.642	.293	-.0621	-.048

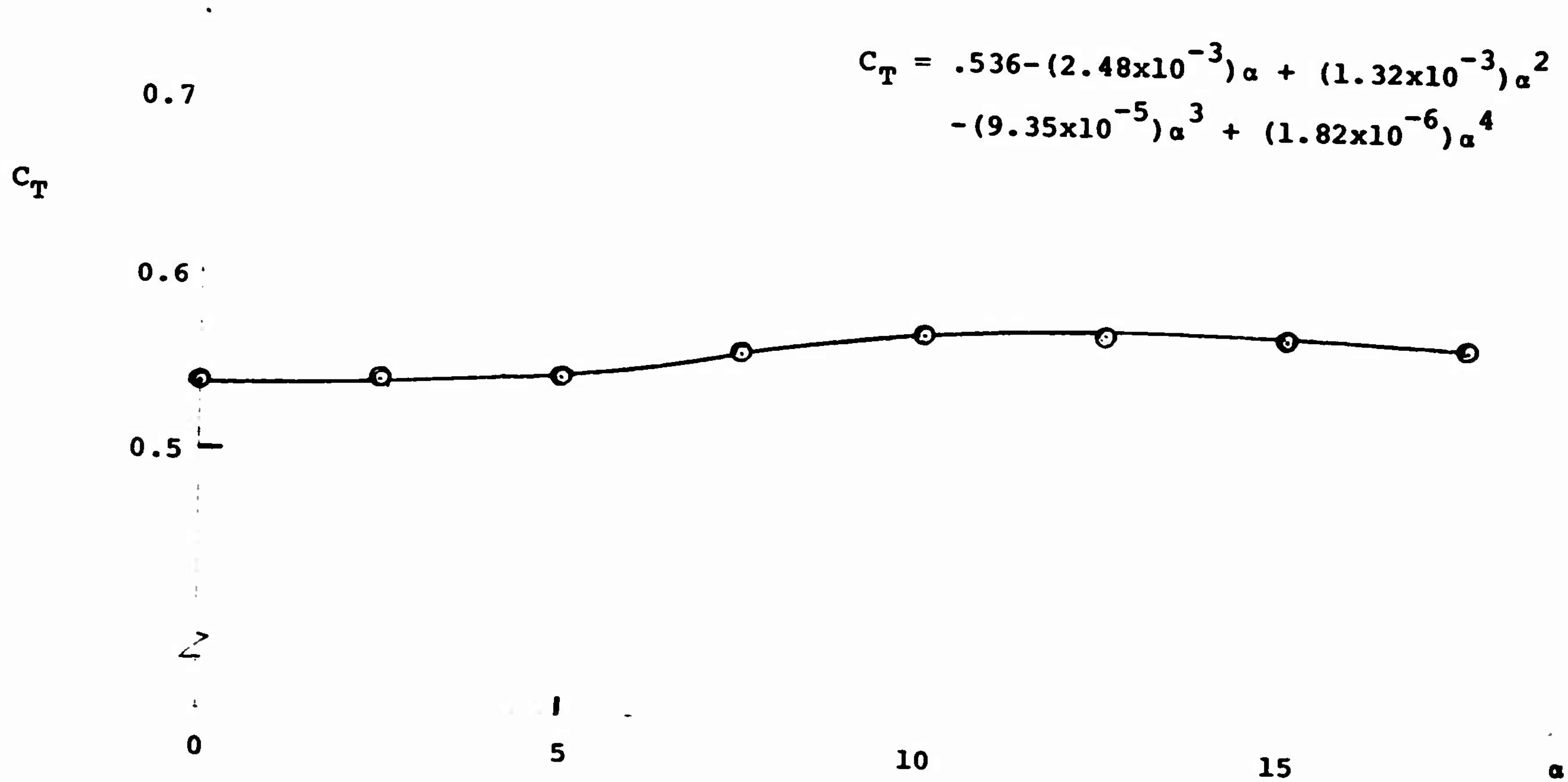

$$C_T = .536-(2.48x10^{-3})\alpha + (1.32x10^{-3})\alpha^2 -(9.35x10^{-5})\alpha^3 + (1.82x10^{-6})\alpha^4$$

FIG. 64 C_T VALUES FOR THE RINGSLOT PARACHUTE MODEL AT L_C/L_S = 1.22 (STANDARD CONFIGURATION)

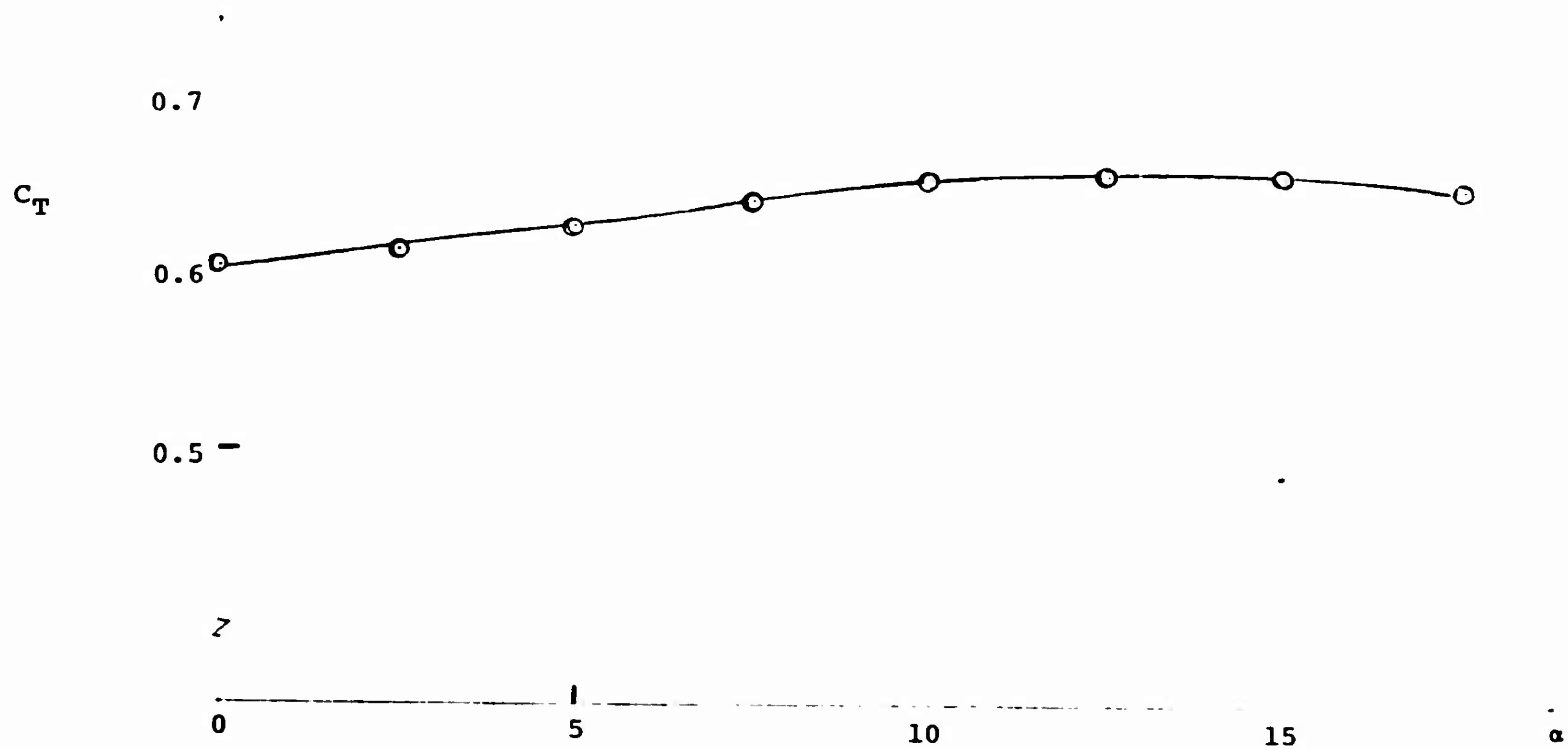

FIG. 65 C_T VALUES FOR THE RINGSLOT PARACHUTE MODEL AT $L_c/L_s = 1.17$

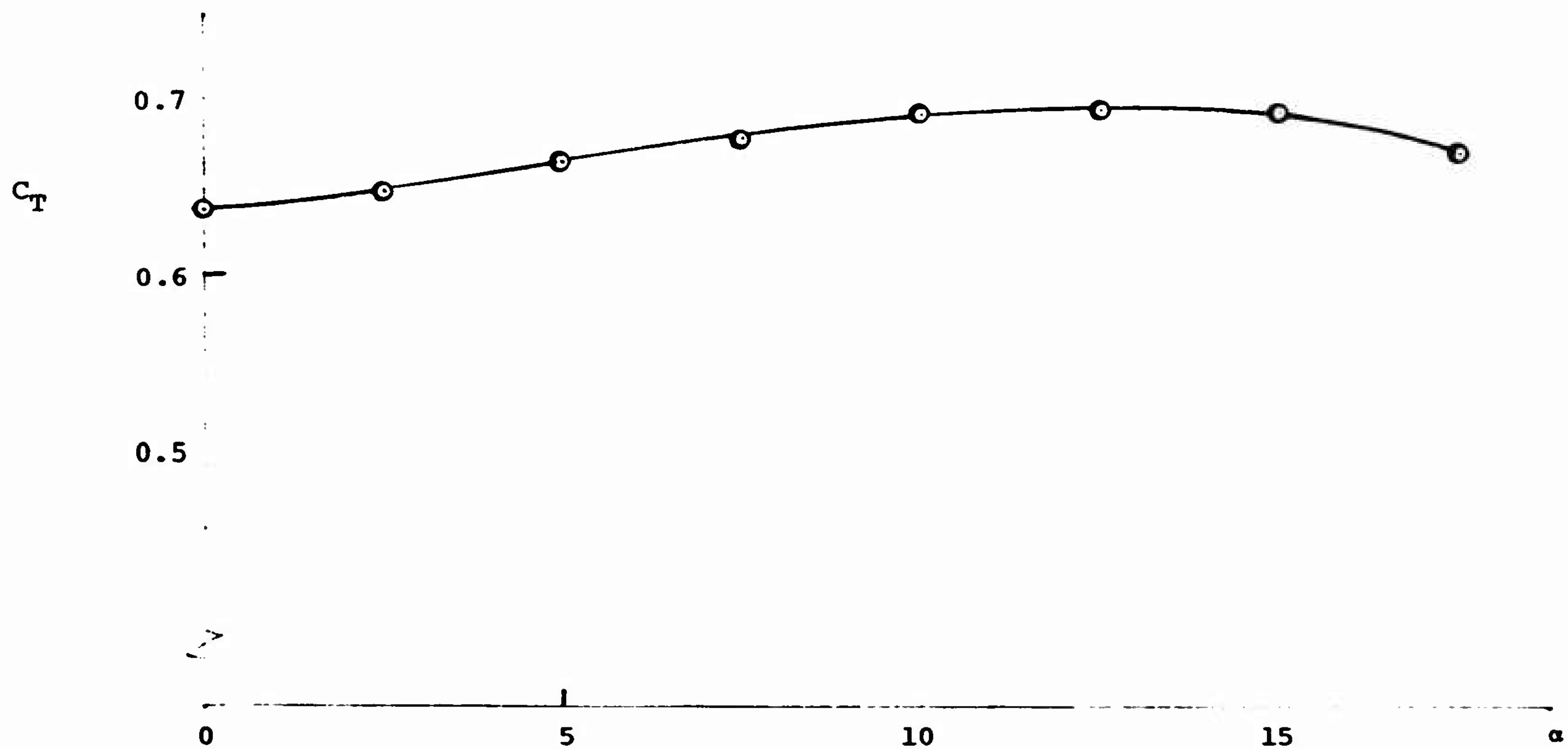

FIG. 66 C_T VALUES FOR THE RINGSLOT PARACHUTE MODEL AT L_c/L_s = 1.12

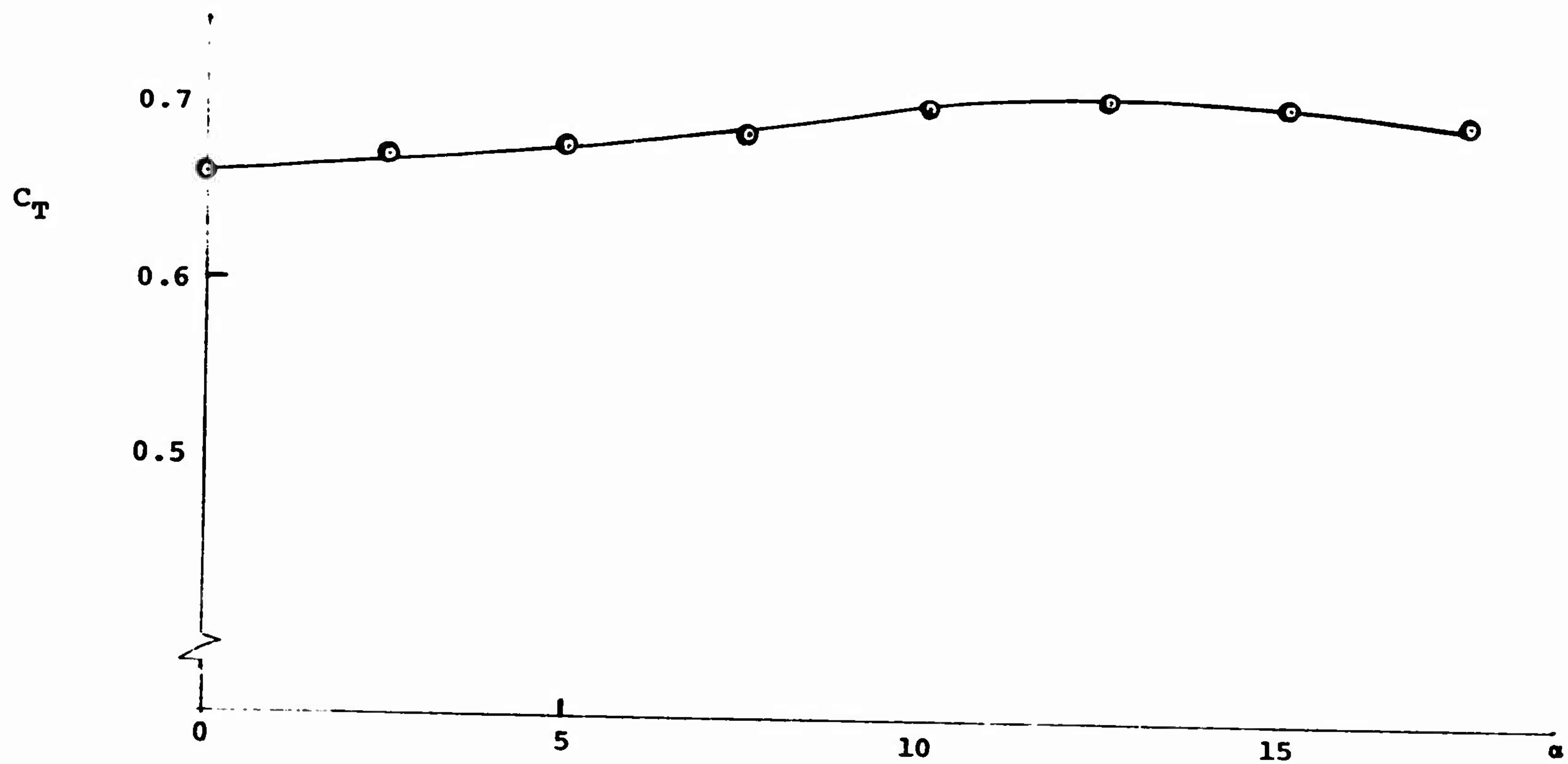

FIG. 67 C_T VALUES FOR THE RINGSLOT PARACHUTE MODEL AT L_c/L_s = 1.07

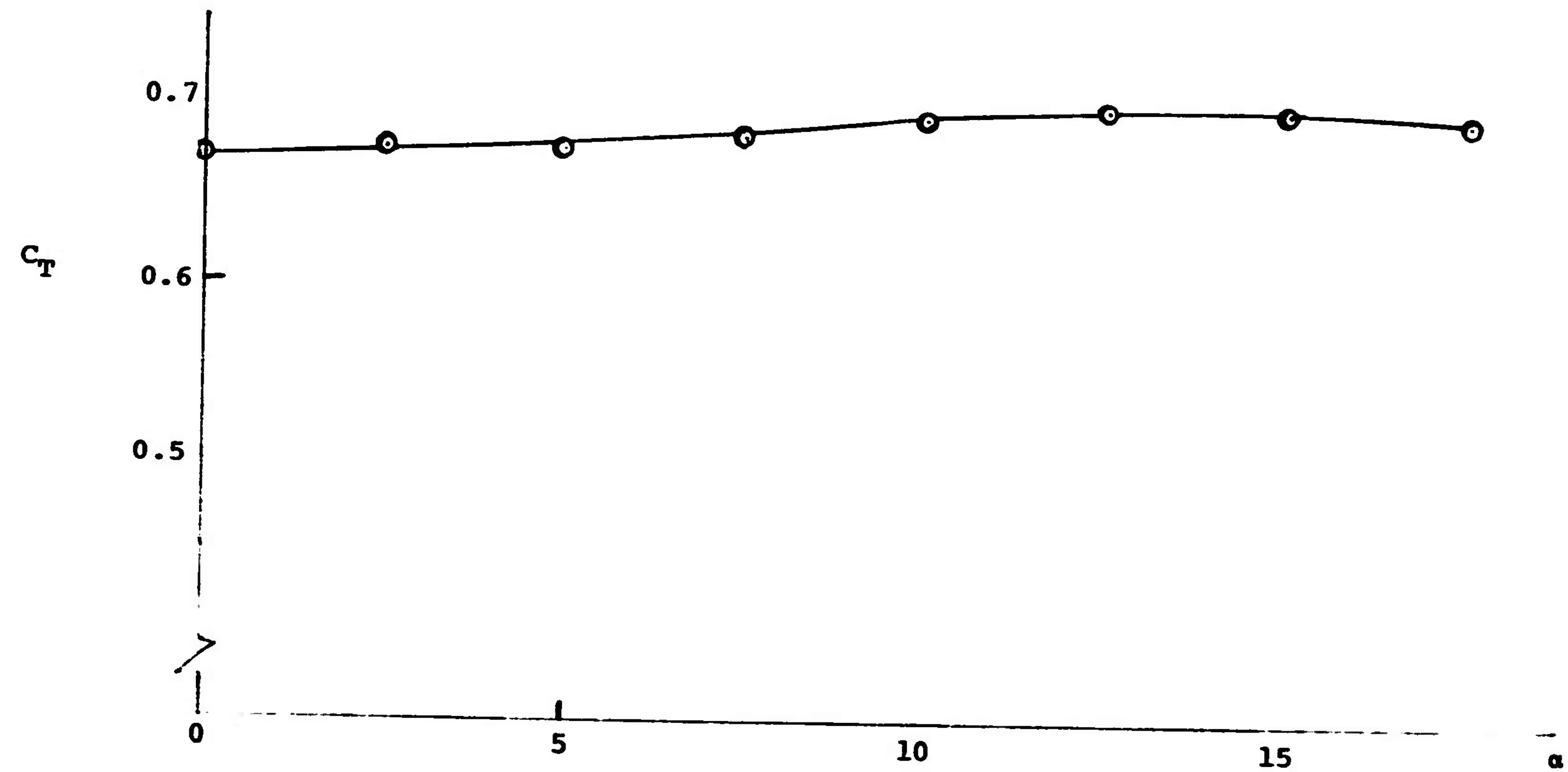

FIG. 68 C_T VALUES FOR THE RINGSLOT PARACHUTE MODEL AT L_C/L_S = 1.02

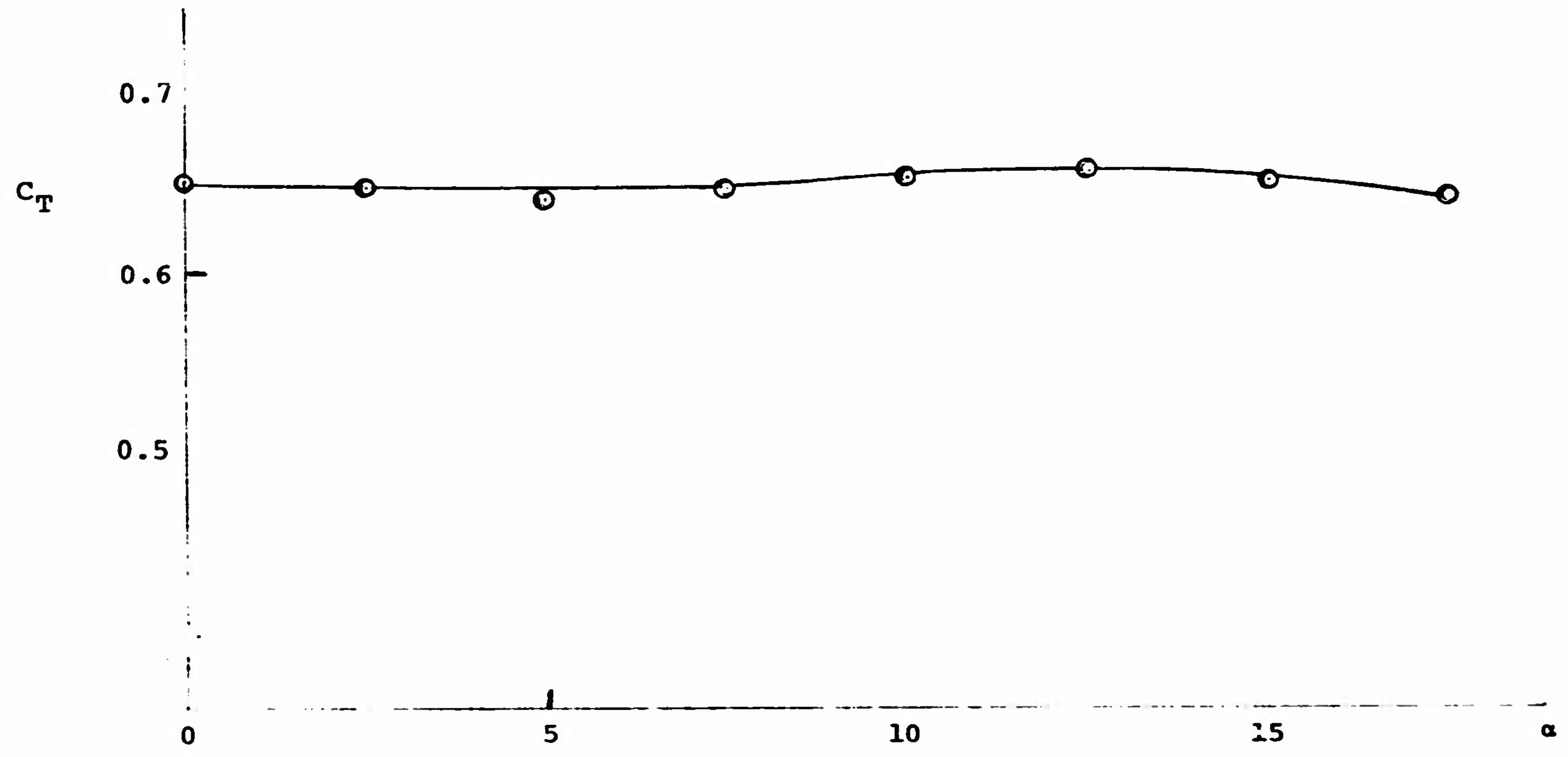

FIG. 69 C_T VALUES FOR THE RINGSLOT PARACHUTE MODEL AT $L_C/L_S = 0.97$

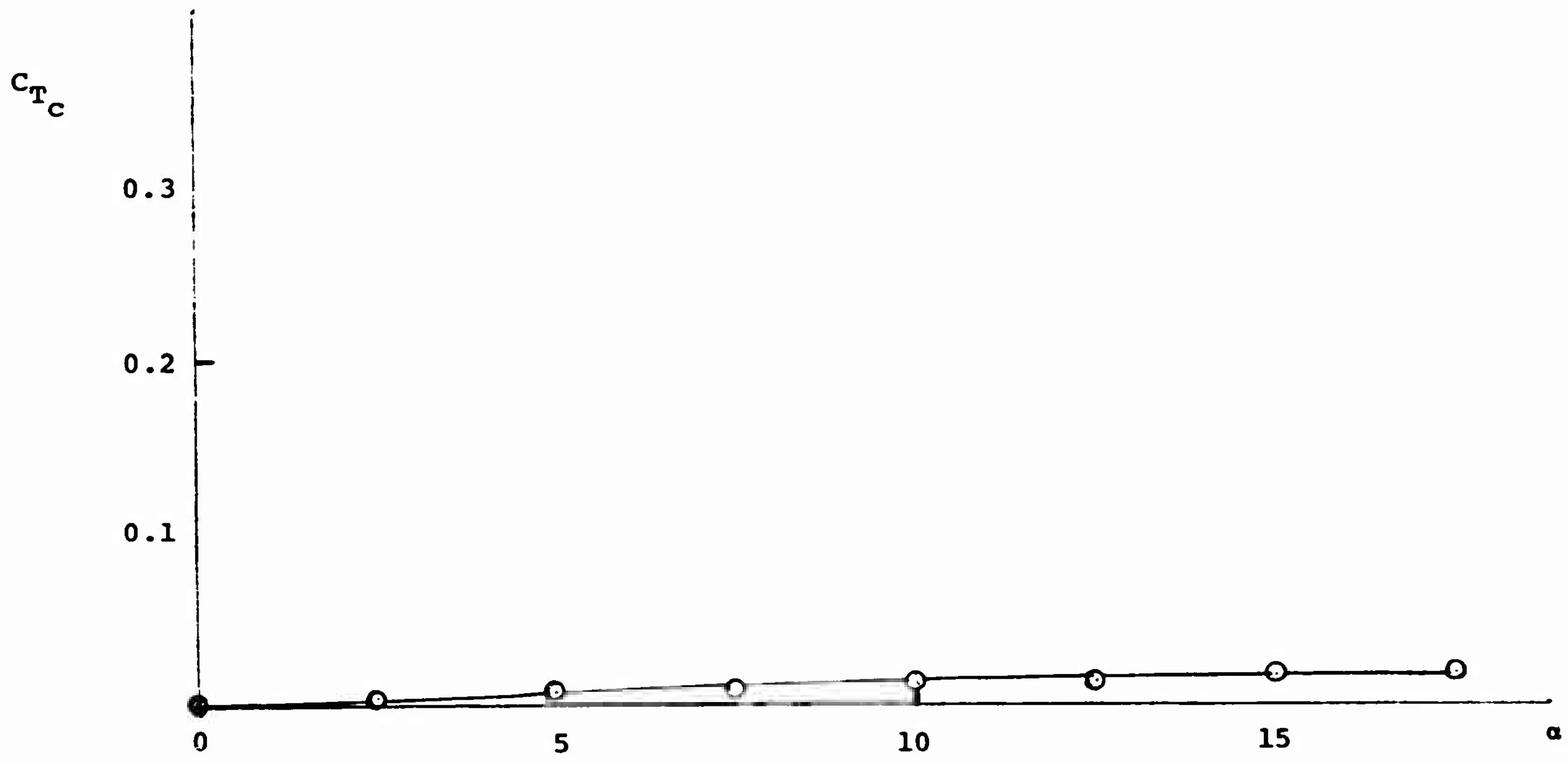

FIG. 70 C_{T_C} VALUES FOR THE RINGSLOT PARACHUTE MODEL AT $L_C/L_S = 1.22$ (STANDARD CONFIGURATION)

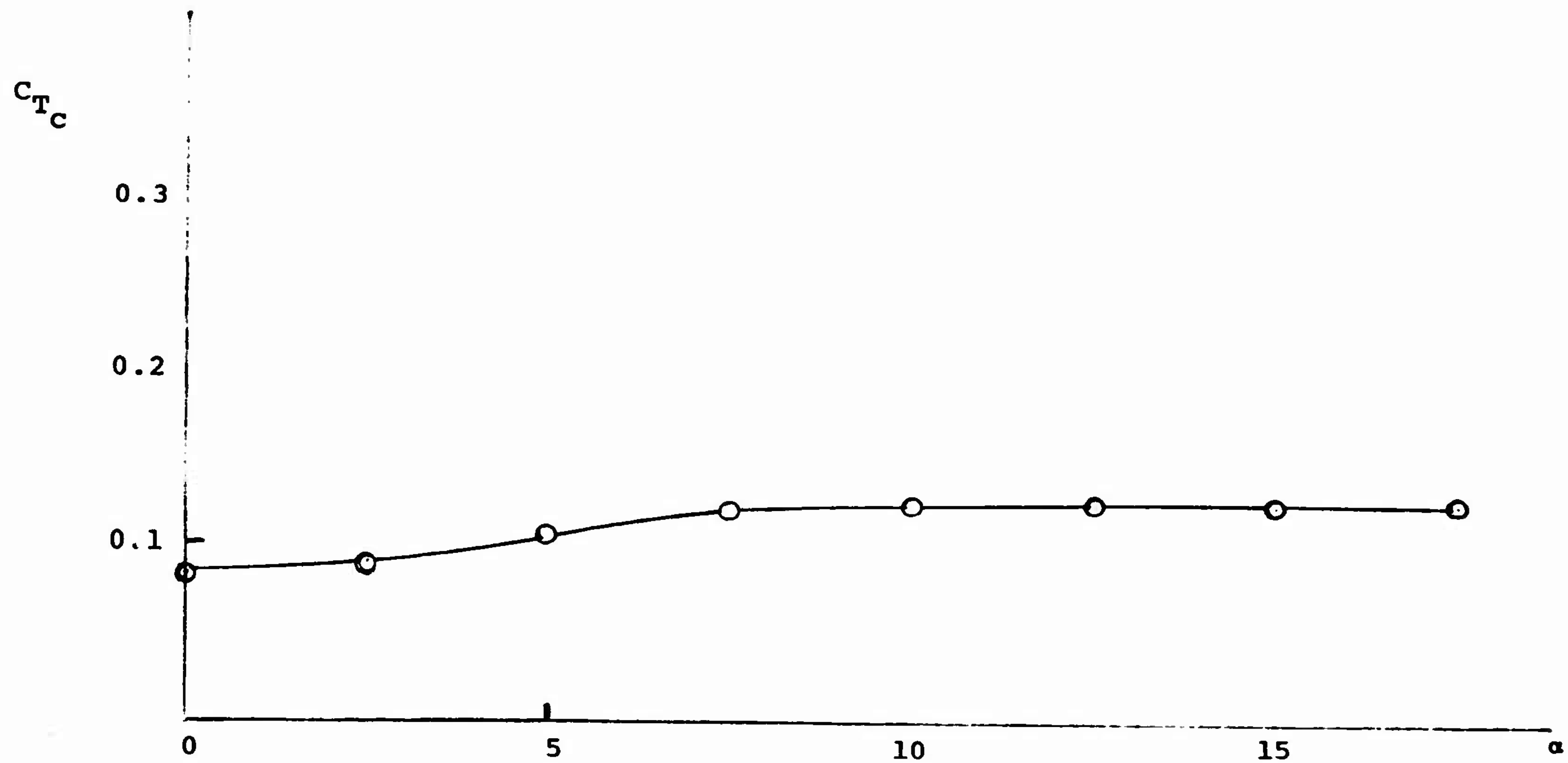

FIG. 71 C_{T_c} VALUES FOR THE RINGSLOT PARACHUTE MODEL AT $L_c/L_s = 1.17$

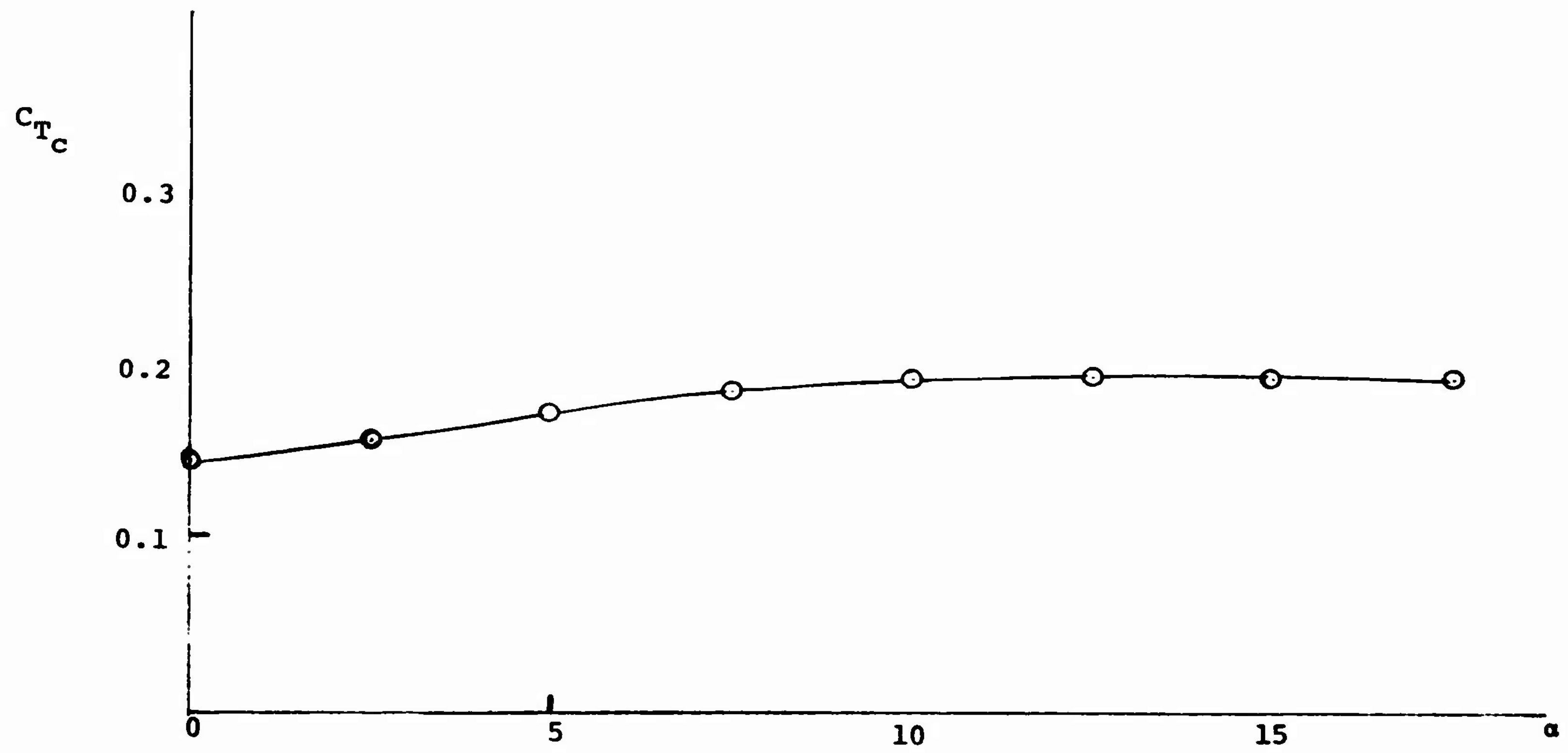

FIG. 72 C_{T_C} VALUES FOR THE RINGSLOT PARACHUTE MODEL AT $L_C/L_S = 1.12$

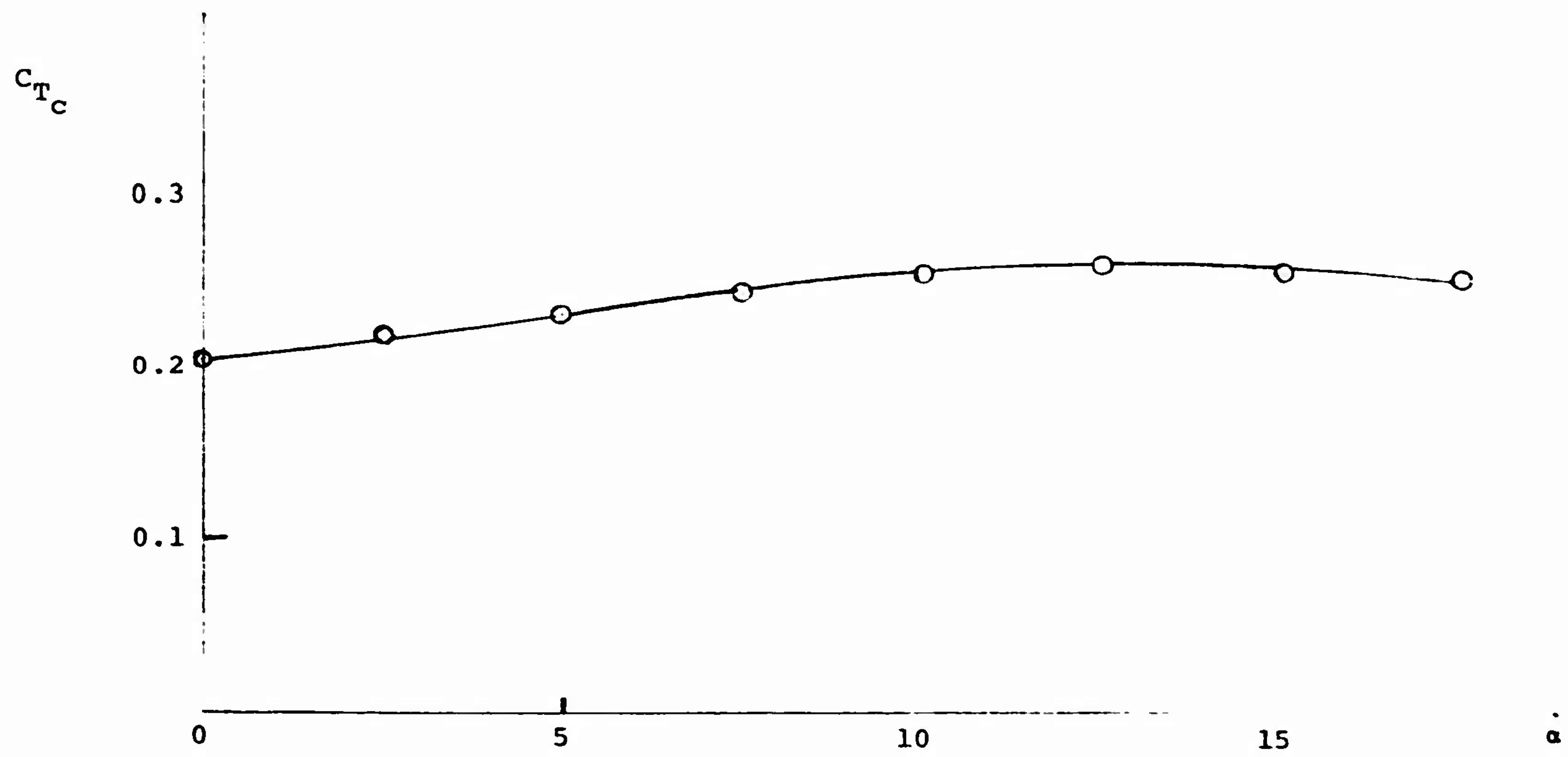

FIG. 73 C_{T_C} VALUES FOR THE RINGSLOT PARACHUTE MODEL AT $L_C/L_S = 1.07$

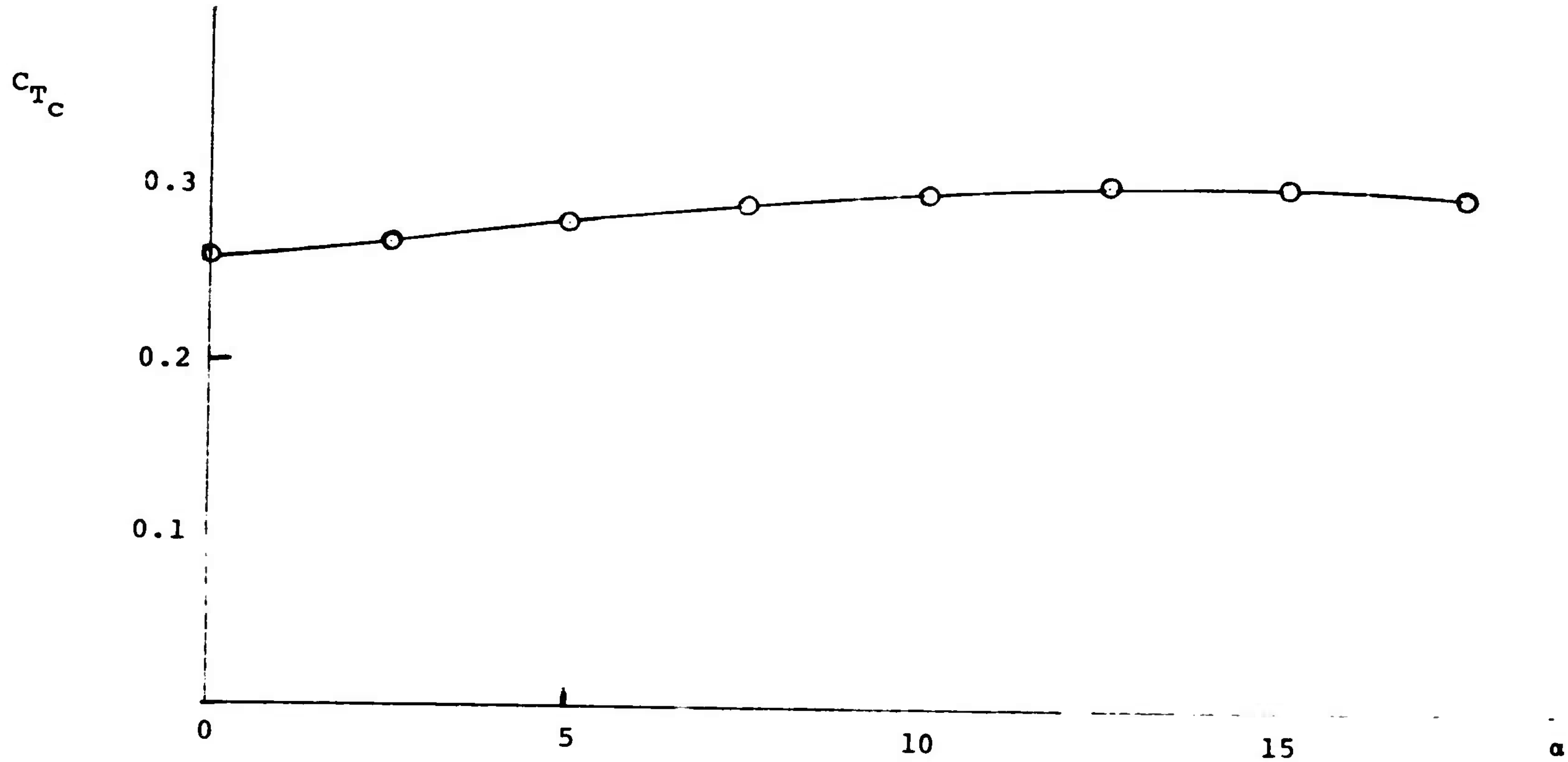

FIG. 74 C_{T_C} VALUES FOR THE RINGSLOT PARACHUTE MODEL AT $L_C/L_S = 1.02$

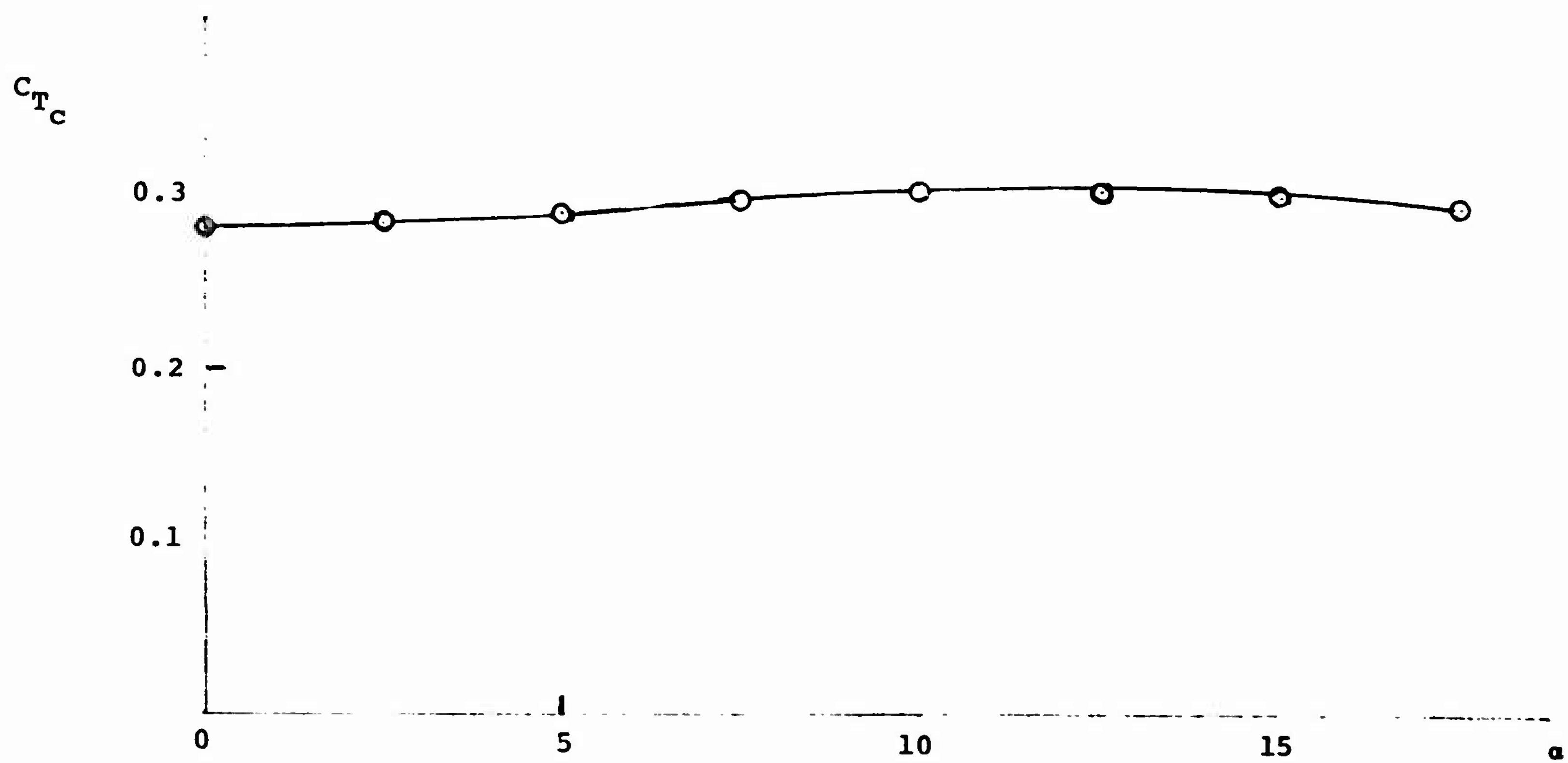

FIG. 75 C_{T_C} VALUES FOR THE RINGSLOT PARACHUTE MODEL AT L_C/L_S = 0.97

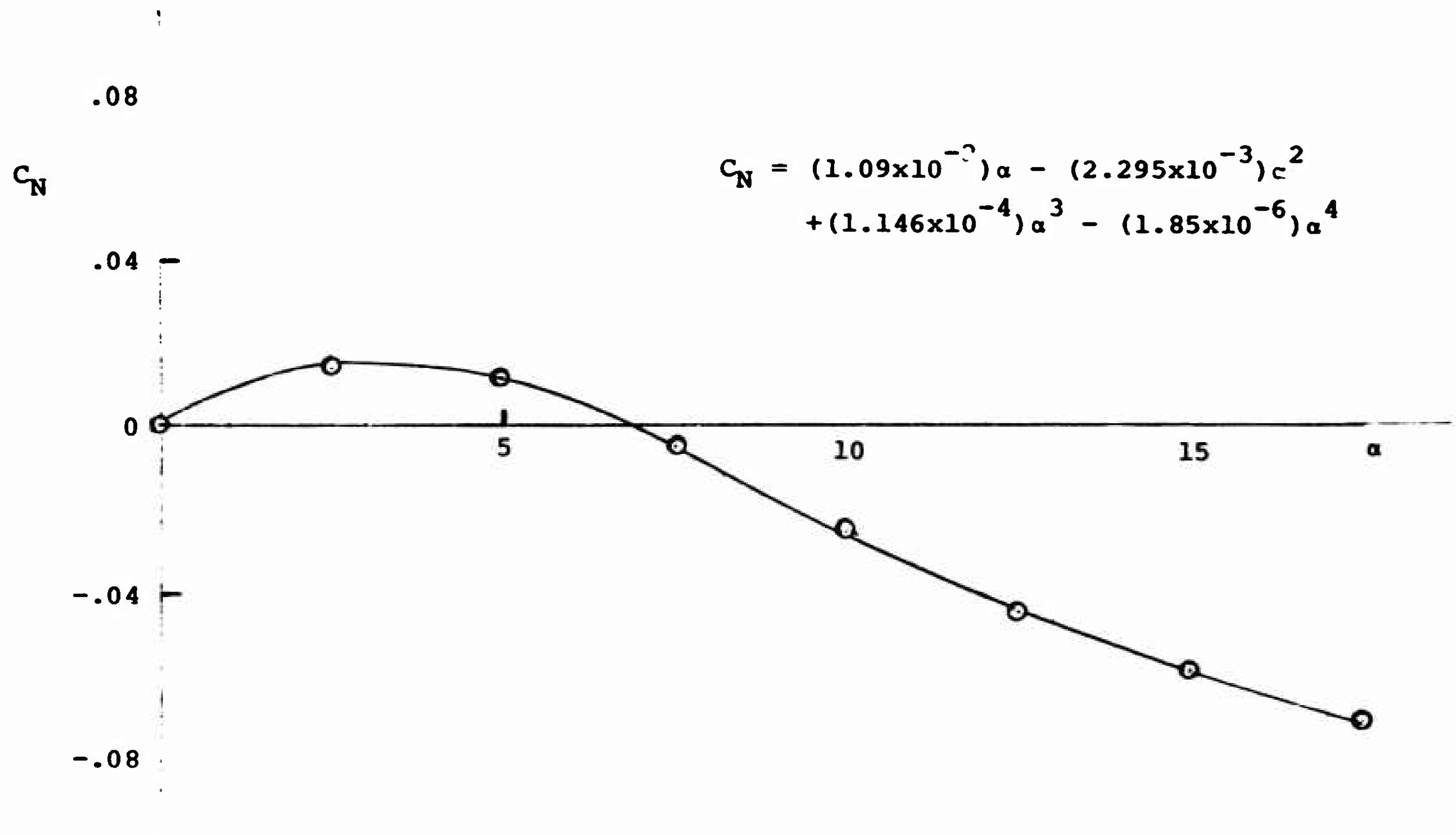

FIG. 76 C_N VALUES FOR THE RINGSLOT PARACHUTE MODEL AT L_C/L_S = 1.22 (STANDARD CONFIGURATION)

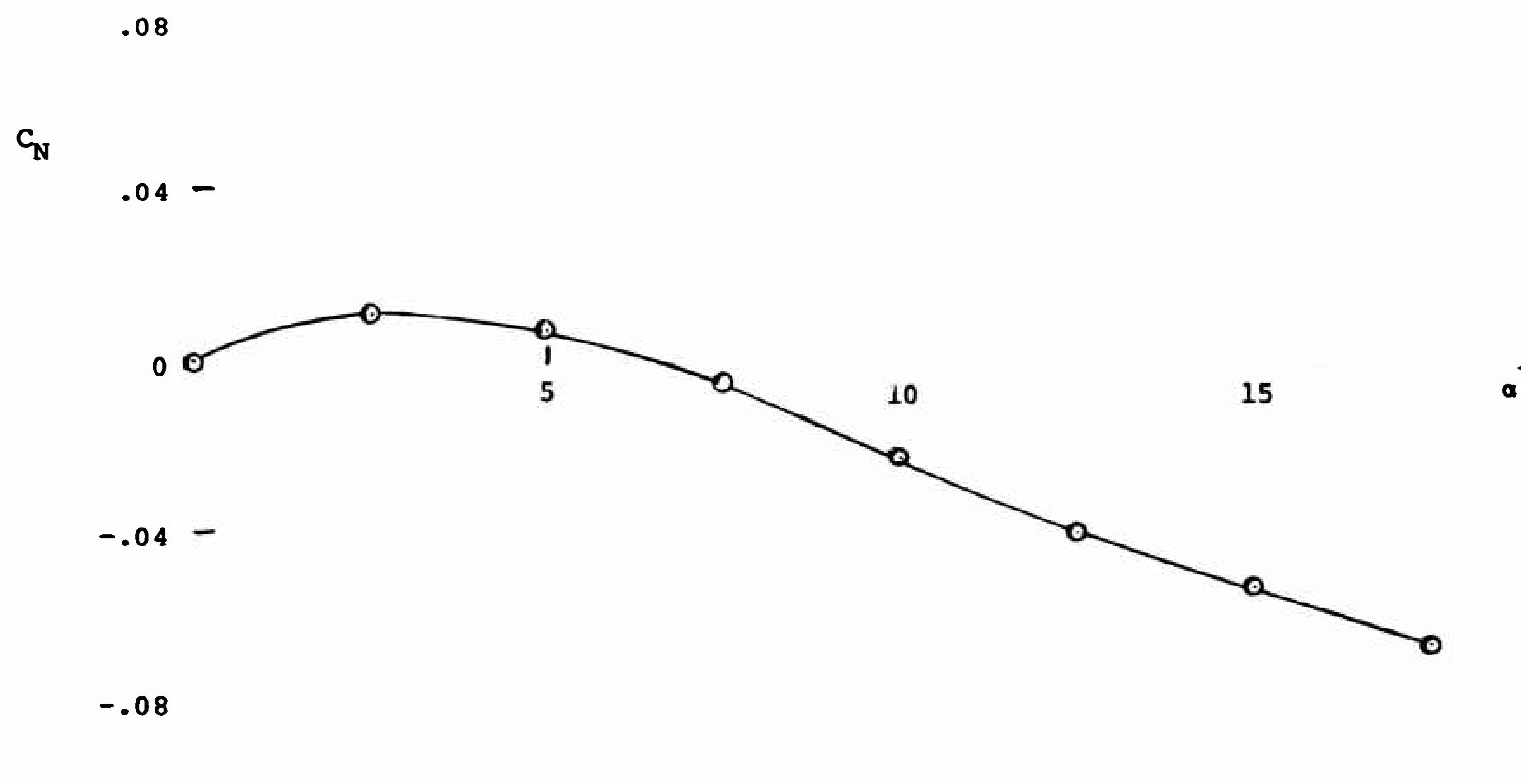

FIG. 77 C_N VALUES FOR THE RINGSLOT PARACHUTE MODEL AT $L_C/L_S = 1.17$

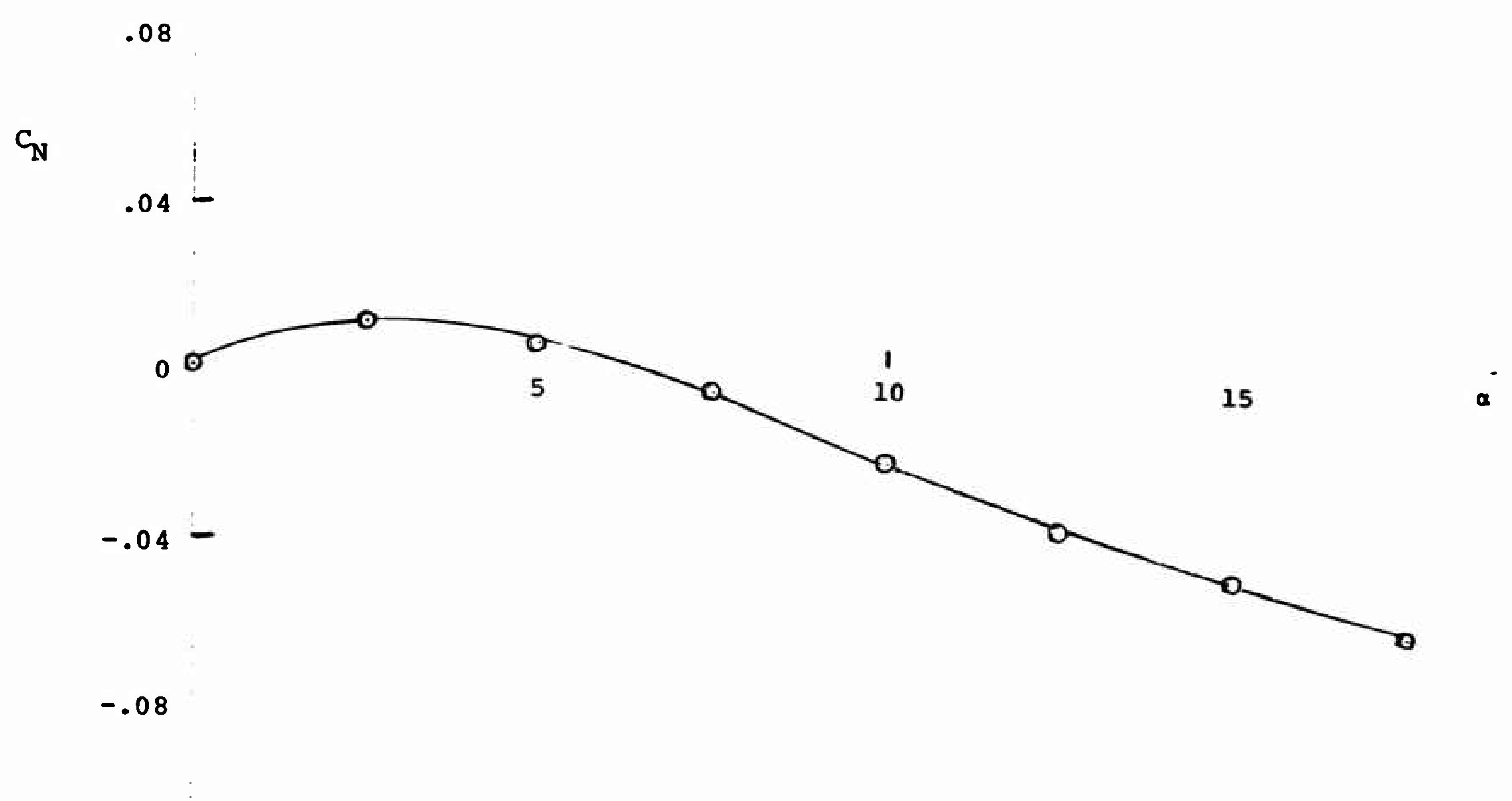

FIG. 78 C_N VALUES FOR THE RINGSLOT PARACHUTE MODEL AT $L_C/L_S = 1.12$

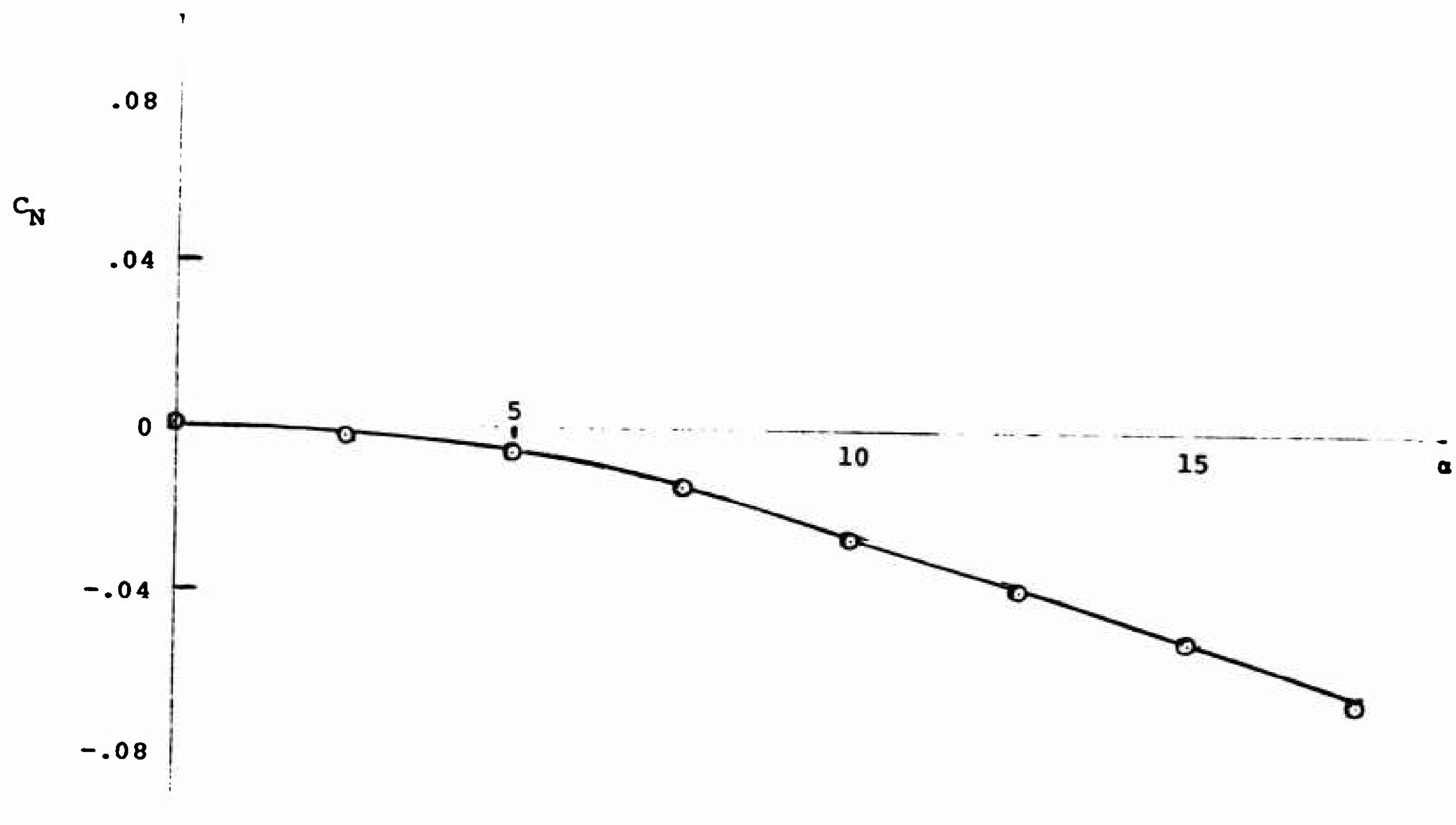

FIG. 79 C_N VALUES FOR THE RINGSLOT PARACHUTE MODEL AT L_C/L_S = 1.07

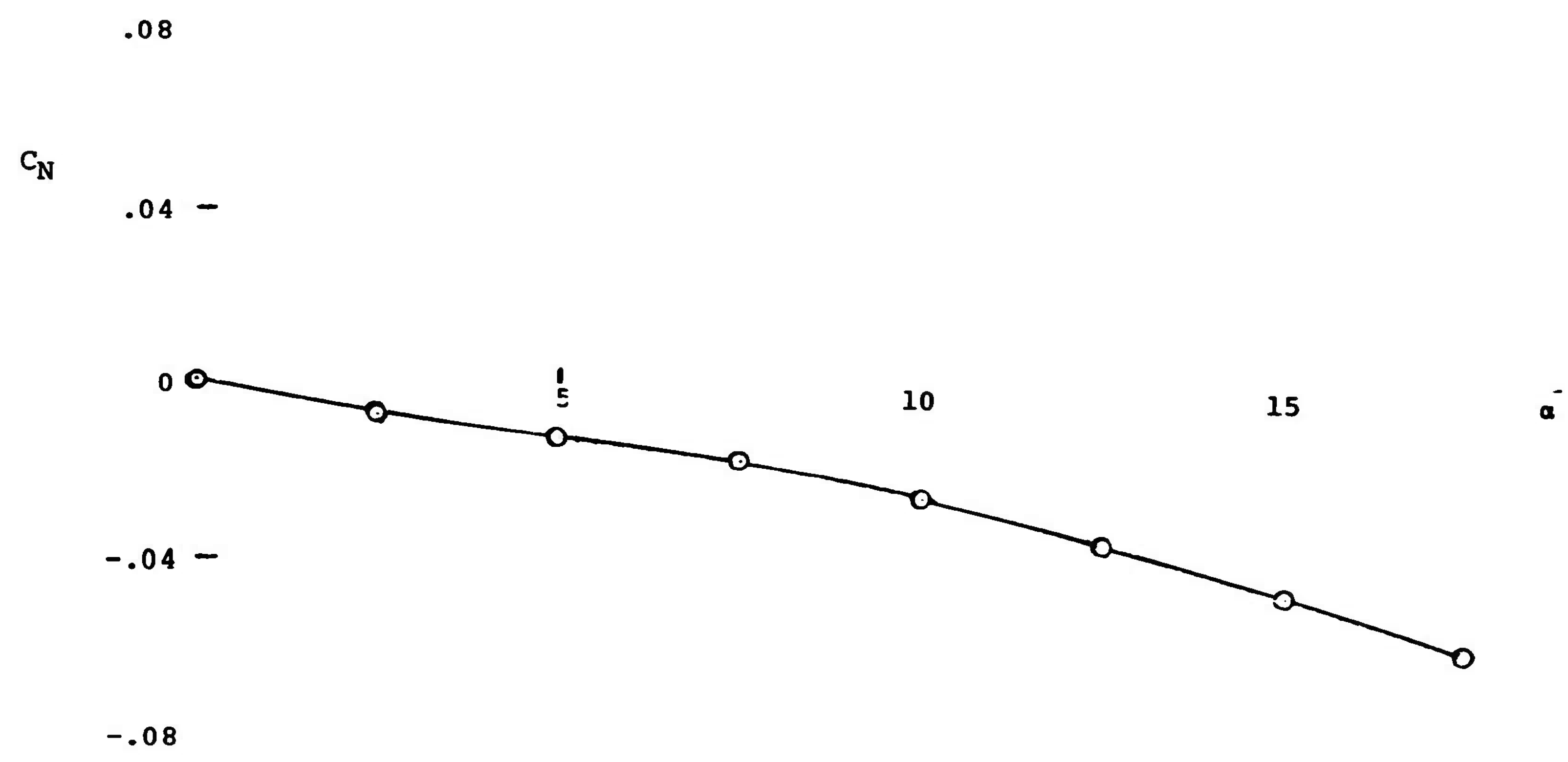

FIG. 80 C_N VALUES FOR THE RINGSLOT PARACHUTE MODEL AT $L_c/L_s = 1.02$

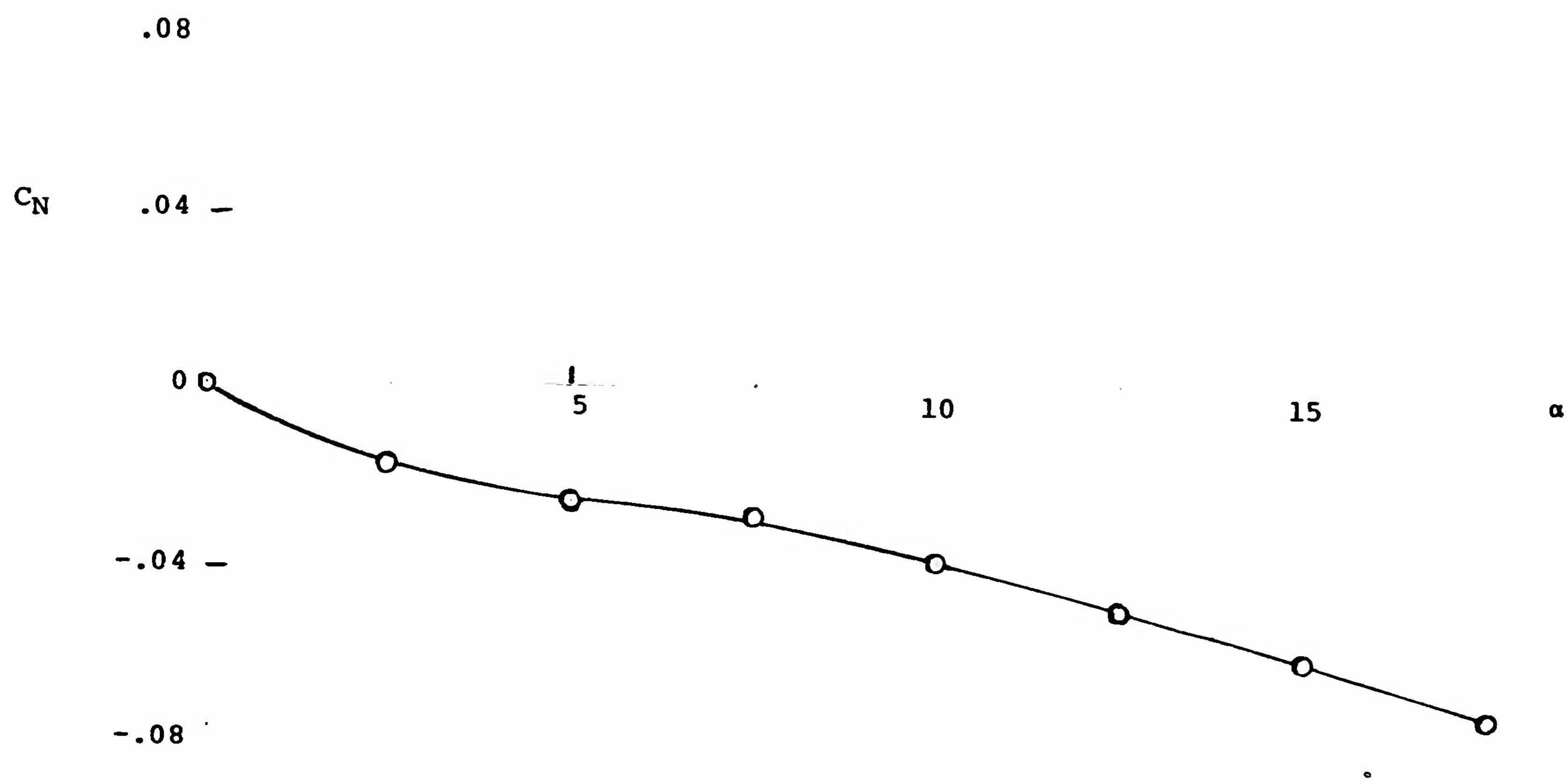

FIG. 81 C_N VALUES FOR THE RINGSLOT PARACHUTE MODEL AT L_C/L_S = .97

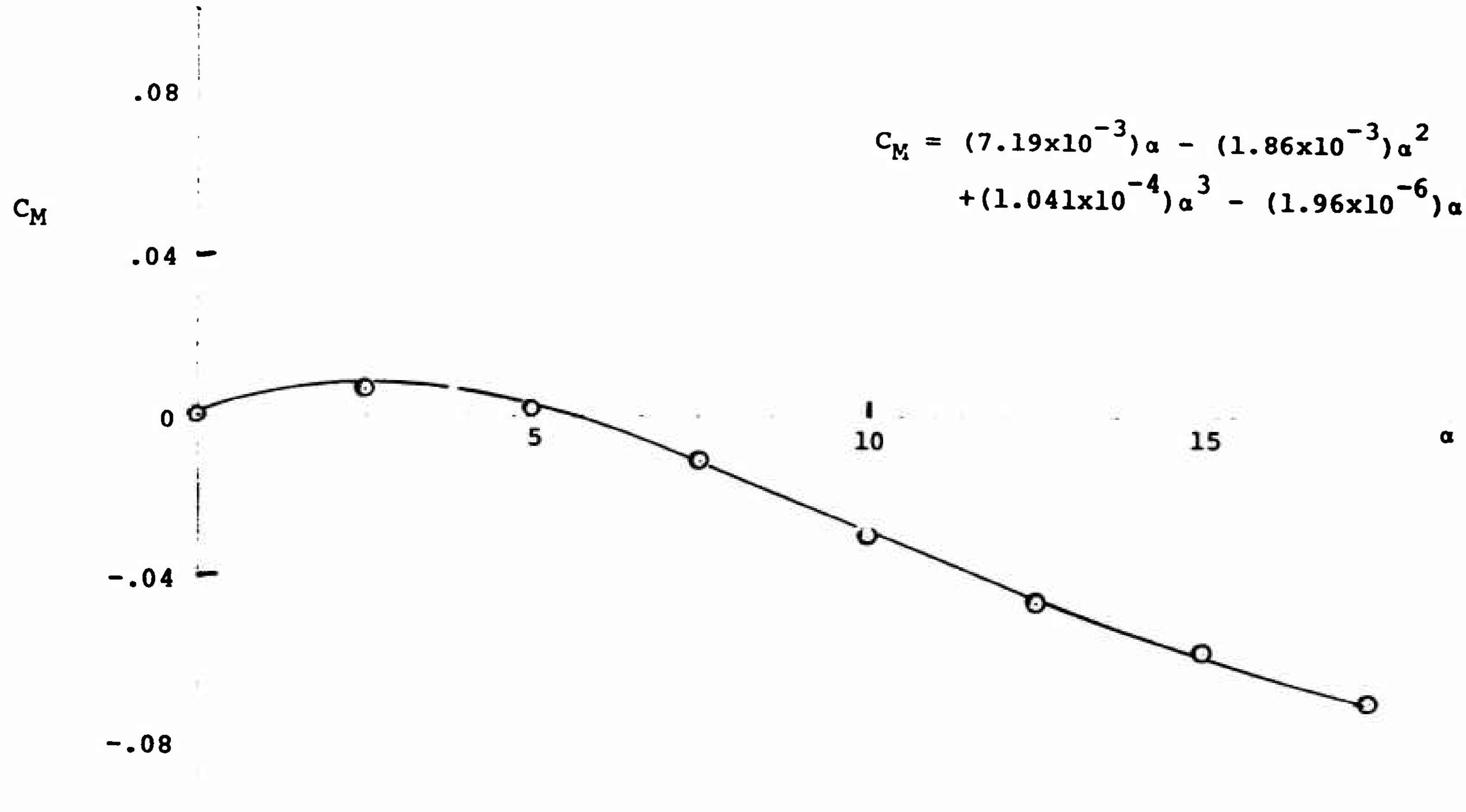

$$C_M = (7.19\times10^{-3})\alpha - (1.86\times10^{-3})\alpha^2 + (1.041\times10^{-4})\alpha^3 - (1.96\times10^{-6})\alpha^4$$

FIG. 82 C_M VALUES FOR THE RINGSLOT PARACHUTE MODEL AT $L_C/L_S = 1.22$ (STANDARD CONFIGURATION)

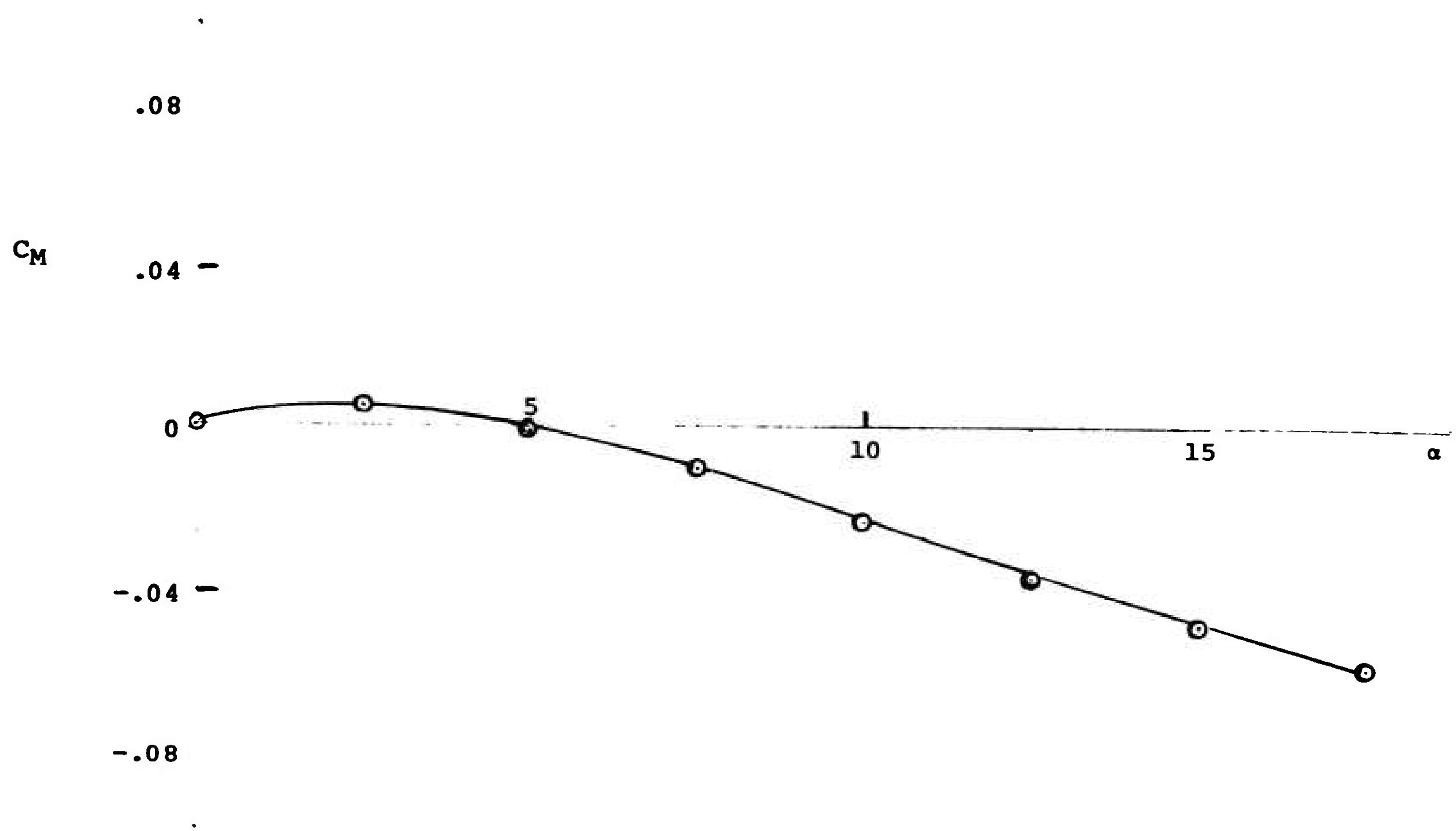

FIG. 83 C_M VALUES FOR THE RINGSLOT PARACHUTE MODEL AT L_C/L_S = 1.17

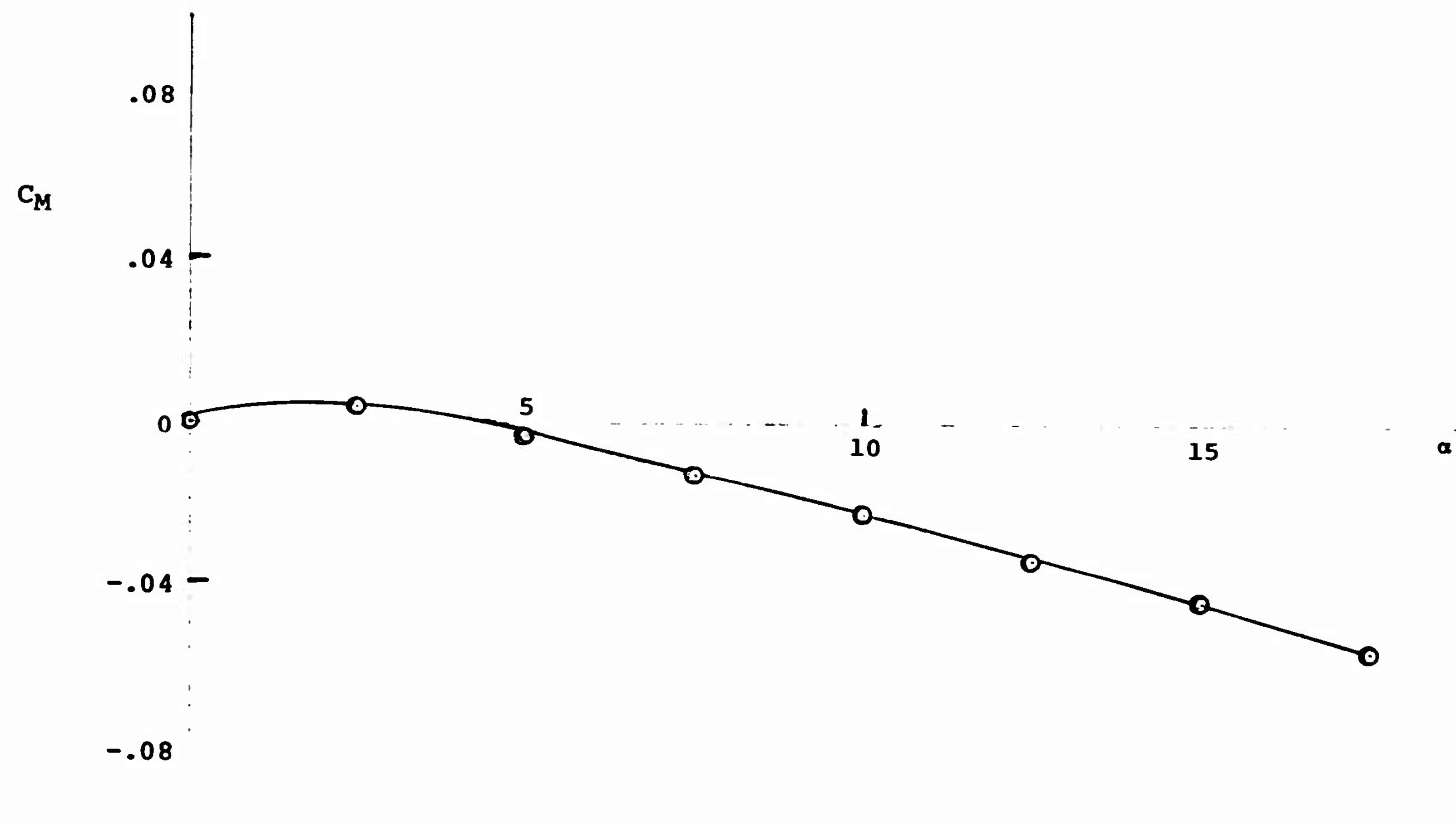

FIG. 84 C_M VALUES FOR THE RINGSLOT PARACHUTE MODEL AT L_C/L_S = 1.12

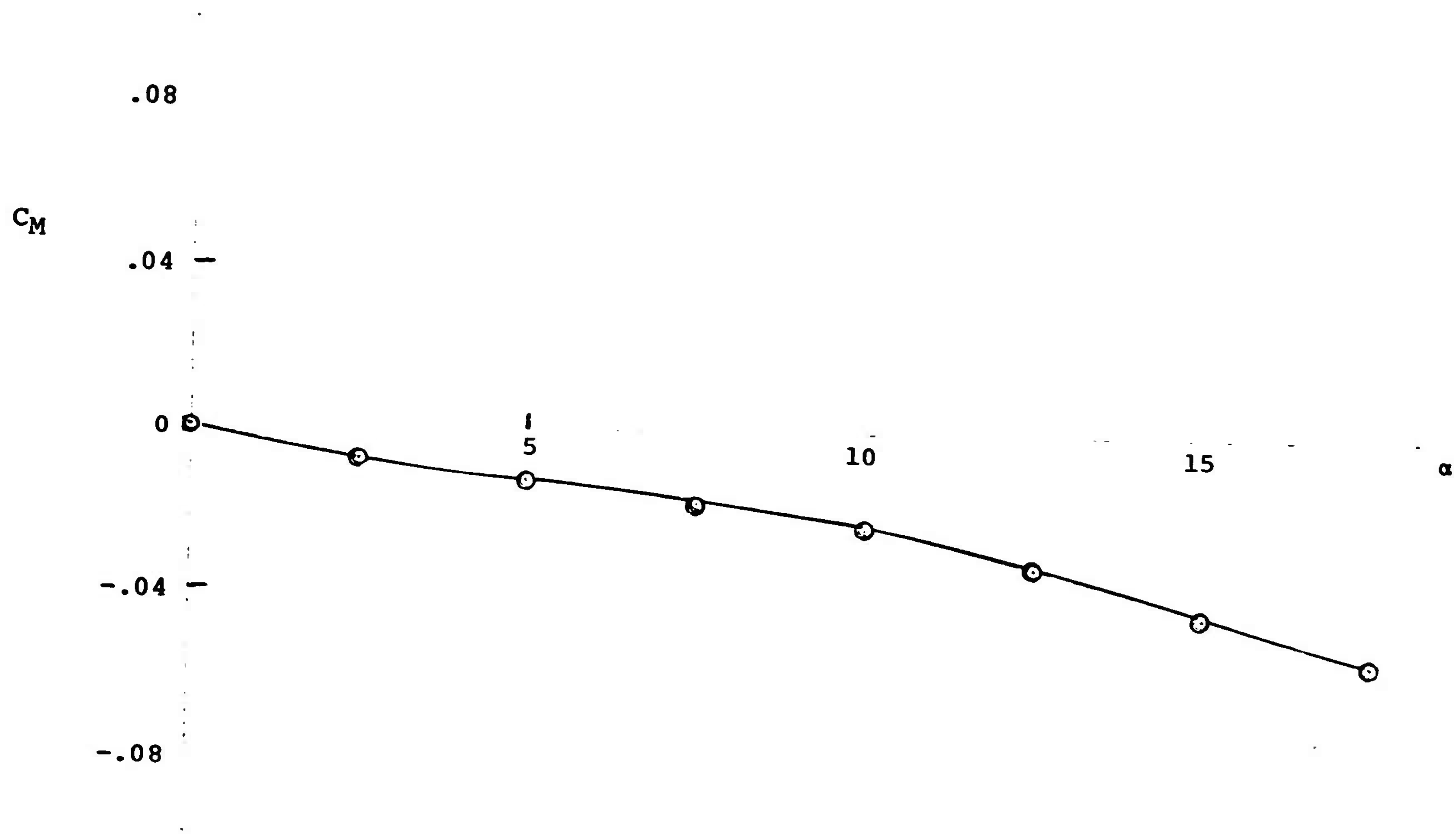

FIG. 85 C_M VALUES FOR THE RINGSLOT PARACHUTE MODEL AT L_c/L_s = 1.07

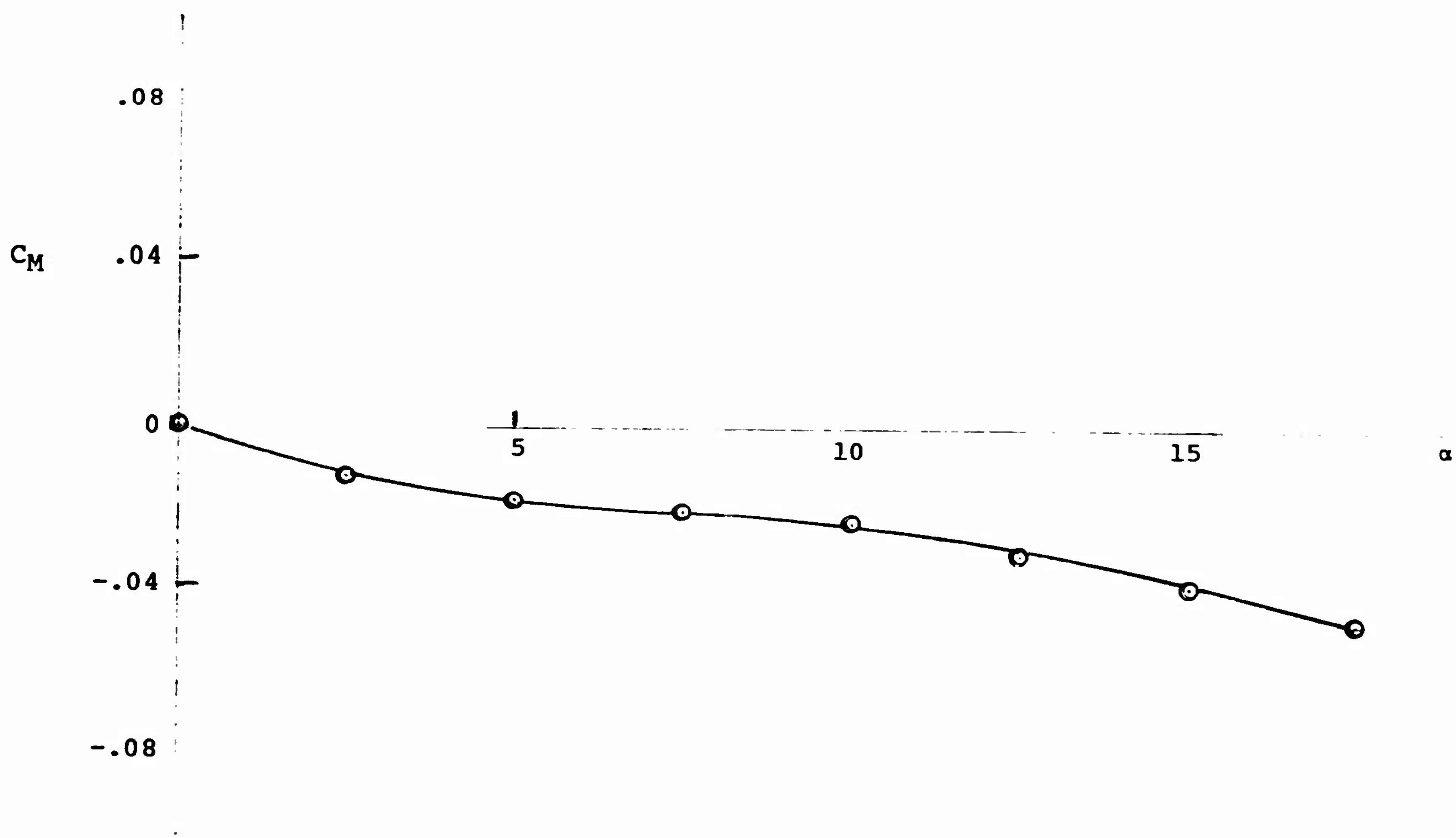

FIG. 86 C_M VALUES FOR THE RINGSLOT PARACHUTE MODEL AT $L_C/L_S = 1.02$

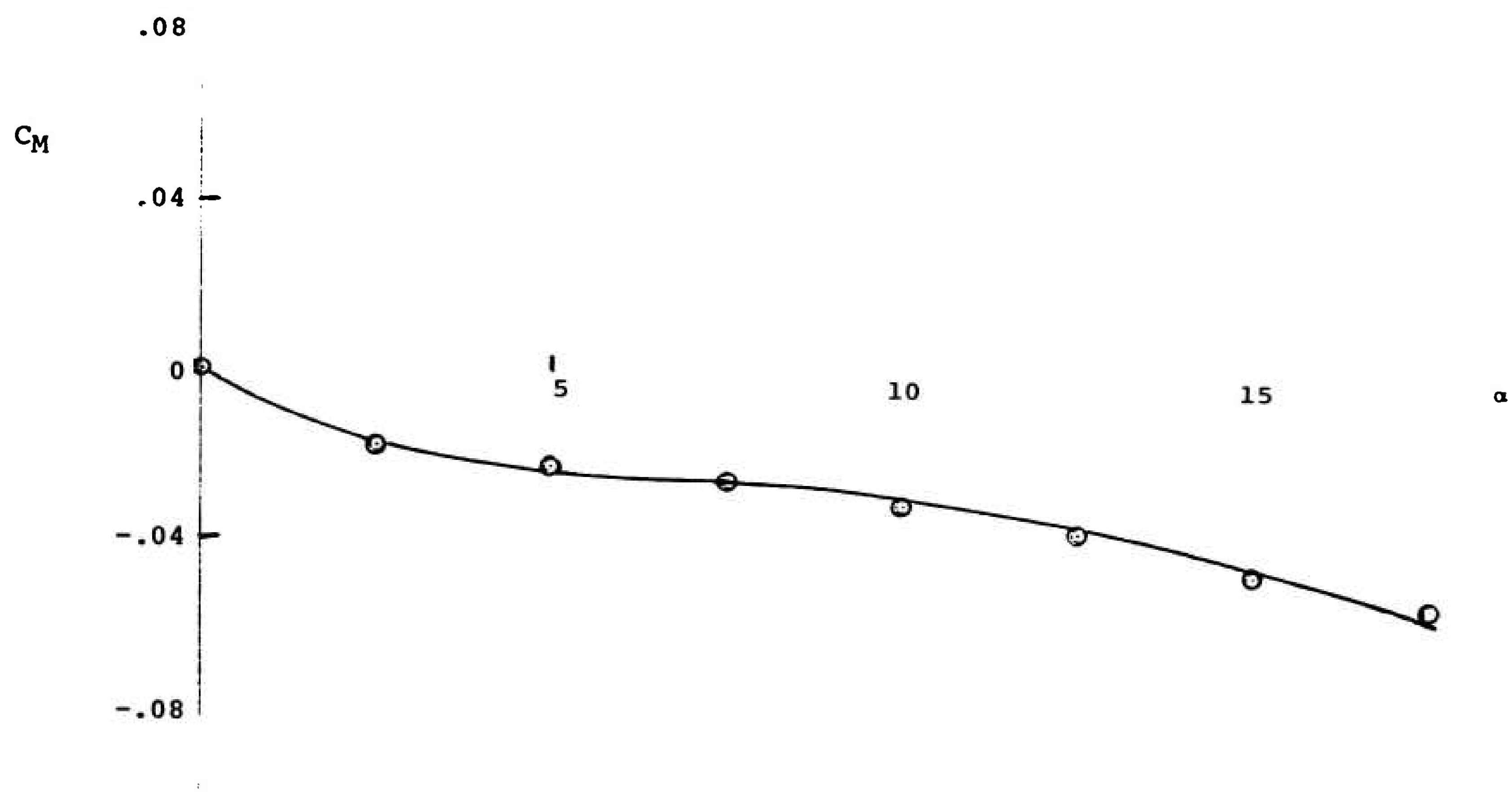

FIG. 87 C_M VALUES FOR THE RINGSLOT PARACHUTE MODEL AT L_C/L_S = .97